

Novel self-similar rotating solutions of nonideal transverse magnetohydrodynamics

M. Shokri* and N. Sadooghi†

Department of Physics, Sharif University of Technology, P.O. Box 11155-9161 Tehran, Iran
(Received 30 April 2017; published 11 December 2017)

The evolution of electromagnetic and thermodynamic fields in a nonideal fluid is studied in the framework of ultrarelativistic transverse magnetohydrodynamics (MHD), which is essentially characterized by electric and magnetic fields being transverse to the fluid velocity and translational invariance in the transverse plane. Extending the method of self-similar solutions of relativistic hydrodynamics to the case of nonconserved charges, the differential equations of nonideal transverse MHD are solved, and two novel sets of self-similar solutions are derived. The first set turns out to be a boost-invariant and exact solution, which is characterized by nonrotating electric and magnetic fields. The second set is a nonboost-invariant solution, which is characterized by rotating electric and magnetic fields. The rotation occurs with increasing rapidity η , as the angular velocity is defined by $\omega_0 \equiv \frac{\partial \zeta}{\partial \eta} = \frac{\partial \phi}{\partial \eta}$, with ζ and ϕ being the angles of local electric and magnetic vectors with respect to a certain fixed axis in the transverse plane. For both sets of solutions, the electric and magnetic fields are either parallel or antiparallel to each other in the local rest frame of the fluid. Performing a complete numerical analysis, the effects of finite electric conductivity as well as electric and magnetic susceptibilities of the medium on the evolution of rotating and nonrotating MHD solutions are explored, and the interplay between the angular velocity ω_0 and these quantities is scrutinized. The lifetime of electromagnetic fields and the evolution of the temperature of the electromagnetized fluid are shown to be affected by ω_0 .

DOI: [10.1103/PhysRevD.96.116008](https://doi.org/10.1103/PhysRevD.96.116008)

I. INTRODUCTION

One of the most significant achievements of relativistic hydrodynamics (RHD) in recent years is in the ability to reproduce experimental data from relativistic heavy ion collisions (HICs) at the Relativistic Heavy Ion Collider (RHIC) and Large Hadron Collider (LHC). In particular, the elliptic flow data of low to intermediate transverse momenta for almost all particle species and for various centralities, beam energies, and colliding nuclei are successfully described by RHD model calculations, performed with realistic initial conditions and the equation of state (EoS) for relativistic HICs [1,2]. These studies have already led to the RHIC discovery that the quark-gluon plasma (QGP) created in relativistic HICs is a strongly coupled nearly perfect fluid [3–6] (for a review see, e.g., [7]).

The nonlinear differential equations describing RHD are remarkably complex. Their major characteristic is, however, that they do not contain any internal scale. Using this special feature, a large class of exact, self-similar solutions of relativistic hydrodynamics has been found in recent years. Motivated by the seminal work by Landau [8,9] and Khalatnikov [10], who presented the first exact one-dimensional implicit solution of RHD, R. C. Hwa [11] and J. D. Bjorken [12] found independently an explicit analytic

solution for RHD equations in the ultrarelativistic limit. This solution, referred to as Bjorken flow, represents a one-dimensional, longitudinally boost-invariant solution of relativistic ideal hydrodynamics (RIHD). Other analytic and self-similar exact solutions of RIHD are presented in [13] and [14,15], where, in particular, a three-dimensional expanding Gaussian fireball is described, which exhibits a Hubble-type linear radial flow. These solutions are then generalized to one- and three-dimensional solutions, exhibiting various cylindrical, spheroidal, and ellipsoidal symmetries. They describe, in particular, the evolution of the fireball with or without rotation and acceleration (for a recent review see [16] and references therein). In combination with the EoS, arising from lattice quantum chromodynamics (QCD), the main goal is, among others, to describe various physical observables in relation with HIC experiments by these exact analytical solutions. They therefore reflect various symmetry properties of HICs before and at hadrochemical freeze-out stage [17].

An important feature of noncentral HICs is the generation of very strong magnetic fields in the early stage of the collisions. Depending on the impact parameter and collision energy, their strengths are estimated to be $eB \sim 1.5m_\pi^2$ at the RHIC and $eB \sim 15m_\pi^2$ at the LHC [18,19], with the pion mass $m_\pi = 0.14 \text{ GeV}$.¹ The magnetic field created

*m_shokri@physics.sharif.ir
†sadooghi@physics.sharif.ir

¹ $eB = 1 \text{ GeV}^2$ corresponds to a magnetic field strength $B \sim 1.7 \times 10^{20} \text{ Gau\ss}$.

at HICs is time dependent, and rapidly decays after $\tau \sim 1\text{--}2$ fm/c. However, as it is argued in [20–22], due to the relatively large electric conductivity of the QGP medium, the external magnetic field is essentially frozen, and its decay is thus substantially delayed. Most theoretical studies deal therefore with the idealized limit of constant and homogeneous magnetic fields.²

One of the possibilities to explore the dynamics of external electromagnetic fields is the relativistic magneto-hydrodynamics (MHD). Recently, MHD methods are used to study the effect of magnetic fields created in HICs on the evolution of the energy density of QGP. A one-dimensional, longitudinally boost-invariant solution of ultrarelativistic ideal MHD is presented in [33,34]. Here, the external magnetic field is assumed to be transverse to the fluid velocity. In [33], it is found that in the ideal MHD limit, where, in particular, the electric conductivity of the medium is assumed to be infinitely large, the (proper) time evolution of the energy density is the same as in the case without any magnetic field. This remarkable result can be best understood by the well-known “frozen-flux theorem” [35], which states that the ratio B/s , with B being the magnetic field and s the entropy density, is conserved, and the magnetic field is thus advected with the fluid, and evolves therefore as $B(\tau) \propto \tau^{-1}$ with $\tau \equiv (t^2 - z^2)^{1/2}$ being the proper time. The deviation from the frozen-flux theorem is also imposed in [33,34] by a parametrized power-law (PL) ansatz for the evolution of the magnetic field, $B(\tau) \propto \tau^{-a}$, where a is an arbitrary free parameter. It is shown that the decay of the energy density depends on whether $a > 1$ or $a < 1$. The additional effect of a constant (temperature-independent) magnetic susceptibility on the energy density of QGP is studied within the same ideal transverse MHD framework in [34]. In [36], the aforementioned power-law decay ansatz of B is generalized to a power-law decay of magnetic fields with spatial inhomogeneity, characterized by a Gaussian distribution in one of the transverse directions.

It is the purpose of this paper to study the dynamics of electromagnetic and thermodynamic fields within a one-dimensional ultrarelativistic nonideal MHD framework with electric and magnetic fields being transverse to the fluid velocity (hereafter nonideal transverse MHD). We present novel nonboost-invariant, self-similar solutions for electromagnetic and thermodynamic fields, appearing in nonideal transverse MHD with finite electric conductivity σ and electric as well as magnetic susceptibilities, χ_e and χ_m . Using the method presented in, e.g., [37], where a

certain self-similar, nonaccelerating exact solution of RIHD is presented, we first show that the boost-invariant solution $B(\tau) \propto \tau^{-1}$, derived in [33,34], is a self-similar exact solution that naturally arises in ideal transverse MHD. Here, apart from the exact solution for B , satisfying the aforementioned frozen-flux theorem, self-similar, exact, and nonboost-invariant solutions for thermodynamic fields, such as temperature T , entropy, and number densities, s and n , arise. To go beyond the ideal limit of infinite electric conductivity [33,34], we extend the method used in [37] to the case of nonconserved charges. We solve the corresponding MHD equations, combined with homogeneous and inhomogeneous Maxwell equations. By appropriately parametrizing these equations in terms of the magnitudes of the electromagnetic fields, E and B , as well as the angles ζ and ϕ of \mathbf{E} and \mathbf{B} with respect to a certain fixed axis in transverse plane, we show that two series of solutions arise, which are particularly characterized by vanishing and nonvanishing angular velocity of \mathbf{E} and \mathbf{B} , ω_0 , defined by $\omega_0 \equiv \frac{d\zeta}{d\eta} = \frac{d\phi}{d\eta}$. Here, $\eta \equiv \frac{1}{2} \ln \frac{t+z}{t-z}$ is the rapidity.

For vanishing angular velocity, nonrotating (NR), boost-invariant, self-similar, and analytic solutions for \mathbf{B} and \mathbf{E} are derived. They are shown to be either parallel or antiparallel with respect to each other in the local rest frame (LRF) of the fluid. Their magnitude is given by $B(\tau) \propto \tau^{-1}$ and $E \propto \tau^{-1} \exp(-f(\sigma, \chi_e)\tau)$, where f is a certain (positive) function of σ and χ_e . As concerns the case of nonvanishing angular velocity of the magnetic and electric vectors, we derive approximate analytical as well as numerical solutions for \mathbf{B} and \mathbf{E} . This is done by solving a second-order and quadratic differential equation for a certain function $\mathcal{M}(\tau)$, describing, in particular, the deviation of the dynamics of the magnetic field from the frozen-flux theorem. It arises in our method of self-similar solutions for nonconserved charges (see below). We show that a power-law solution $B(\tau) \propto \tau^{-a}$, similar to the one previously used in [33,34],³ naturally arises as one of the approximate analytical solutions to this differential equation, where, in particular, the ratio E/B is assumed to be constant in τ . Here, the power a in $B(\tau) \propto \tau^{-a}$ is shown to be expressed in terms of the angular velocity ω_0 , which, by its part, turns out to be a function of σ , χ_e , and χ_m . A second series of approximate analytical solutions to the above-mentioned nonlinear differential equation for \mathcal{M} is also derived. It eventually leads to slowly rotating (SR) \mathbf{B} and \mathbf{E} fields. We present the corresponding self-similar and nonboost-invariant solutions to the temperature T in these approximations. As concerns the nonboost invariance of the solutions for \mathbf{E} and \mathbf{B} , it is shown that in contrast to the nonboost invariance of T , which reflects itself in the

²See [23,24] for a complete analysis of the effect of constant magnetic fields on QCD phase diagram, including magnetic catalysis [25,26] and inverse magnetic catalysis effects [27], and [28–30] in relation with the effect of constant magnetic fields on various particle production rates in HICs. See also [31,32] for recent reviews on the effect of constant magnetic fields on quark matter.

³In contrast to the power-law solution that is derived in the present paper, the power-law decay ansatz used in [33,34] turns out to be a solution of transverse MHD, where, in particular, $\sigma \rightarrow \infty$, and thus $E \rightarrow 0$.

appearance of an η -dependent scale factor, the nonboost invariance of electromagnetic fields is particularly characterized by the dependence of the angles ζ and ϕ on the rapidity η .

We also numerically solve the aforementioned differential equation for \mathcal{M} . The aim is to quantitatively study the effects of free parameters σ, χ_e, χ_m , and $\sigma_0 \equiv \frac{B_0^2}{\epsilon_0}$ on B , E , and T . Here, B_0 and ϵ_0 are the magnetic field and energy density of the fluid at the initial (proper) time. The effects of the angular velocity ω_0 on the evolution of B , E , T , and the interplay between ω_0 and other free parameters is further scrutinized. We, in particular, show that the evolution of thermodynamic fields T is strongly affected by rotating and nonrotating solutions to nonideal transverse MHD equations, as well as the magnetic susceptibility of the medium.

The organization of this paper is as follows: In Sec. II, we first apply the method presented in [37] on ideal transverse MHD, and derive self-similar, boost-invariant, and exact solutions for the number density n , temperature T , energy density ϵ , and magnetic field B . Then, we extend the method from [37] to nonideal transverse MHD, where we are, in particular, faced with inhomogeneous continuity equations with the generic form $\partial_\mu(fu^\mu) = f\mathfrak{D}\lambda$ for B , E , and T . The corresponding inhomogeneity functions for $f = \{B, E, T\}$ in $\partial_\mu(fu^\mu) = f\mathfrak{D}\lambda$ are denoted in the rest of this paper by $\lambda = \{\mathcal{M}, \mathcal{N}, \mathcal{L}\}$, respectively. In Sec. III, after presenting the necessary definition of the nonideal transverse MHD with finite σ , χ_e , and χ_m , we derive the corresponding differential equations of MHD and Maxwell equations in terms of variables B , E , and ζ, ϕ as well as free parameters σ, χ_e , and χ_m (Sec. III A). Assuming the boost invariance of p , B , and E in a uniformly expanding fluid, and using the formal self-similar solutions to the inhomogeneous continuity equations for B , E , and T , arising from our generalized self-similar method for nonconserved charges (Sec. III B), we then combine, in Sec. III C, the aforementioned differential equations for nonideal transverse MHD, and arrive, in particular, at the corresponding differential equations to \mathcal{M} . We show that \mathcal{M} satisfies either $\frac{d\mathcal{M}}{du} = 0$ with $u \equiv \ln(\frac{r}{r_0})$ or a second-order nonlinear differential equation. Solutions to these differential equations play a major role in determining \mathcal{N} and \mathcal{L} , and thus in determining rotating and nonrotating solutions for B , E , and T . In Secs. IV A and IV B, we introduce the exact and approximate analytical, self-similar nonrotating and rotating solutions of B , E , and T . Numerical solutions of the second-order, nonlinear differential equation corresponding to \mathcal{M} are presented in Sec. V. In Sec. V A, we qualitatively compare the space-time evolutions of B , E , and T in ideal MHD with their nonrotating and rotating solutions in nonideal MHD. In Sec. V B, the reliability of approximate analytical solutions from Sec. III C is quantitatively studied. The effects of free sets of parameters σ, χ_e, χ_m , as well as ω_0, σ_0 , and $\beta_0 \equiv E_0/B_0$ on the evolution of B , E , and T

are studied in Sec. V C. Here, E_0 and B_0 are the electric and magnetic fields at initial proper time. Although for the choice of free set of parameters, we have strongly oriented ourselves to sets that may be relevant for QGP, the considerations in this paper are quite general, and can be applied to every magnetized fluid with finite electric and magnetic susceptibilities. Section VI is devoted to a summary of the results and a number of concluding remarks. A number of useful proofs and a general analysis of the solutions of the nontrivial differential equation for \mathcal{M} are presented in Appendixes A and B.

II. SELF-SIMILAR SOLUTIONS OF RELATIVISTIC IDEAL HYDRODYNAMICS AND THE METHOD OF NONCONSERVED CHARGES

As aforementioned, self-similar solutions of RHD are generalizations of the Hwa-Bjorken flow [11,12]. They provide the possibility of nonboost-invariant temperature profiles [37], and are naturally generalized to $3+1$ dimensions [38]. In this section, we briefly review these solutions in $1+1$ dimensions. In this setup, one assumes that the fluid is expanding in time and only one spatial dimension, which, without loss of generality, can be taken to be the z -direction. The system is also assumed to possess translational invariance in the transverse plane, i.e., the x - y plane. The latter assumption implies that the hydrodynamical fields, such as four-velocity $u^\mu(x) = \gamma(1, \mathbf{v})$ and entropy density $s(x)$, are independent of the transverse coordinates [39].⁴ Here, $\gamma = (1 - v_z^2)^{-1/2}$ is the Lorentz factor. The equations of RIHD, consisting of conservation laws of the energy-momentum tensor of the fluid $T^{\mu\nu} = (\epsilon + p)u^\mu u^\nu - pg^{\mu\nu}$, and entropy density current su^μ , read

$$\partial_\mu T^{\mu\nu} = 0, \quad (2.1)$$

$$\partial_\mu (su^\mu) = 0. \quad (2.2)$$

In $T^{\mu\nu}$, ϵ and p are the energy density and pressure of the fluid, respectively. In what follows, we introduce the method used in [37], where, in particular, general self-similar solutions for the above hydrodynamical fields are found.

To this purpose, let us first consider an arbitrary continuity equation

$$\partial_\mu (fu^\mu) = 0. \quad (2.3)$$

Here, $f(t, z)$ is a conserved quantity such as the entropy density s . To determine the self-similar solution to (2.3), one introduces the scaling parameter $Z(t)$ and the scaling variable $\Theta(z, Z)$, such that

⁴Here, $g^{\mu\nu} = \text{diag}(1, -1, -1, -1)$ and $u_\mu u^\mu = 1$.

- (i) if $f(t, z)$ is a solution to Eq. (2.3), then $f(t, z)\mathcal{F}_f(\Theta)$ is also a solution to the same equation. Here, \mathcal{F}_f is any differentiable function of the parameter Θ , which is defined below. In addition, if $f(t, z)$ is a positive quantity, then \mathcal{F}_f must be positive as well,
- (ii) the longitudinal velocity obeys a Hubble-like expansion law as $v_z = H(t)z$ with $H(t) = \frac{\dot{Z}}{Z}$.

Assumption (i) requires

$$\mathfrak{D}\Theta = 0. \tag{2.4}$$

Here, $\mathfrak{D} \equiv u^\mu \partial_\mu$ is the conductive derivative. Assumption (ii) can be used to solve (2.4) as

$$\Theta = \left(\frac{z}{Z}\right)^\alpha, \tag{2.5}$$

where α is a parameter, which is fixed later. Having these in hand, the most general self-similar solution of (2.3) reads

$$f(t, z) = f_0 \left(\frac{Z_0}{Z\gamma}\right) \mathcal{F}_f(\Theta), \tag{2.6}$$

with $Z_0 = Z(t_0)$ and $f_0 = f(t_0, 0)$. In (2.6), \mathcal{F}_f is normalized as $\mathcal{F}_f(0) = 1$.

Let us consider again the RIHD equations (2.1) and (2.2). These equations can be closed by incorporating a thermodynamic EoS, which is assumed to be

$$\epsilon = \kappa p, \tag{2.7}$$

with $\kappa = \text{const.}$ ⁵ Plugging (2.7) into the longitudinal component of (2.1),

$$\mathfrak{D}\epsilon + (\epsilon + p)\theta = 0, \tag{2.8}$$

and exploiting the entropy conservation of RIHD from (2.2), leads to the following continuity equation for the temperature T ,

$$\partial_\mu(T^\kappa u^\mu) = 0. \tag{2.9}$$

Here, the thermodynamic relation $\epsilon + p = Ts$ is used.⁶ According to (2.6), the solutions for T , s , and p then read [37]

$$s(t, z) = s_0 \left(\frac{Z_0}{Z\gamma}\right) \mathcal{S}(\Theta), \tag{2.10}$$

$$T(t, z) = T_0 \left(\frac{Z_0}{Z\gamma}\right)^{1/\kappa} \mathcal{T}(\Theta), \tag{2.11}$$

$$p(t, z) = p_0 \left(\frac{Z_0}{Z\gamma}\right)^{1+1/\kappa} \mathcal{T}(\Theta)\mathcal{S}(\Theta), \tag{2.12}$$

where $p_0 = \frac{T_0 s_0}{1+\kappa}$. As concerns the power α in (2.5), we put (2.12) into the Euler equation

$$\mathfrak{D}u_\mu = \frac{1}{\epsilon + p} \nabla_\mu p, \tag{2.13}$$

which arises from $\Delta_{\mu\nu} \partial_\rho T^{\rho\nu} = 0$, with $\nabla_\mu \equiv \Delta_{\mu\nu} \partial^\nu$ and $\Delta_{\mu\nu} \equiv g_{\mu\nu} - u_\mu u_\nu$, and arrive at an expression for \ddot{Z} in terms of Z , \dot{Z} , and Θ . The requirement that \ddot{Z} is finite leads to $\alpha = 2$.⁷ Moreover, the fact that Z is Θ independent leads to $\ddot{Z}(\Theta, \dots) = \ddot{Z}(0, \dots)$. This, for its part, translates into a second-order equation for \dot{Z}^2 whose coefficients are only functions of Θ . It thus has a solution of the form⁸

$$\dot{Z}^2 = \dot{Z}^2(\Theta). \tag{2.14}$$

Exploiting, at this stage, the Θ independence of Z requires \dot{Z} to be constant, and thus $\ddot{Z} = 0$. This immediately results in vanishing of the proper acceleration, $\mathfrak{D}u_\mu = 0$, and the emergence of the Hwa-Bjorken velocity profile $v_z = z/t$.

Since $\mathfrak{D}\gamma = \frac{\partial\gamma}{\partial\tau} = 0$, one is able to introduce new scaling functions

$$\mathcal{U}(\Theta) = \frac{\mathcal{S}(\Theta)}{\gamma^2}, \tag{2.15}$$

$$\mathcal{V}(\Theta) = \frac{\mathcal{T}(\Theta)}{\gamma^{2/\kappa}}. \tag{2.16}$$

Using $\mathfrak{D}u_\mu = 0$, we arrive at the boost invariance (η independence) of p and automatically at $\mathcal{U}\mathcal{V} = 1$. If the process is isentropic [40], then s and the number density n share the same scaling function, and the ideal gas equation $p = nT$ holds.⁹ The latter can then be used to give the final results for n , T , and p ,

$$n = n_0 \left(\frac{\tau_0}{\tau}\right) \mathcal{U} \left(\frac{\tanh^2 \eta}{\dot{Z}_0^2}\right), \tag{2.17}$$

$$T = T_0 \left(\frac{\tau_0}{\tau}\right)^{1/\kappa} \mathcal{U}^{-1} \left(\frac{\tanh^2 \eta}{\dot{Z}_0^2}\right), \tag{2.18}$$

⁷This result is in line with [37], where $\alpha = 2$ is *a priori* assumed.

⁸The functional form of $\dot{Z}(\Theta)$ does not matter.

⁹The ideal gas equation that was used as an assumption in the original derivation of the solutions in [37] seems not to be required for the case of baryon-free RIHD.

⁵For our purposes, it is enough that $\mathfrak{D}\kappa = 0$.

⁶The system is assumed to be baryon free [40].

$$p = p_0 \left(\frac{\tau_0}{\tau} \right)^{1+1/\kappa}. \quad (2.19)$$

Here, we have introduced the Milne coordinates $z = \tau \sinh \eta$ and $t = \tau \cosh \eta$, with $\tau = (t^2 - z^2)^{1/2}$ and $\eta = \frac{1}{2} \ln \frac{t+z}{t-z}$ being the proper time and space-time rapidity, respectively.¹⁰ To derive (2.17)–(2.19), $Z(t) = \dot{Z}_0 t$ is used. The evolution of the energy density ϵ is determined by plugging (2.19) into (2.8). It is given by

$$\epsilon = \epsilon_0 \left(\frac{\tau_0}{\tau} \right)^{1+1/\kappa}, \quad (2.20)$$

with $\epsilon_0 = \kappa p_0$. Let us note that although the velocity and pressure profile are the same as the Hwa-Bjorken solution, the temperature, number, and entropy densities have an arbitrary rapidity dependence through the factors $\mathcal{U}(\frac{\tanh^2 \eta}{Z_0^2})$. It is also worth mentioning that although in deriving (2.9) κ was only assumed to have vanishing conductive derivative, the treatment of the Euler equation was based on κ being a constant.

Transverse MHD was previously studied in [33,34]. It is found that the Hwa-Bjorken solution for the energy density (and temperature profile) is also valid for 1 + 1-dimensional ideal MHD.¹¹ This is not surprising since ideal MHD has no extra energy dissipation channel in addition to RIHD, and the energy equation (2.8) still holds. Therefore any solution of the RIHD energy density holds in ideal MHD as well. It thus seems that self-similar solutions of thermodynamic fields in RIHD are automatically generalized to the case of ideal MHD. However, the boost invariance needs extra care. As it is shown in the following sections, in the transverse MHD setup [33] electrical charge density vanishes. The inspection of the equation of motion for the fluid parcels shows that proper acceleration gains therefore no contribution from electromagnetic fields. Since the equation of motion is linear, one can take the proper acceleration to remain 0 by superposition. As we show, any additive term in the Euler equation becomes boost invariant when proper acceleration $\mathfrak{D}u_\mu$ vanishes. The results of self-similar solutions of thermodynamic fields in RIHD are thus generalized to the case of ideal MHD.

However, in the treatment of MHD one is not only concerned about the evolution of hydrodynamical fields, but also wants to know how the electromagnetic fields evolve as observed in the LRF of the fluid. As it turns out, the frozen-flux theorem of ideal transverse MHD [33] is

¹⁰Let us note that in these coordinates $\mathfrak{D} = u^\mu \partial_\mu$, $\theta \equiv \partial_\mu u^\mu$, and ∇_μ translate into $\mathfrak{D} = \frac{\partial}{\partial \tau}$, $\theta = \frac{1}{\tau}$, and $\nabla_\mu = -\frac{1}{\tau} (\sinh \eta, 0, 0, -\cosh \eta) \frac{\partial}{\partial \eta}$.

¹¹In ideal MHD, apart from hydrodynamical dissipative effects, the resistivity of the medium is assumed to vanish.

translated into another continuity equation for the magnitude of the local magnetic field, B ,¹²

$$\partial_\mu (B u^\mu) = 0. \quad (2.21)$$

The most general self-similar solution of B is therefore given by

$$B = B_0 \left(\frac{\tau_0}{\tau} \right) \mathcal{B} \left(\frac{\tanh^2 \eta}{\dot{Z}_0^2} \right). \quad (2.22)$$

Here, as in the case of pressure in the RIHD case, the η -dependent scaling factor $\mathcal{B} = 1$, because, by inspecting the Euler equation, it turns out that an additional term B^2 appears on the rhs of the Euler equation (2.13) (see also Sec. III). The fact that $\mathfrak{D}u_\mu = 0$ thus leads to the boost invariance (η independence) of B , or equivalently to $\mathcal{B} = 1$.

In nonideal transverse MHD, when one relaxes the assumption of infinite conductivity, things becomes more complicated. The frozen flux (2.21) and the continuity equation for the temperature (2.9) are then violated, and the evolution of the electric field becomes also important. In this case, we have found it useful to introduce a method to solve the nonideal MHD equations, which for further convenience is referred to as the method of nonconserved charges. Here, one basically considers a nonconserved charge $f(t, z)$, which satisfies

$$\partial_\mu (f u^\mu) = f \mathfrak{D} \lambda, \quad (2.23)$$

with $\lambda = \lambda(t, z)$ being a differentiable function of space and time. From (2.23), one finds

$$\partial_\mu (f u^\mu \exp(-\lambda)) = 0, \quad (2.24)$$

leading to

$$f(t, z) = f_0 \left(\frac{Z_0}{\gamma Z} \right) \exp(\lambda - \lambda_0) \mathbb{F}_f(\Theta), \quad (2.25)$$

with $\lambda = \lambda(t, z)$ and $\lambda_0 = \lambda(t_0, 0)$. One can add any function $g(t, z)$ to λ as long as $\mathfrak{D}g = 0$. Specifically, any differentiable function of Θ can be added to λ . The resulting factor $\exp(g - g_0)$ can however be absorbed into \mathbb{F}_f , as a purely η -dependent function. In a uniformly expanding fluid, where v_z satisfies the Hwa-Bjorken profile $v_z = \frac{z}{t}$, the final result of the nonconserved charge f can thus be given in terms of τ and η as

¹²To show (2.21), let us consider the homogeneous Maxwell equation $\partial_\mu \tilde{F}^{\mu\nu} = 0$, which for $E^\mu = 0$ in ideal MHD reads $\partial_\mu (B^\mu u^\nu - B^\nu u^\mu) = 0$. Using $\partial \cdot B = B \cdot \partial = 0$ in transverse ideal MHD (see below) and using $B \cdot B = -B^2$, we arrive after some work at the frozen-flux theorem (2.21) in transverse ideal MHD. Here, $a \cdot b \equiv a_\mu b^\mu$.

$$f(\tau, \eta) = f_0 \left(\frac{\tau_0}{\tau} \right) \exp(\lambda - \lambda_0) \mathcal{U} \left(\frac{\tanh^2 \eta}{\dot{Z}_0^2} \right), \quad (2.26)$$

where $\lambda = \lambda(\tau)$ and $\lambda_0 = \lambda(\tau_0)$. Without loss of generality, we set $\lambda_0 = 0$ in the rest of this work. In the next sections, we apply this method to nonideal MHD, and, in particular, find a master equation that governs the deviation of an electromagnetized nonideal fluid from the frozen-flux theorem. The latter leads to the solutions of the equations of transverse MHD in some specific cases. We show that the η dependence of the relative angle of the B field with a certain axis in the LRF of the fluid may distinguish between various solutions of this master equation.

III. RELATIVISTIC MAGNETOHYDRODYNAMICS

In this section, we first focus on transverse MHD in $1+1$ dimensions, and introduce the main definitions and a number of useful relations (Sec. III A). To be brief, we only consider the case of nonideal magnetized fluid with finite magnetization M , electric polarization P , and electric conductivity σ . Taking the limit $\sigma \rightarrow \infty$ as well as $M, P \rightarrow 0$, the case of ideal MHD can be retrieved. We compare the results of ideal and nonideal fluid whenever necessary. Apart from energy and Euler equations, we consider the homogeneous and nonhomogeneous Maxwell equations. Combining these equations, we derive in Sec. III C the aforementioned master equation, whose solutions are explored in Sec. IV. The aim is to use the method of nonconserved charges in order to determine the space-time evolution of thermodynamic quantities n, T, p, ϵ as well as those of electric and magnetic fields E^μ and B^μ . Formal self-similar solutions to these fields are presented in III B.

A. Transverse MHD: Definitions and useful relations

A locally equilibrated relativistic fluid in $1+1$ dimensions is characterized by the four-velocity $u_\mu = \gamma(1, 0, 0, v_z)$, which is defined by the variation of the four coordinate $x^\mu = (t, \mathbf{x})$ with respect to proper time $\tau = (t^2 - z^2)^{1/2}$ and satisfies $u_\mu u^\mu = 1$. Continuity equations

$$\partial_\mu (n u^\mu) = 0, \quad \partial_\mu T^{\mu\nu} = 0, \quad \partial_\mu J^\mu = 0 \quad (3.1)$$

then govern the dynamics of the fluid. Here, n is the baryonic number density and $T^{\mu\nu}$ and J^μ are the total energy-momentum tensor and electric current, respectively.

In the presence of electromagnetic fields, $T^{\mu\nu}$ is given by a combination of the fluid and electromagnetic energy-momentum tensor, $T_F^{\mu\nu}$ and $T_{EM}^{\mu\nu}$, as

$$T^{\mu\nu} = T_F^{\mu\nu} + T_{EM}^{\mu\nu}, \quad (3.2)$$

with¹³

$$T_F^{\mu\nu} = (\epsilon + p) u^\mu u^\nu - p g^{\mu\nu} - \frac{1}{2} (M^{\mu\lambda} F_{\lambda}{}^\nu + M^{\nu\lambda} F_{\lambda}{}^\mu), \quad (3.3)$$

and

$$T_{EM}^{\mu\nu} = -F^{\mu\lambda} F_{\lambda}{}^\nu + \frac{1}{4} F^{\rho\sigma} F_{\rho\sigma} g^{\mu\nu}. \quad (3.4)$$

The antisymmetric field strength and polarization tensors, $F^{\mu\nu}$ and $M^{\mu\nu}$, are defined by

$$F^{\mu\nu} = E^\mu u^\nu - E^\nu u^\mu - \epsilon^{\mu\nu\alpha\beta} B_\alpha u_\beta, \\ M^{\mu\nu} = -\chi_e (E^\mu u^\nu - E^\nu u^\mu) - \chi_m \epsilon^{\mu\nu\alpha\beta} B_\alpha u_\beta, \quad (3.5)$$

where $\epsilon^{\mu\nu\alpha\beta}$ is the totally antisymmetric Levi-Civita symbol,¹⁴ and the four-vector of electric and magnetic fields is given by $E^\mu \equiv F^{\mu\nu} u_\nu$ and $B^\mu \equiv \frac{1}{2} \epsilon^{\mu\nu\alpha\beta} F_{\nu\alpha} u_\beta$. They satisfy $E^\mu E_\mu = -E^2$ and $B^\mu B_\mu = -B^2$. In the LRF of the fluid, with $u^\mu = (1, \mathbf{0})$, we have $E^\mu = (0, \mathbf{E})$ and $B^\mu = (0, \mathbf{B})$. Moreover, using the definitions of E^μ and B^μ in terms of $F^{\mu\nu}$, we arrive at $u_\mu E^\mu = 0$ and $u_\mu B^\mu = 0$. Combining these relations with $\mathbf{v} \cdot \mathbf{E} = 0$ as well as $\mathbf{v} \cdot \mathbf{B} = 0$, which are valid in $1+1$ -dimensional transverse MHD, we have, in particular, $E^\mu = (0, E_x, E_y, 0)$ as well as $B^\mu = (0, B_x, B_y, 0)$. In what follows, we strongly use the above properties of transverse MHD leading to $\partial \cdot E = 0$, $\partial \cdot B = 0$, $E \cdot \partial = 0$, $B \cdot \partial = 0$.¹⁵

For later convenience, we parametrize E^μ and B^μ in terms of the magnitudes of the fields, E and B , as well as the relative angles of \mathbf{E} and \mathbf{B} fields with respect to the x -axis in the LRF of the fluid, ζ and ϕ ,

$$E^\mu = (0, E \cos \zeta, E \sin \zeta, 0), \\ B^\mu = (0, B \cos \phi, B \sin \phi, 0). \quad (3.6)$$

The antisymmetric polarization tensor $M^{\mu\nu}$ in Sec. (3.4) describes the response of the system to an applied electromagnetic field. Assuming a linear response from the medium, the electric and magnetic susceptibilities χ_e and χ_m are defined by $\chi_e \equiv P/E$ and $\chi_m \equiv M/B$, where P and M are given by $P^2 = -P^\mu P_\mu$ and $M^2 = -M^\mu M_\mu$, with the electric polarization $P^\mu \equiv -M^{\mu\nu} u_\nu$ and magnetization

¹³Apart from electric conductivity, other dissipative effects, such as shear and bulk viscosities, will not be considered in this paper.

¹⁴Here, $\epsilon^{0123} = -\epsilon_{0123} = 1$.

¹⁵In Appendix A 2, we present a number of results by making use of the assumption of translational invariance of the system in the transverse plane as well as the aforementioned properties of transverse MHD.

$M^\mu \equiv \frac{1}{2}\epsilon^{\mu\nu\alpha\beta}M_{\nu\alpha}u_\beta$. In this paper, $\partial_\mu\chi_e = 0$ and $\partial_\mu\chi_m = 0$ as well as $\chi_e \neq -1$ are assumed.

The electromagnetic field strength tensor satisfies the homogeneous Maxwell equation

$$\partial_\mu\tilde{F}^{\mu\nu} = 0, \quad (3.7)$$

with $\tilde{F}^{\mu\nu} \equiv \frac{1}{2}\epsilon^{\mu\nu\alpha\beta}F_{\alpha\beta}$, or equivalently,

$$\tilde{F}^{\mu\nu} = B^\mu u^\nu - B^\nu u^\mu + \epsilon^{\mu\nu\alpha\beta}E_\alpha u_\beta, \quad (3.8)$$

and the inhomogeneous Maxwell equation

$$\partial_\mu F^{\mu\nu} = J^\nu, \quad (3.9)$$

with the electromagnetic current

$$J^\mu = \rho_e u^\mu + \partial_\rho M^{\rho\mu} + \sigma E^\mu. \quad (3.10)$$

Here, ρ_e is the electric charge density, and $\partial_\rho M^{\rho\mu}$ is the magnetization current. Differentiating (3.9) with respect to x^ν leads to the third continuity equation $\partial_\nu J^\nu = 0$ in (3.1). Contracting further (3.9) with u_ν leads to $\rho_e = 0$ (see Appendix A 1 for a more rigorous proof of $\rho_e = 0$).

Let us consider at this stage the Euler equation arising from $\Delta_{\mu\nu}\partial_\rho T^{\rho\nu} = 0$, with $T^{\mu\nu}$ defined in (3.2). It reads

$$\mathfrak{D}u_\mu = \frac{\nabla_\mu p_{\text{tot}} - C_\mu}{(\epsilon + p + (1 - \chi_m)B^2 + (1 + \chi_e)E^2)}, \quad (3.11)$$

where

$$p_{\text{tot}} \equiv p - \chi_m B^2 + \frac{1}{2}(E^2 + B^2),$$

$$C_\mu \equiv \chi[\theta E^\lambda B_{\lambda\mu} + \Delta_{\mu\nu}D(E_\lambda B^{\lambda\nu}) + E_\lambda B^{\lambda\rho}\partial_\rho u_\mu], \quad (3.12)$$

with $B^{\mu\nu} \equiv \epsilon^{\mu\nu\alpha\beta}B_\alpha u_\beta$ and $\chi \equiv \frac{1}{2}[(1 + \chi_e) + (1 - \chi_m)]$.

Assuming $\mathfrak{D}u_\mu = 0$ and the boost invariance of p , E , and B , or equivalently $\nabla_\mu p_{\text{tot}} = 0$, (3.12) yields $C_\mu = 0$. To determine the time evolution of the electromagnetic and thermodynamic fields, we later derive a number of constituent equations, arising from the homogeneous and inhomogeneous Maxwell equations as well as $\Delta_{\mu\nu}\partial_\rho T^{\rho\nu} = \Delta_{\mu\nu}J_\rho F^{\rho\nu}$. We show that the combination of these equations with $C_\mu = 0$ leads among others to $\sin\delta = 0$, where $\delta \equiv \phi - \zeta$. It turns out that in the LRF of the fluid, the electric and magnetic fields \mathbf{E} and \mathbf{B} are either parallel or antiparallel to each other (see Secs. III B and III C).

More complicated solutions for the evolution of electromagnetic and thermodynamic fields in a uniformly expanding fluid with $\mathfrak{D}u_\mu = 0$ arise by turning off the assumption of the boost invariance of p , E , and B . In this case, $\mathfrak{D}u_\mu = 0$ is guaranteed once the numerator of (3.11)

vanishes. Using $\mathfrak{D} = \frac{1}{\tau}$, $\theta = \frac{1}{\tau}$, and $\nabla_\mu = -\frac{1}{\tau}(\sinh\eta, 0, 0, -\cosh\eta)\frac{\partial}{\partial\eta}$ as well as

$$u^\mu = (\cosh\eta, 0, 0, \sinh\eta), \quad (3.13)$$

and

$$\frac{\partial}{\partial t} = +\cosh\eta\frac{\partial}{\partial\tau} - \frac{1}{\tau}\sinh\eta\frac{\partial}{\partial\eta},$$

$$\frac{\partial}{\partial z} = -\sinh\eta\frac{\partial}{\partial\tau} + \frac{1}{\tau}\cosh\eta\frac{\partial}{\partial\eta}, \quad (3.14)$$

the resulting expression $\nabla_\mu p_{\text{tot}} = C_\mu$ translates into

$$\frac{1}{\tau}\frac{\partial p_{\text{tot}}}{\partial\eta} + \chi\left(\frac{\partial}{\partial\tau} + \frac{2}{\tau}\right)(EB\sin\delta) = 0. \quad (3.15)$$

In the present work, we exclusively assume the boost invariance of p , E , and B . Other more complicated solutions corresponding to (3.15) in combination with other constituent equations of electromagnetic and thermodynamic fields are presented elsewhere [41].

In what follows, we derive a number of useful relations, which help us to determine the space and time evolution of n , T , p , ϵ as well as E and B . To do this, let us first consider the homogeneous Maxwell equation (3.7). Plugging the definition of $\tilde{F}^{\mu\nu}$ from (3.8) into this equation, and using the fact that in a nonaccelerating expansion u^μ is given by (3.13), we arrive for $\nu = 1$ and $\nu = 2$ at

$$\partial_\mu(Bu^\mu)\cos\phi - B\sin\phi\frac{\partial\phi}{\partial\tau} - \frac{E}{\tau}\cos\zeta\frac{\partial\zeta}{\partial\eta} = 0,$$

$$\partial_\mu(Bu^\mu)\sin\phi + B\cos\phi\frac{\partial\phi}{\partial\tau} - \frac{E}{\tau}\sin\zeta\frac{\partial\zeta}{\partial\eta} = 0, \quad (3.16)$$

respectively. Here, the parametrization (3.6) for the electromagnetic fields and (3.14) are used. Combining the relations arising in (3.16), we arrive at

$$\partial_\mu(Bu^\mu) - \frac{E}{\tau}\cos\delta\frac{\partial\zeta}{\partial\eta} = 0,$$

$$B\frac{\partial\phi}{\partial\tau} + \frac{E}{\tau}\sin\delta\frac{\partial\zeta}{\partial\eta} = 0, \quad (3.17)$$

where $\delta = \phi - \zeta$ the relative angle between \mathbf{E} and \mathbf{B} . As concerns the inhomogeneous Maxwell equation, plugging $F^{\mu\nu}$ from (3.5) into the lhs of (3.9), we arrive for J^μ from (3.10) first at

$$(1 + \chi_e)\partial_\nu(E^\mu u^\nu) - (1 - \chi_m)\epsilon^{0\mu\nu 3}\frac{1}{\tau}\frac{\partial B_\nu}{\partial\eta} + \sigma E^\mu = 0. \quad (3.18)$$

Here, we have, in particular, used $\partial \cdot E = 0$, $\partial \cdot B = 0$ as well as $E \cdot \partial = 0$, and $B \cdot \partial = 0$, which are valid in 1 + 1-dimensional transverse MHD. For $\mu = 1$ and $\mu = 2$, (3.18) then yields

$$\begin{aligned} & (1 + \chi_e) \partial_\mu (Eu^\mu) \cos \zeta - (1 + \chi_e) E \sin \zeta \frac{\partial \zeta}{\partial \tau} \\ & + (1 - \chi_m) \frac{B}{\tau} \cos \phi \frac{\partial \phi}{\partial \eta} + \sigma E \cos \zeta = 0, \\ & (1 + \chi_e) \partial_\mu (Eu^\mu) \sin \zeta + (1 + \chi_e) E \cos \zeta \frac{\partial \zeta}{\partial \tau} \\ & + (1 - \chi_m) \frac{B}{\tau} \sin \phi \frac{\partial \phi}{\partial \eta} + \sigma E \sin \zeta = 0. \end{aligned} \quad (3.19)$$

Combining these two equations results in

$$\begin{aligned} & (1 + \chi_e) E \frac{\partial \zeta}{\partial \tau} + (1 - \chi_m) \frac{B}{\tau} \sin \delta \frac{\partial \phi}{\partial \eta} = 0, \\ & (1 + \chi_e) \partial_\mu (Eu^\mu) + (1 - \chi_m) \frac{B}{\tau} \cos \delta \frac{\partial \phi}{\partial \eta} + \sigma E = 0. \end{aligned} \quad (3.20)$$

Using, at this stage, the previously assumed boost invariance of p , E , and B in transverse MHD in combination with $\Delta_{\mu\nu} \partial_\rho T_{EM}^{\rho\nu} = \Delta_{\mu\nu} J_\rho F^{\rho\nu}$, we also obtain

$$[\chi_e \partial_\mu (Eu^\mu) + \sigma E] \sin \delta = \chi_e E \cos \delta \frac{\partial \zeta}{\partial \tau}. \quad (3.21)$$

Another useful relation, which is used later to determine the evolution of thermodynamic quantities T , p , and ϵ arises from $u_\nu \partial_\mu T_F^{\mu\nu} = -u_\nu J_\mu F^{\mu\nu}$, and reads

$$\begin{aligned} & \mathfrak{D} \left(\epsilon + \frac{1}{2} \chi_e E^2 \right) + \theta (\epsilon + p - \chi_m B^2) \\ & = \sigma E^2 - \chi_m \frac{EB}{\tau} \cos \delta \frac{\partial \phi}{\partial \eta}. \end{aligned} \quad (3.22)$$

Here,

$$\epsilon^{0\mu\nu 3} E_\mu \frac{\partial B_\nu}{\partial \eta} = EB \cos \delta \frac{\partial \phi}{\partial \eta} \quad (3.23)$$

is used. The full energy equation

$$\begin{aligned} & \mathfrak{D} \left[\epsilon + \left(\frac{1}{2} + \chi_e \right) E^2 + \frac{1}{2} B^2 \right] \\ & + \theta [\epsilon + p + (1 + \chi_e) E^2 + (1 - \chi_m) B^2] = 0 \end{aligned} \quad (3.24)$$

is derived from $u_\nu \partial_\mu T^{\mu\nu} = 0$. In the next section, we use the relations (3.17), (3.20), and (3.21) to derive a differential equation, whose solution yields the space and time dependence of the \mathbf{E} and \mathbf{B} vectors. In particular, the evolution of the magnitude of these fields, $E = |\mathbf{E}|$ and

$B = |\mathbf{B}|$, as well as their relative angles ζ and ϕ with respect to the x -axis in the LRF of the fluid, is determined as functions of independent coordinates τ and η . Moreover, the method of self-similar solutions for nonconserved charges, introduced in Sec. II, is used to determine the space-time evolution of thermodynamic quantities n , T , p , and ϵ .

B. Formal self-similar solutions for electromagnetic and thermodynamic quantities in nonideal transverse MHD

In nonideal transverse MHD, the dynamics of the electromagnetic fields B and E as well as the thermodynamic quantities n , T , p and ϵ are governed by the following homogeneous and inhomogeneous differential equations:

$$\partial_\mu (nu^\mu) = 0, \quad (3.25)$$

$$\partial_\mu (T^\kappa u^\mu) = T^\kappa \mathfrak{D} \mathcal{L}, \quad (3.26)$$

$$\partial_\mu (Bu^\mu) = B \mathfrak{D} \mathcal{M}, \quad (3.27)$$

$$\partial_\mu (Eu^\mu) = E \mathfrak{D} \mathcal{N}, \quad (3.28)$$

where functions \mathcal{L} , \mathcal{M} , and \mathcal{N} are to be determined. Here, the baryonic current $\partial_\mu (nu^\mu)$ is assumed to be conserved. This leads to (3.25). Whereas the last two equations (3.27) and (3.28) are only assumed to be valid at this stage, the second equation (3.26) arises by assuming the ideal gas equation $p = nT$, as in the previous Sec. II, and by plugging the EoS (2.7), with κ satisfying $\mathfrak{D} \kappa = 0$, into (3.22). Using (3.25), we thus obtain (3.26) with

$$\mathfrak{D} \mathcal{L} = \frac{1}{p} \left(\sigma E^2 - \chi_e E \frac{\partial E}{\partial \tau} + \chi_m B^2 \theta - \chi_m \frac{EB}{\tau} \cos \delta \frac{\partial \phi}{\partial \eta} \right). \quad (3.29)$$

As expected, in ideal MHD, with $\sigma E^2 \rightarrow 0$ and $\chi_e = \chi_m = 0$, we have $\mathfrak{D} \mathcal{L} = 0$. In this case, the self-similar solution of the resulting equation $\partial_\mu (T^\kappa u^\mu) = 0$ is given by (2.18).

Following the method presented in the previous section, the self-similar solution of n reads

$$n(\tau, \eta) = n_0 \left(\frac{\tau_0}{\tau} \right) \mathcal{U} \left(\frac{\tanh^2 \eta}{Z_0^2} \right) \quad (3.30)$$

[see (2.17)]. Here, \mathcal{U} is an arbitrary η -dependent scaling factor. Using further the method of nonconserved charges from Sec. II, the formal solution of (3.26) reads

$$T(\tau, \eta) = T_0 \left(\frac{\tau_0}{\tau} \right)^{1/\kappa} e^{\frac{\epsilon}{\kappa} \mathfrak{V}} \left(\frac{\tanh^2 \eta}{Z_0^2} \right) \quad (3.31)$$

[see (2.26)]. Here, $\mathbb{V} = \mathcal{U}^{-1}$ guarantees the boost invariance of p , whose formal solution can be derived from the ideal gas equation $p = nT$,

$$p = p_0 \left(\frac{\tau_0}{\tau} \right)^{1+\frac{1}{\kappa}} e^{\frac{\mathcal{L}}{\kappa}}. \quad (3.32)$$

Here, $p_0 = n_0 T_0$. Using further the EoS $\epsilon = \kappa p$, the formal solution of the energy density is given by

$$\epsilon = \epsilon_0 \left(\frac{\tau_0}{\tau} \right)^{1+\frac{1}{\kappa}} e^{\frac{\mathcal{L}}{\kappa}}, \quad (3.33)$$

with $\epsilon_0 = \kappa p_0$. To determine \mathcal{L} explicitly from (3.29) the space-time evolutions of B and E are first to be determined.

Using the boost invariance of E and B , which arises from the Euler equation (3.11) in a uniformly expanding fluid with $\mathfrak{D}u_\mu = 0$, the formal solutions of B and E are given by

$$B(\tau) = B_0 \left(\frac{\tau_0}{\tau} \right) e^{\mathcal{M}}, \quad (3.34)$$

$$E(\tau) = E_0 \left(\frac{\tau_0}{\tau} \right) e^{\mathcal{N}}. \quad (3.35)$$

Here, \mathcal{M} and \mathcal{N} are functions of τ , and \mathcal{M}_0 and \mathcal{N}_0 are chosen to be $\mathcal{M}_0 = \mathcal{M}(\tau_0) = 0$ and $\mathcal{N}_0 = \mathcal{N}(\tau_0) = 0$. Plugging finally (3.32), (3.34), and (3.35) into (3.29), we arrive at

$$\begin{aligned} e^{\frac{\mathcal{L}}{\kappa}} = & 1 + \frac{\sigma E_0^2}{\epsilon_0} \int_{\tau_0}^{\tau} d\tau' \left(\frac{\tau_0}{\tau'} \right)^{1-\frac{1}{\kappa}} e^{2\mathcal{N}} + \frac{\chi_e E_0^2}{\epsilon_0 \tau_0} \int_{\tau_0}^{\tau} d\tau' \left(\frac{\tau_0}{\tau'} \right)^{2-\frac{1}{\kappa}} e^{2\mathcal{N}} - \frac{\chi_e E_0^2}{\epsilon_0} \int_{\tau_0}^{\tau} d\tau' \left(\frac{\tau_0}{\tau'} \right)^{1-\frac{1}{\kappa}} e^{2\mathcal{N}} \frac{d\mathcal{N}}{d\tau'} \\ & + \frac{\chi_m B_0^2}{\epsilon_0 \tau_0} \int_{\tau_0}^{\tau} d\tau' \left(\frac{\tau_0}{\tau'} \right)^{2-\frac{1}{\kappa}} e^{2\mathcal{M}} - \frac{\chi_m E_0 B_0}{\epsilon_0 \tau_0} \int_{\tau_0}^{\tau} d\tau' \left(\frac{\tau_0}{\tau'} \right)^{2-\frac{1}{\kappa}} e^{\mathcal{M}+\mathcal{N}} \cos \delta \frac{\partial \phi}{\partial \eta}. \end{aligned} \quad (3.36)$$

Here, $\delta = \phi - \zeta$. To have the full τ dependence of T , p , ϵ as well as B and E , the τ dependence of \mathcal{M} and \mathcal{N} as well as the η dependence of ϕ and δ are to be determined. This is done in the following section.

C. Master equation for \mathcal{M} in nonideal transverse MHD

Let us start by considering (3.17), (3.20), and (3.21). These are a set of five constituent equations, whose solutions lead to (τ, η) dependence of \mathcal{M} , \mathcal{N} as well as ϕ and ζ . To arrive at these solutions, the following assumptions in the nonideal transverse MHD setup are essential:

- (1) The system is translational invariant in the transverse plane, i.e., in our setup no quantity depends on x and y .¹⁶
- (2) The system evolves uniformly at all times, i.e., $\mathfrak{D}u_\mu = 0$, $\forall t$.
- (3) The pressure p and the magnitude of electric and magnetic fields $E = |\mathbf{E}|$ and $B = |\mathbf{B}|$ are boost invariant, i.e., in general we have $\frac{\partial p_{\text{tot}}}{\partial \eta} = 0$, where p_{tot} is defined in (3.12). According to our arguments above this assumption together with $\mathfrak{D}u_\mu = 0$ leads automatically to $\mathcal{C}_\mu = 0$.

The outline of our method is as follows.

- (i) We first show that a combination of these equations leads automatically to $\sin \delta = 0$. Mathematically, $\sin \delta = 0$ leads to $\delta = \phi - \zeta = n\pi$ with $n = 0, 1, 2, \dots$. Physically, this would mean that in a uniformly

expanding fluid, where a transverse MHD setup is applicable, the electric and magnetic vectors, \mathbf{E} and \mathbf{B} , are either parallel or antiparallel with respect to each other in the LRF of the fluid. Moreover, since the relative angle, δ , of these fields remains constant in τ and η , if at τ_0 they are parallel/antiparallel, they remain so at any later time $\tau > \tau_0$ and for any $\eta = -\infty, \dots, \infty$. Let us notice that the fact that electric and magnetic fields are either parallel or antiparallel leads to vanishing local Poynting vector $\mathbf{S} = \mathbf{E} \times \mathbf{B}$, and consequently to vanishing electromagnetic energy flow between fluid parcels. This result is fully consistent with $\mathcal{C}_\mu = 0$, where \mathcal{C}_μ is defined in (3.12).

- (ii) By solving these equations, we, in particular, show that ϕ and η evolves as

$$\phi(\eta) = \omega_0 \eta + \phi_0, \quad \zeta(\eta) = \omega_0 \eta + \zeta_0, \quad (3.37)$$

with $\phi(\eta) - \zeta(\eta) = \phi_0 - \zeta_0 = \delta = n\pi$. Here, $\omega_0 = \frac{\partial \phi}{\partial \eta} = \frac{\partial \zeta}{\partial \eta} = \text{const}$. A nonvanishing ω_0 implies a rotation of \mathbf{B} and \mathbf{E} vectors around an axis parallel to the z -axis. It can also be regarded as the source for nonboost invariance (η dependence) of rotating solutions in nonideal transverse MHD.

- (iii) Finally, by combining these equations, we show that \mathcal{M} either satisfies

$$\frac{d\mathcal{M}}{du} = 0, \quad (3.38)$$

¹⁶See Appendix A 2 for more discussions concerning the symmetry properties in transverse MHD.

where $u \equiv \ln(\frac{\tau}{\tau_0})$, or the following second-order nonlinear differential equation:

$$\frac{d^2\mathcal{M}}{du^2} + \frac{d\mathcal{M}}{du} \left(\frac{d\mathcal{M}}{du} + \frac{\sigma\tau_0 e^u}{1+\chi_e} \right) + \omega_0^2 \frac{(1-\chi_m)}{1+\chi_e} = 0. \quad (3.39)$$

Here, $\omega_0 = \frac{\partial\phi}{\partial\eta} = \frac{\partial\zeta}{\partial\eta}$, being part of the initial condition, remains constant for all τ and η . We show that (3.38) corresponds to $\omega_0 = 0$, which leads, using (3.37), to constant ϕ and ζ . Physically, this corresponds to nonrotating vectors \mathbf{E} and \mathbf{B} . Moreover, for \mathcal{M} satisfying (3.38), we have $\mathcal{M} = 0$. Using (3.27), this leads to frozen-flux relation $\partial_\mu(Bu^\mu) = 0$, even in the nonideal MHD with nonvanishing magnetization and electric polarization. In addition, any solution of (3.39) leads to a deviation from frozen-flux theorem in such a medium. Since for the derivation of (3.39), ω_0 is assumed to be nonzero, these solutions correspond to rotating \mathbf{E} and \mathbf{B} fields.

Let us finally notice that whenever $\mathcal{M}(\tau)$ and $\phi(\tau, \eta)$ are computed, it is then easy to determine $\mathcal{N}(\tau)$ from the second equation in (3.20) in combination with the ansatz (3.28). The τ dependence of T arises then from (3.36) in combination with the formal self-similar solution (3.31) of T . Important self-consistency checks concerning the evolution of E_0, E_z as well as B_0, B_z with τ and η are presented in Appendix A 2. We, in particular, show that apart from $E_i = B_i = 0$, $\frac{\partial E_i}{\partial\tau} = \frac{\partial E_i}{\partial\eta} = 0$, and $\frac{\partial B_i}{\partial\tau} = \frac{\partial B_i}{\partial\eta} = 0$, $i = 0, z$ are always valid. This guarantees the persistence of the aforementioned conditions of transverse MHD during the uniform expansion of the fluid.

Proofs:

- (i) In order to show that $\sin \delta = 0$, let us consider the first equation in (3.20). Plugging

$$\chi_e E \frac{\partial\zeta}{\partial\tau} = -E \frac{\partial\zeta}{\partial\tau} - (1-\chi_m) \frac{B}{\tau} \sin \delta \frac{\partial\phi}{\partial\eta},$$

from this equation into the rhs of (3.21), we arrive, in particular, at

$$\begin{aligned} & [\chi_e \partial_\mu(Eu^\mu) + \sigma E] \sin \delta \\ &= -E \cos \delta \frac{\partial\zeta}{\partial\tau} - (1-\chi_m) \sin \delta \cos \delta \frac{B}{\tau} \frac{\partial\phi}{\partial\eta}. \end{aligned} \quad (3.40)$$

From the second equation in (3.20), we then have

$$\chi_e \partial_\mu(Eu^\mu) + \sigma E = -\partial_\mu(Eu^\mu) - (1-\chi_m) \cos \delta \frac{B}{\tau} \frac{\partial\phi}{\partial\eta}. \quad (3.41)$$

Plugging (3.40) into the lhs of (3.41) results in

$$E \cos \delta \frac{\partial\zeta}{\partial\tau} = \partial_\mu(Eu^\mu) \sin \delta, \quad (3.42)$$

which together with (3.21) leads to

$$\sigma E \sin \delta = 0. \quad (3.43)$$

In nonideal transverse MHD, where $\sigma E \neq 0$, (3.43) leads to $\sin \delta = 0$, and consequently to $\delta = n\pi$ with $n = 0, 1, 2, \dots$, and $\ell \equiv \cos \delta = \pm 1$. Here, the plus and minus signs correspond to parallel and antiparallel orientation of \mathbf{E} and \mathbf{B} fields with respect to each other.

- (ii) Let us now reconsider the relations from (3.17), (3.20), and (3.21) with $\sin \delta = 0$ and $\cos \delta = \pm 1$. In this case, (3.21) leads to

$$\frac{\partial\zeta(\tau, \eta)}{\partial\tau} = 0, \quad \forall \tau, \eta. \quad (3.44)$$

This is also compatible with the first equation of (3.20). From the second equation of (3.17), we also obtain

$$\frac{\partial\phi(\tau, \eta)}{\partial\tau} = 0, \quad \forall \tau, \eta. \quad (3.45)$$

Introducing at this stage $u = \ln(\frac{\tau}{\tau_0})$, the first equation in (3.17) leads to

$$\frac{\partial\zeta(\tau, \eta)}{\partial\eta} = \ell \frac{B(\tau)}{E(\tau)} \frac{d\mathcal{M}(u)}{du}. \quad (3.46)$$

Here, (3.27) is used. Let us note that since $\delta = \phi - \zeta = \text{const.}$, we also have

$$\frac{\partial\zeta(\tau, \eta)}{\partial\eta} = \frac{\partial\phi(\tau, \eta)}{\partial\eta}. \quad (3.47)$$

Bearing in mind that the electromagnetic fields, E and B , are boost invariant (η independent), and that \mathcal{M} depends only on τ , the rhs of (3.46) turns out to be independent of η . We thus have

$$\frac{\partial^2\zeta(\tau, \eta)}{\partial\eta^2} = 0, \quad \forall \tau, \eta, \quad (3.48)$$

and upon using (3.47),

$$\frac{\partial^2\phi(\tau, \eta)}{\partial\eta^2} = 0, \quad \forall \tau, \eta. \quad (3.49)$$

The last two relations together with (3.47) lead first to

$$\begin{aligned}\phi(\tau, \eta) &= \omega(\tau)\eta + \phi_0(\tau), \\ \zeta(\tau, \eta) &= \omega(\tau)\eta + \zeta_0(\tau).\end{aligned}\quad (3.50)$$

Using then

$$\frac{\partial}{\partial \tau} \left(\frac{\partial \phi}{\partial \eta} \right) = \frac{\partial}{\partial \tau} \left(\frac{\partial \zeta}{\partial \eta} \right) = 0, \quad (3.51)$$

arising from (3.44) and (3.45), we obtain

$$\frac{\partial \zeta}{\partial \eta} = \frac{\partial \phi}{\partial \eta} \equiv \omega_0 = \text{const.}, \quad (3.52)$$

as well as

$$\begin{aligned}\phi_0(\tau) &\equiv \phi_0 = \text{const.}, \\ \zeta_0(\tau) &\equiv \zeta_0 = \text{const.}\end{aligned}\quad (3.53)$$

Plugging the above results into (3.50), we arrive at (3.37), as claimed.

- (iii) To derive the differential equation (3.39) for \mathcal{M} , we use (3.37) together with (3.46), and arrive at

$$\frac{d\mathcal{M}}{du} = \ell \omega_0 \frac{E}{B}, \quad (3.54)$$

which, upon using (3.27) and (3.28), yields

$$\frac{d\mathcal{M}}{du} = \ell \omega_0 \beta_0 e^{\mathcal{N} - \mathcal{M}}, \quad (3.55)$$

with $\beta_0 \equiv \frac{E_0}{B_0}$. For $\omega_0 = 0$, (3.55) leads to (3.38). For $\omega_0 \neq 0$, we use the second equation of (3.20), together with (3.28) and (3.55), and arrive, for $\chi_e \neq -1$ and $\frac{d\mathcal{M}}{du} \neq 0$, at the differential equation (3.39).

As aforementioned, the solutions of (3.38) and (3.39) correspond to nonrotating and rotating electromagnetic fields, respectively. In the next section, we present exact and approximate solutions to these equations.

IV. ANALYTICAL SOLUTIONS OF (3.38) AND (3.39)

A. Nonrotating electric and magnetic fields

As we have argued in the previous section, in nonideal transverse MHD with nonvanishing electric field, the case $\frac{d\mathcal{M}}{du} = 0$ corresponds to $\omega_0 = 0$. This implies constant angles of \mathbf{B} and \mathbf{E} fields with respect to a certain x -axis in the transverse plane, i.e.,

$$\phi(\tau, \eta) = \phi_0 = \text{const.} \quad \text{and} \quad \zeta(\tau, \eta) = \zeta_0 = \text{const.} \quad (4.1)$$

[see (3.37)]. To determine the magnitude of the electric and magnetic fields, let us consider $\frac{d\mathcal{M}}{du} = 0$, or equivalently, $\mathfrak{D}\mathcal{M} = 0$. Using (3.27) and $\mathcal{M}_0 = 0$, we have

$$\mathcal{M} = 0. \quad (4.2)$$

Plugging this relation into (3.27), it turns out that B satisfies (2.21), as in the ideal case. In other words, the fluxes are, as in the case of ideal MHD, frozen. Bearing in mind that $B = |\mathbf{B}|$ is η independent, the most general self-similar solution of B reads

$$B(\tau) = B_0 \left(\frac{\tau_0}{\tau} \right) \quad (4.3)$$

[see (3.34)]. Using, at this stage, the second relation in (3.20) with $\frac{\partial \phi}{\partial \eta} = 0$, we arrive at

$$\partial_\mu (E u^\mu) = -E \frac{\sigma}{1 + \chi_e}, \quad (4.4)$$

which, upon comparing with (3.28), leads to

$$\mathcal{N} = -\frac{\sigma(\tau - \tau_0)}{1 + \chi_e}. \quad (4.5)$$

Hence, according to (3.35), $E(\tau)$ evolves as

$$E(\tau) = E_0 \left(\frac{\tau_0}{\tau} \right) e^{-\frac{\sigma(\tau - \tau_0)}{1 + \chi_e}}. \quad (4.6)$$

The ideal transverse MHD limit $E \rightarrow 0$ is thus recovered for $\frac{\sigma}{1 + \chi_e} \ll \frac{1}{\tau - \tau_0}$. Let us notice that in the ideal MHD, where E is assumed to vanish, $\frac{d\mathcal{M}}{du} = 0$ leads also to (4.3). Combining now (4.3) and (4.6), we also arrive at

$$\frac{E}{B} = \beta_0 e^{-\frac{\sigma(\tau - \tau_0)}{1 + \chi_e}}, \quad (4.7)$$

with $\beta_0 = \frac{E_0}{B_0}$.

In Fig. 1, the spatial components of nonrotating $B^\mu = (0, \mathbf{B})$ and $E^\mu = (0, \mathbf{E})$ fields with

$$\begin{aligned}\frac{\mathbf{B}}{B_0} &= \left(\frac{\tau_0}{\tau} \right) (\cos \phi_0, \sin \phi_0, 0), \\ \frac{\mathbf{E}}{E_0} &= \left(\frac{\tau_0}{\tau} \right) e^{-\frac{\sigma(\tau - \tau_0)}{1 + \chi_e}} (\cos \zeta_0, \sin \zeta_0, 0),\end{aligned}\quad (4.8)$$

are plotted in an η vs τ/τ_0 plane. Here, $\phi_0 = \frac{\pi}{6}$ and $\zeta_0 = \frac{7\pi}{6}$. Moreover, $\tau_0 = 0.5$ fm/c, $\sigma = 4$ MeVc, and $\chi_e = 0$ are assumed. In this case, $\delta = \phi_0 - \zeta_0 = \pi$. This corresponds to antiparallel \mathbf{B} (blue arrows) and \mathbf{E} (red arrows) vectors. As it is shown, whereas $B = |\mathbf{B}|$ and $E = |\mathbf{E}|$ decrease with increasing τ , the orientations of magnetic and electric fields remain constant in the η direction.

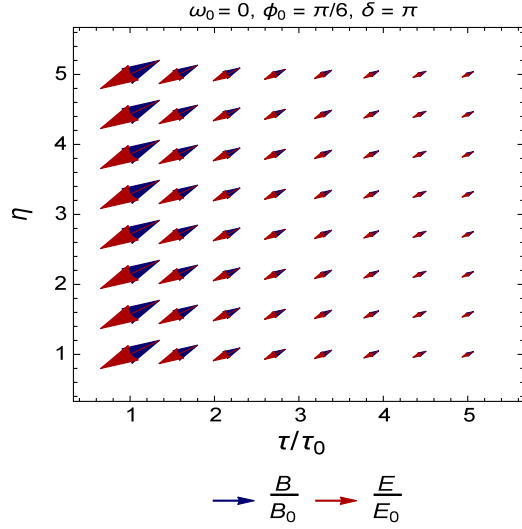


FIG. 1. Nonrotating $\frac{\mathbf{B}}{B_0}$ and $\frac{\mathbf{E}}{E_0}$ from (4.8) are plotted in an η vs τ/τ_0 plane. Blue (red) arrows correspond to the magnetic (electric) vector field. Here, $\phi_0 = \pi/6$ and $\delta = \pi$, i.e., \mathbf{B} and \mathbf{E} are antiparallel. For \mathbf{E} , $\sigma = 4$ MeVc and $\tau_0 = 0.5$ fm/c. Whereas the magnetic flux is frozen, $\partial_\mu(Bu^\mu) = 0$, the electric field satisfies (4.4).

Plugging, at this stage, \mathcal{M} and \mathcal{N} from (4.2) and (4.5) into (3.36), and performing the integration over τ' by making use of

$$\begin{aligned} & \int_{\tau_0}^{\tau} d\tau' \left(\frac{\tau_0}{\tau'}\right)^{n-\frac{1}{\kappa}} e^{-\frac{m\sigma(\tau'-\tau_0)}{1+\chi_e}} \\ &= \tau_0 \left(\frac{m\sigma\tau_0}{1+\chi_e}\right)^{n-\frac{1}{\kappa}-1} e^{\frac{m\sigma\tau_0}{1+\chi_e}} \left\{ \Gamma\left(\frac{1}{\kappa} - n + 1, \frac{m\sigma\tau_0}{1+\chi_e}\right) \right. \\ & \quad \left. - \Gamma\left(\frac{1}{\kappa} - n + 1, \frac{m\sigma\tau}{1+\chi_e}\right) \right\}, \end{aligned}$$

which arises from

$$\int_{\tau_1}^{\tau_2} dt t^{a-1} e^{-t} = \Gamma(a, \tau_1) - \Gamma(a, \tau_2), \quad (4.9)$$

we obtain

$$\begin{aligned} e^{\frac{\ell}{\kappa}} &= 1 + \frac{(1+2\chi_e)E_0^2}{2\epsilon_0} \left(\frac{2\sigma\tau_0}{1+\chi_e}\right)^{1-c_s^2} e^{\frac{2\sigma\tau_0}{1+\chi_e}} \\ & \times \left\{ \Gamma\left(c_s^2, \frac{2\sigma\tau_0}{1+\chi_e}\right) - \Gamma\left(c_s^2, \frac{2\sigma\tau}{1+\chi_e}\right) \right\} \\ & + \frac{\chi_e E_0^2}{\epsilon_0} \left(\frac{2\sigma\tau_0}{1+\chi_e}\right)^{1-c_s^2} e^{\frac{2\sigma\tau_0}{1+\chi_e}} \\ & \times \left\{ \Gamma\left(c_s^2 - 1, \frac{2\sigma\tau_0}{1+\chi_e}\right) - \Gamma\left(c_s^2 - 1, \frac{2\sigma\tau}{1+\chi_e}\right) \right\} \\ & - \frac{\chi_m B_0^2}{\epsilon_0(1-c_s^2)} \left(\left(\frac{\tau_0}{\tau}\right)^{1-c_s^2} - 1 \right). \end{aligned} \quad (4.10)$$

Here, $c_s^2 \equiv \kappa^{-1}$ is the sound velocity and $\epsilon_0 = \kappa p_0$. In Sec. V, we use (4.10) to demonstrate the evolution of thermodynamic fields T , p , and ϵ , whose self-similar solutions are presented in (3.31)–(3.33). In particular, we compare the evolution of these fields for nonrotating and rotating electromagnetic fields, characterized by $\omega_0 = 0$ and $\omega_0 \neq 0$, respectively. The latter case is discussed as a next step.

B. Rotating electric and magnetic fields: Approximate analytical solutions

In this section, we present approximate analytical solutions to (3.39). We consider two different cases,

$$\text{Case 1: } \frac{E}{B} \sim \frac{E_0}{B_0} \left(\frac{\tau_0}{\tau}\right)^n \quad \text{for } n \neq 0 \quad \text{and } n = 0,$$

$$\text{Case 2: Small } \omega_0 \quad \text{with } \mathcal{M}(\tau) \sim \omega_0 f(\tau).$$

In both cases, \mathbf{B} and \mathbf{E} are either parallel ($\ell = +1$) or antiparallel ($\ell = -1$), and rotate gradually with increasing η . The angular velocity is given by $\omega_0 = \text{const}$. The τ dependence of the magnitudes of the electromagnetic fields turns out to be given by any nonvanishing solution of (3.39), which, in particular, represents a deviation from frozen-flux theorem. Apart from the evolution of \mathbf{B} and \mathbf{E} , we are interested in the evolution of T , p , and ϵ . To this purpose, we insert the corresponding \mathcal{M} and \mathcal{N} from these two cases into (3.36), and arrive at $\exp(\frac{\ell}{\kappa})$, which, upon insertion into (3.31)–(3.33) leads to the evolution of T , p , and ϵ , respectively.

1. Case 1: $\frac{E}{B} \sim \frac{E_0}{B_0} \left(\frac{\tau_0}{\tau}\right)^n$ for $n \neq 0$ and $n = 0$

Plugging $\frac{E}{B} = \frac{E_0}{B_0} \left(\frac{\tau_0}{\tau}\right)^n$ into the rhs of (3.54), we arrive first at

$$\mathcal{M}(u) = -\frac{\ell\omega_0\beta_0}{n} (e^{-nu} - 1), \quad (4.11)$$

with $u = \ln(\frac{\tau}{\tau_0})$. Then, using the formal solution of $B(\tau)$ from (3.34), arising from the method of nonconserved charges introduced in Sec. II, the most general self-similar solution for $B = |\mathbf{B}|$ reads

$$B(\tau) = B_0 \left(\frac{\tau_0}{\tau}\right) e^{-\mathfrak{b}_n(\tau, \omega_0)}, \quad (4.12)$$

with

$$\mathfrak{b}_n(\tau, \omega_0) \equiv \frac{\ell\omega_0\beta_0}{n} \left(\left(\frac{\tau_0}{\tau}\right)^n - 1 \right). \quad (4.13)$$

To determine \mathcal{N} , we insert (4.13) into the rhs of (3.55). We obtain

$$\begin{aligned}\mathcal{N}(u) &= \mathcal{M}(u) - nu \\ &= -\frac{\ell\omega_0\beta_0}{n}(e^{-nu} - 1) - nu,\end{aligned}\quad (4.14)$$

which leads, upon using (3.35), to

$$E = E_0 \left(\frac{\tau_0}{\tau} \right)^{1+n} e^{-\mathfrak{b}_n(\tau, \omega_0)}, \quad (4.15)$$

with $\mathfrak{b}_n(\tau, \omega_0)$ from (4.13). As concerns the evolution of ϕ and ζ , the relative angles of \mathbf{B} and \mathbf{E} with respect to the x -axis in the LRF of the fluid, they are, as before, given by (3.37), where the constant angular velocity of these fields ω_0 can be fixed from the master equation (3.39) evaluated at $u = 0$ (or equivalently $\tau = \tau_0$). To this purpose, we use (3.54), which for \mathcal{M} from (4.11) yields

$$\begin{aligned}\frac{d\mathcal{M}}{du}\Big|_{u=0} &= \ell\omega_0\beta_0, \\ \frac{d^2\mathcal{M}}{du^2}\Big|_{u=0} &= -n\ell\omega_0\beta_0.\end{aligned}\quad (4.16)$$

Plugging these expressions into (3.39), and setting $u = 0$, we obtain

$$\tilde{\omega}_0 = \frac{\ell\beta_0[n(1 + \chi_e) - \sigma\tau_0]}{1 - \chi_m + \beta_0^2(1 + \chi_e)}. \quad (4.17)$$

We are, in particular, interested in the evolution of \mathbf{B} and \mathbf{E} in the limit $n \rightarrow 0$. Using (4.12) and (4.15), and taking the limit $n \rightarrow 0$, we arrive at the power-law solutions

$$B = B_0 \left(\frac{\tau_0}{\tau} \right)^a, \quad E = E_0 \left(\frac{\tau_0}{\tau} \right)^a, \quad (4.18)$$

with $a \equiv 1 - \ell\omega_0\beta_0$ and

$$\omega_0 = -\frac{\ell\beta_0\sigma\tau_0}{1 - \chi_m + \beta_0^2(1 + \chi_e)}, \quad (4.19)$$

which arises from (4.17) by taking the limit $n \rightarrow 0$. Let us notice, at this stage, that the power-law solution (4.18) for the B field is similar to the power-law decay ansatz that was previously introduced in [33]. In contrast to our method, the authors took the ansatz $B(\tau) \sim \tau^{-a}$, with a being an arbitrary constant free parameter, as the starting point of their analysis, without bringing the power a into relation with ω_0 and β_0 . Let us note that according to (4.19), two cases of $a > 1$ and $a < 1$, discussed in [33,34], are controlled by

$$\begin{aligned}\chi_m &< 1 + \beta_0^2(1 + \chi_e), \\ \chi_m &> 1 + \beta_0^2(1 + \chi_e),\end{aligned}$$

leading to $\ell\omega_0 < 0$ and $\ell\omega_0 > 0$, respectively.

In Fig. 2, we have demonstrated the spatial components of rotating magnetic and electric fields $B^\mu = (0, \mathbf{B})$ and $E^\mu = (0, \mathbf{E})$ with

$$\begin{aligned}\frac{\mathbf{B}}{B_0} &= \left(\frac{\tau_0}{\tau} \right) e^{-\mathfrak{b}_n(\tau, \tilde{\omega}_0)} (\cos \phi(\eta), \sin \phi(\eta), 0), \\ \frac{\mathbf{E}}{E_0} &= \left(\frac{\tau_0}{\tau} \right)^{1+n} e^{-\mathfrak{b}_n(\tau, \tilde{\omega}_0)} (\cos \zeta(\eta), \sin \zeta(\eta), 0).\end{aligned}\quad (4.20)$$

Here, $\mathfrak{b}_n(\tau, \tilde{\omega}_0)$ is defined in (4.13) and $\tilde{\omega}_0$ in (4.17). The angles $\phi(\eta)$ and $\zeta(\eta)$ are given in (3.37) with ω_0 replaced by $\tilde{\omega}_0$. In Figs. 2(a) and 2(b), the vectors corresponding to \mathbf{B}/B_0 [blue arrows in Fig. 2(a)] and $\frac{\mathbf{E}}{E_0}$ [red arrows in Fig. 2(b)] are plotted for the set of free parameters $\{n, \sigma, \beta_0, \phi_0, \chi_e, \chi_m, \ell\} = \{4, 400, 1, \frac{\pi}{3}, 0, 0, +1\}$ in an η

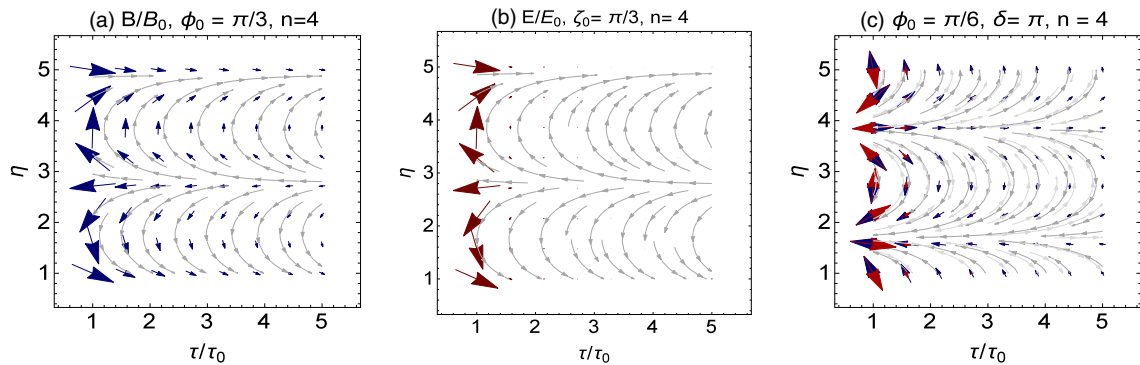


FIG. 2. \mathbf{B}/B_0 (a) and \mathbf{E}/E_0 (b) from (4.20) are plotted for the set of free parameters $\{n, \sigma, \beta_0, \phi_0, \chi_e, \chi_m, \ell\} = \{4, 400, 1, \frac{\pi}{3}, 0, 0, +1\}$ in an η vs τ/τ_0 plane. The magnetic and electric vectors, indicated by blue (a) and red (b) vectors, are parallel. This implies a clockwise rotation of \mathbf{B} and \mathbf{E} vectors while η increases. This is demonstrated with gray stream lines. The angular velocity $\tilde{\omega}_0$ is given in (4.17). (c) \mathbf{B}/B_0 (blue arrows) and \mathbf{E}/E_0 (red arrows) from (4.20) are plotted for the set of free parameters $\{n, \sigma, \beta_0, \phi_0, \chi_e, \chi_m, \ell\} = \{4, 400, 1, \frac{\pi}{6}, 0, 0, -1\}$ in an η vs τ/τ_0 plane. In this case, \mathbf{B} and \mathbf{E} are antiparallel, and rotate counterclockwise while η increases. The electric field decreases much faster than the magnetic field with increasing τ/τ_0 .

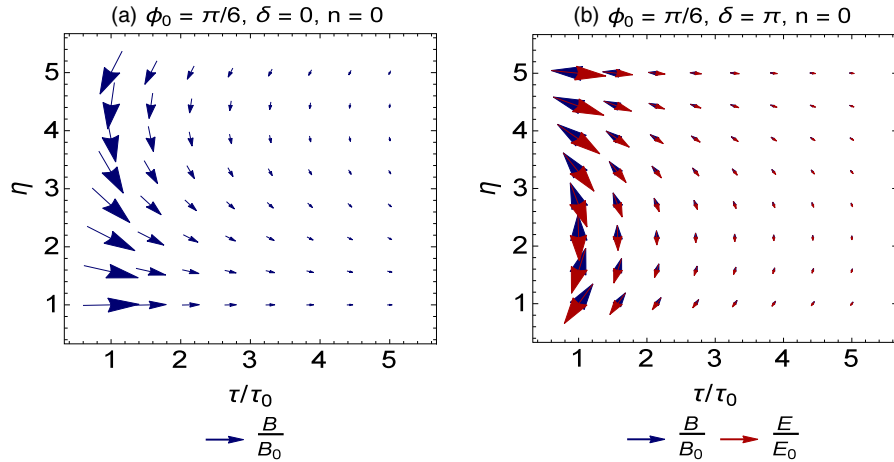


FIG. 3. (a) \mathbf{B}/B_0 from (4.21) is plotted for the set of free parameters $\{\sigma, \beta_0, \phi_0, \chi_e, \chi_m, \ell\} = \{400, 1, \frac{\pi}{6}, 0, 0, +1\}$ in an η vs τ/τ_0 plane. The electric field vectors are parallel to the magnetic field vectors (denoted by blue arrows), and are not demonstrated in this plot. A clockwise rotation is set up with increasing η . The angular velocity is given by (4.19). (b) \mathbf{B}/B_0 (blue arrows) and \mathbf{E}/E_0 (red arrows) from (4.21) are plotted for the set of free parameters $\{\sigma, \beta_0, \phi_0, \chi_e, \chi_m, \ell\} = \{400, 1, \frac{\pi}{6}, 0, 0, -1\}$ in an η vs τ/τ_0 plane. The rotation turns out to be counterclockwise while η increases.

vs τ/τ_0 plane. The gray stream lines are plotted to demonstrate the rotation of \mathbf{B} and \mathbf{E} vectors, which are, in this case, parallel to each other ($\ell = +1$).¹⁷ Here, the rotation turns out to be clockwise while η increases. The magnitudes of the fields B and E decrease with increasing τ . Because of an additional power n of $\frac{\tau_0}{\tau}$, E decays much faster than B with increasing τ [see (4.20)].

In Fig. 2(c), \mathbf{B} (blue arrows) and \mathbf{E} (red arrows) are antiparallel ($\ell = -1$).¹⁸ In this case, a counterclockwise rotation occurs with increasing η . Here, the set of free parameters is chosen to be $\{n, \sigma, \beta_0, \phi_0, \chi_e, \chi_m, \ell\} = \{4, 400, 1, \frac{\pi}{6}, 0, 0, -1\}$. As in the previous case, with increasing τ , E decreases much faster than B .

In Fig. 3, we have plotted the spatial components of rotating magnetic and electric fields $B^\mu = (0, \mathbf{B})$ and $E^\mu = (0, \mathbf{E})$,

$$\begin{aligned} \frac{\mathbf{B}}{B_0} &= \left(\frac{\tau_0}{\tau}\right)^a (\cos \phi(\eta), \sin \phi(\eta), 0), \\ \frac{\mathbf{E}}{E_0} &= \left(\frac{\tau_0}{\tau}\right)^a (\cos \zeta(\eta), \sin \zeta(\eta), 0), \end{aligned} \quad (4.21)$$

with $a = 1 - \ell \omega_0 \beta_0$ and $\phi(\eta)$ as well as $\zeta(\eta)$ from (3.37). Here, ω_0 from (4.19) are to be inserted into a , $\phi(\eta)$, and $\zeta(\eta)$. Let us recall that for $n = 0$, $\frac{E}{B} = \frac{E_0}{B_0} = \text{const}$. Hence B and E decrease with the same slope as τ increases. In Fig. 3(a), where the set of free parameters is chosen to be $\{\sigma, \beta_0, \phi_0, \chi_e, \chi_m, \ell\} = \{400, 1, \frac{\pi}{6}, 0, 0, +1\}$, \mathbf{B} and \mathbf{E} are parallel, and a clockwise rotation occurs with increasing η .

¹⁷ $\ell = +1$ corresponds to $\delta = \phi_0 - \zeta_0 = 2n\pi$ with $n = 0, 1, 2, \dots$
¹⁸ $\ell = -1$ corresponds to $\delta = \phi_0 - \zeta_0 = (2n + 1)\pi$ with $n = 0, 1, 2, \dots$

In Fig. 3(b), \mathbf{B} (blue arrows) and \mathbf{E} (red arrows) are antiparallel. As expected, a counterclockwise rotation occurs with increasing η , and B as well as E decrease with increasing τ with the same slope. Here, we have worked with $\{\sigma, \beta_0, \phi_0, \chi_e, \chi_m, \ell\} = \{400, 1, \frac{\pi}{6}, 0, 0, -1\}$.

As concerns $e^{\frac{\zeta}{s}}$ from (3.36), in the limit $n \rightarrow 0$, it is given by

$$\begin{aligned} e^{\frac{\zeta}{s}} &= 1 + \frac{\sigma \tau_0 E_0^2}{(c_s^2 - 2(a-1))\epsilon_0} \left(\left(\frac{\tau_0}{\tau}\right)^{-c_s^2 + 2(a-1)} - 1 \right) \\ &+ \frac{a(\chi_e E_0^2 + \chi_m B_0^2)}{(c_s^2 + 1 - 2a)\epsilon_0} \left(\left(\frac{\tau_0}{\tau}\right)^{-c_s^2 - 1 + 2a} - 1 \right), \end{aligned} \quad (4.22)$$

where $a = 1 - \ell \omega_0 \beta_0$ with ω_0 given in (4.19). Plugging this expression into (3.31)–(3.33), we arrive at the evolution of thermodynamic fields T , p , and ϵ in the case, where \mathbf{B} and \mathbf{E} evolve as presented in (4.21).

2. Case 2: Slowly rotating E and B fields

In this case, the angular velocity ω_0 is assumed to be small ($\omega_0 \ll 1$). Consequently, \mathcal{M} may be approximated by

$$\mathcal{M}(u) \sim \omega_0 f(u), \quad (4.23)$$

with $f(u)$ satisfying the differential equation

$$f''(u) + A e^u f'(u) = 0. \quad (4.24)$$

Here, $A \equiv \frac{\sigma \tau_0}{1 + \chi_e}$. This differential equation arises by inserting the ansatz (4.23) into the master equation (3.39), and neglecting terms proportional to ω_0^2 . To solve (4.24), we use the first relation in (4.16), and arrive for $f'(u)$ at

$$f'(u) = \ell \beta_0 e^{-A(e^u - 1)}. \quad (4.25)$$

The final result for $\mathcal{M}(\tau)$ then reads

$$\begin{aligned} \mathcal{M}(\tau) \sim \omega_0 f(\tau) &= \ell \omega_0 \beta_0 e^{\frac{\sigma \tau_0}{1+\chi_e}} \\ &\times \left\{ \Gamma\left(0, \frac{\sigma \tau_0}{1+\chi_e}\right) - \Gamma\left(0, \frac{\sigma \tau}{1+\chi_e}\right) \right\}. \end{aligned} \quad (4.26)$$

To perform the integration over τ , (4.9) is used. Using (3.55) together with (4.25), \mathcal{N} is given by

$$\mathcal{N}(\tau) = \mathcal{M}(\tau) - \frac{\sigma(\tau - \tau_0)}{1 + \chi_e}, \quad (4.27)$$

with \mathcal{M} from (4.26). The proper time evolution of the magnetic and electric fields thus reads

$$B = B_0 \left(\frac{\tau_0}{\tau}\right) e^{\mathcal{M}(\tau)}, \quad E = E_0 \left(\frac{\tau_0}{\tau}\right) e^{\mathcal{N}(\tau)}, \quad (4.28)$$

with \mathcal{M} and \mathcal{N} from (4.26) and (4.27), respectively. The ratio E/B is then given by

$$\frac{E}{B} = \beta_0 e^{-\frac{\sigma(\tau - \tau_0)}{1 + \chi_e}}, \quad (4.29)$$

with $\beta_0 = E_0/B_0$. The above results can be studied in two different limits $\sigma(\tau - \tau_0) \ll (1 + \chi_e)$ and $\sigma(\tau - \tau_0) \gg (1 + \chi_e)$, by using

$$\Gamma(0, z) \stackrel{z \rightarrow 0}{\approx} -\gamma_E - \ln z + z, \quad \Gamma(0, z) \stackrel{z \rightarrow \infty}{\approx} \frac{e^{-z}}{z}. \quad (4.30)$$

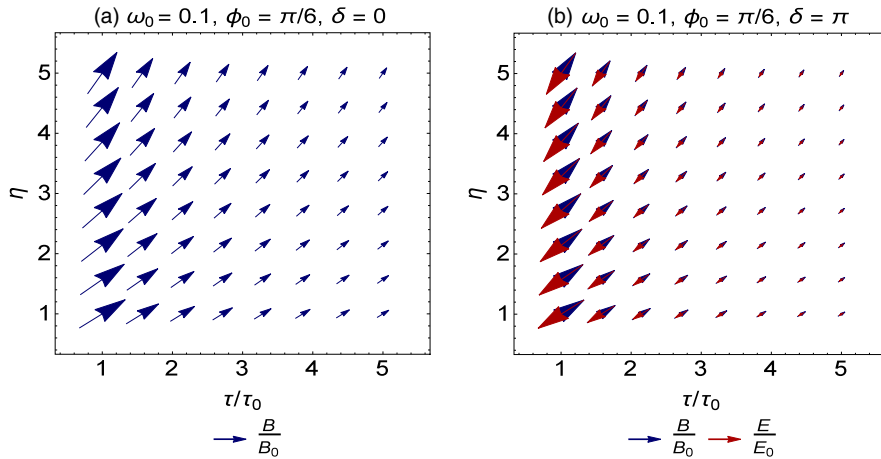


FIG. 4. (a) \mathbf{B}/B_0 from (4.35) is plotted for the set of free parameters $\{\sigma, \omega_0, \beta_0, \phi_0, \chi_e, \chi_m, \ell\} = \{40, 0.1, 0.1, \frac{\pi}{6}, 0, 0, +1\}$ in an η vs τ/τ_0 plane. The electric field vectors are parallel to the magnetic field vectors (denoted by blue arrows), and are not demonstrated in this plot. A slow rotation sets up with increasing η . (b) \mathbf{B}/B_0 (blue arrows) and \mathbf{E}/E_0 (red arrows) from (4.35) are plotted for the set of free parameters $\{\sigma, \omega_0, \beta_0, \phi_0, \chi_e, \chi_m, \ell\} = \{40, 0.1, 0.1, \frac{\pi}{6}, 0, 0, -1\}$ in an η vs τ/τ_0 plane. A slow rotation sets up with increasing η .

For small conductivity, $\sigma \ll \frac{(1+\chi_e)}{\tau - \tau_0}$, we thus arrive at

$$B \approx B_0 \left(\frac{\tau_0}{\tau}\right)^a \left\{ 1 - \frac{\sigma(1-a)}{1+\chi_e} \left[\tau_0 \ln\left(\frac{\tau_0}{\tau}\right) + (\tau - \tau_0) \right] \right\}, \quad (4.31)$$

and

$$\begin{aligned} E \approx E_0 \left(\frac{\tau_0}{\tau}\right)^a \left\{ 1 - \frac{\sigma}{1+\chi_e} \left[(1-a)\tau_0 \ln\left(\frac{\tau_0}{\tau}\right) \right. \right. \\ \left. \left. + (2-a)(\tau - \tau_0) \right] \right\}, \end{aligned} \quad (4.32)$$

with $a = 1 - \ell \omega_0 \beta_0$, as in the previous case. Hence, as it turns out, (4.31) and (4.32) represent a deviation from the power-law solution (4.18).

In the case of large conductivity, $\sigma \gg \frac{(1+\chi_e)}{\tau - \tau_0}$, the magnetic field behaves as

$$B \approx B_0 \left(\frac{\tau_0}{\tau}\right) \left(1 + \frac{\ell \omega_0 \beta_0 (1 + \chi_e)}{\sigma \tau_0} \right), \quad (4.33)$$

while, as expected, the electric field vanishes,

$$E = B \beta_0 e^{-\frac{\sigma(\tau - \tau_0)}{1 + \chi_e}} \rightarrow 0. \quad (4.34)$$

In Fig. 4, we have plotted the spatial components of rotating magnetic and electric fields $B^\mu = (0, \mathbf{B})$ and $E^\mu = (0, \mathbf{E})$,

$$\begin{aligned}\frac{\mathbf{B}}{B_0} &= \left(\frac{\tau_0}{\tau}\right) e^{\mathcal{M}(\tau)} (\cos \phi(\eta), \sin \phi(\eta), 0), \\ \frac{\mathbf{E}}{E_0} &= \left(\frac{\tau_0}{\tau}\right) e^{\mathcal{N}(\tau)} (\cos \zeta(\eta), \sin \zeta(\eta), 0),\end{aligned}\quad (4.35)$$

with \mathcal{M} and \mathcal{N} from (4.26) and (4.27), respectively. The angles $\phi(\eta)$ and $\zeta(\eta)$ are given in (4.34). In Fig. 4(a), the vectors of \mathbf{B}/B_0 (blue arrows) are plotted with the set of free parameters $\{\sigma, \omega_0, \beta_0, \phi_0, \chi_e, \chi_m, \ell\} = \{40, 0.1, 0.1, \frac{\pi}{6}, 0, 0, +1\}$. The electric vectors \mathbf{E}/E_0 are parallel to \mathbf{B}/B_0 , and are not demonstrated in this plot. The vectors are slowly rotating with increasing η . In Fig. 4(b), antiparallel vectors \mathbf{B}/B_0 (blue arrows) and \mathbf{E}/E_0 (red arrows) are plotted with the set of free parameters $\{\sigma, \omega_0, \beta_0, \phi_0, \chi_e, \chi_m, \ell\} = \{40, 0.1, 0.1, \frac{\pi}{6}, 0, 0, -1\}$. A slow rotation is set up with increasing η .

V. NUMERICAL RESULTS

As it is demonstrated in previous sections, the combination of five partial differential equations (3.17), (3.20), and (3.21), arising from the energy conservation law and Maxwell equations of motion, leads to two different series of solutions for the evolution of electromagnetic and thermodynamic fields. They are essentially characterized by $\frac{d\mathcal{M}}{du} = 0$ and $\frac{d\mathcal{M}}{du} \neq 0$. Here, nonvanishing \mathcal{M} describes the deviation from frozen-flux theorem $\partial_\mu(Bu^\mu) = 0$ of ideal transverse MHD [see (3.27) and the most general solution of the magnetic field B in nonideal transverse MHD from (3.34)]. Whereas the solution corresponding to $\frac{d\mathcal{M}}{du} = 0$ leads to nonrotating parallel or antiparallel electric and magnetic fields, the solutions corresponding to $\frac{d\mathcal{M}}{du} \neq 0$ describe rotating \mathbf{B} and \mathbf{E} fields. The proper time evolution of the magnitudes of these fields is shown to be determined by exact and approximate analytical solutions to (3.38) and (3.39). We have, in particular, shown that, apart from B and E , the proper time evolution of thermodynamic fields T , p , and ϵ is also affected by vanishing or nonvanishing \mathcal{M} .

In this section, we use the numerical solution to the master equation (3.39), and numerically determine the time evolution of $E = |\mathbf{E}|$, $B = |\mathbf{B}|$ and T .¹⁹ To demonstrate the effect of rotation, we qualitatively compare the space-time evolution of rotating and NR solutions of nonideal transverse MHD for E , B , and T [Sec. VA]. The cases of vanishing and nonvanishing susceptibilities are discussed separately. In Sec. VB, we present a quantitative analysis on the reliability of approximate solutions corresponding to (3.39) presented in Sec. IV B. This is done by comparing the PL and SR solutions from (4.21) and (4.28) with the numerical solutions for B , E , and T arising from (3.39) and

(3.55), from which we particularly determine \mathcal{M} and \mathcal{N} , in combination with (3.34)–(3.36).

In Sec. VC, we study the effect of various free parameters $\{\Omega_0, \sigma, \chi_m\}$ on the proper time evolution of electromagnetic and thermodynamic fields B , E , and T . We focus on potentially different effects of $\Omega_0 > 0$ and $\Omega_0 < 0$, as well as $\chi_m < 0$ and $\chi_m > 0$, corresponding to dia- and paramagnetic fluids. We show that with our specific choices of free parameters,²⁰ $\Omega_0 > 0$ leads to negative E/E_0 , and is therefore unphysical. We therefore consider only the case of $\Omega_0 < 0$ along with other free parameters. The effect of $\sigma_0 \equiv \frac{B_0^2}{\epsilon_0}$, with $B_0 = B(\tau_0)$ and $\epsilon_0 = \epsilon(\tau_0)$, on the proper time evolution of T is also discussed in detail. Reformulating σ_0 in terms of eB_0/m_π^2 , with the pion mass $m_\pi \sim 0.140$ GeV, it is then possible to plot T/T_0 in terms of eB_0/m_π^2 , and compare, in this way, the effect of B_0 on T/T_0 at the RHIC and LHC. We choose different sets of $\{\chi_e, \chi_m\}$ as well as Ω_0 , and scrutinize the interplay between these parameters on the gradient of temperature once eB_0 increases from its value at the RHIC ($eB_0 \sim 1.5m_\pi^2$) to its value at the LHC ($eB_0 \sim 15m_\pi^2$).

A. Space-time evolution of E , B , and T

In Sec. II, we studied the proper time evolution of ideal transverse MHD. We argued that in this case, B evolves as (2.22) with $\mathcal{B} = 1$, while $E = 0$. We have also shown that the evolution of T is given by (2.18). Using these relations, we have presented, in Fig. 5, the contour plots of B/B_0 [Fig. 5(a)] and T/T_0 [Fig. 5(b)] with $\mathcal{U} = 1$. A qualitative comparison shows that the magnetic field decays much faster than the temperature.²¹ It declines within $t = 5$ fm/c down to 10 percent of its original value at $\tau_0 = 0.5$ fm/c.

In Figs. 6(a)–6(i), the contour plots of B/B_0 [Figs. 6(a)–6(c)], E/E_0 [Figs. 6(d)–6(f)], and T/T_0 [Figs. 6(g)–6(i)] are demonstrated for nonrotating and rotating electromagnetic fields. The results for NR solutions, characterized by vanishing $d\mathcal{M}/du$, are demonstrated in Figs. 6(a), 6(d), and 6(g). They correspond to (4.8) and (3.31) with $\exp(\frac{\ell}{\kappa})$ from (4.10) and $\mathbb{V} = 1$. Here, the set of free parameters is chosen to be

$$\{\sigma_0, \sigma, \beta_0, \chi_e, \chi_m\} = \{10, 400 \text{ MeVc}, 0.01, 0, 0\}. \quad (5.1)$$

To plot the space-time evolution of the numerical solutions for B/B_0 , E/E_0 , and T/T_0 , denoted by “NumIso” B/B_0 , E/E_0 , and T/T_0 , the set of free parameters

$$\begin{aligned}\{\sigma_0, \sigma, \Omega_0, \beta_0, \chi_e, \chi_m\} \\ = \{10, 400 \text{ MeVc}, -1.5, 0.01, 0, 0\}\end{aligned}\quad (5.2)$$

¹⁹The time evolution of p and ϵ is similar to that of T , and is not presented here.

²⁰Free parameters are chosen particularly with regard to the realistic example of QGP.

²¹This is related with the fact that $c_s < 1$.

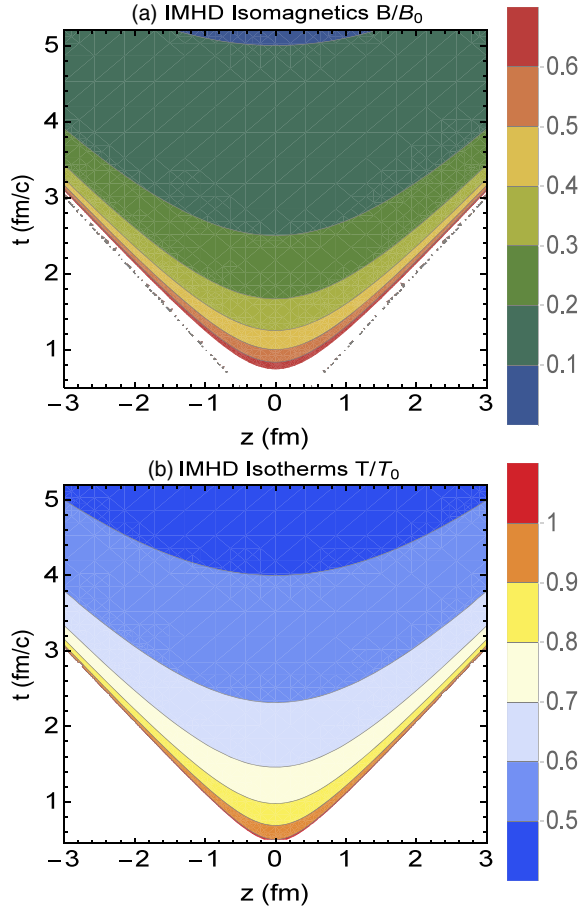


FIG. 5. Space-time evolution of B and T in ideal transverse MHD. (a) Isomagnetic fluxes of B/B_0 ; (b) isothermal fluxes of T/T_0 .

[Figs. 6(b), 6(e), and 6(h)] as well as

$$\{\sigma_0, \sigma, \Omega_0, \beta_0, \chi_e, \chi_m\} \\ = \{10, 400 \text{ MeVc}, -1.5, 0.01, 0.01, 0.01\} \quad (5.3)$$

[Figs. 6(c), 6(f), and 6(i)] are used. First, using these parameters, the master equation (3.39) is numerically solved. Plugging then \mathcal{M} arising from this equation into (3.55), \mathcal{N} is determined. The space-time evolution of B/B_0 , E/E_0 , and T/T_0 is then determined by plugging \mathcal{M} and \mathcal{N} into (3.34)–(3.36). The latter leads, in combination with (3.31) with $\mathbb{V} = 1$, to the numerical solution of T/T_0 .

A comparison between NR result for the space-time evolution B/B_0 from Fig. 6(a) shows that the magnetic field decays faster in the case of nonvanishing $\frac{d\mathcal{M}}{du}$ (rotating electromagnetic fields) with vanishing [Fig. 6(b)] and nonvanishing susceptibilities [Fig. 6(c)]. In all these cases B/B_0 decays monotonically with t to values of $B \ll B_0$. In contrast, the numerical results for E/E_0 and T/T_0 exhibit a completely different behavior. Qualitatively, E/E_0 and

T/T_0 increase rapidly with increasing $t \lesssim 2 \text{ fm/c}$ to values of E and T larger than their original values E_0 and T_0 . Then, in the interval $2 \lesssim t \lesssim 5 \text{ fm/c}$, they decay slowly to values that are still larger than E_0 and T_0 [see Sec. V C and Appendix B]. Nonvanishing susceptibilities do not affect this qualitative picture too much.

In Sec. V C, we present, among others, a careful quantitative analysis of the effect of Ω_0 and χ_m on the proper time evolution of B/B_0 , E/E_0 , and T/T_0 .

B. Reliability of analytical solutions of the master equation (3.39): A qualitative analysis

In Sec. IV B, two approximate analytical solutions for the master equation (3.39) have been presented. The first case, for which $\frac{E}{B} \sim \frac{E_0}{B_0}$ was assumed, leads to PL, and the second one, for which ω_0 was assumed to be small, leads to SR solutions for the proper time evolution of B , E , and T .

In this section, we quantitatively determine the deviation of these approximate analytical solutions from the numerical solutions of these fields. This deviation is determined from

Error in %

$$\equiv \left| \frac{\text{approx analytical} - \text{numerical solution}}{\text{numerical solution}} \right| \times 100. \quad (5.4)$$

The τ dependence of these errors for B/B_0 and E/E_0 is presented in Fig. 7. The sets of free parameters

$$\{\tau_0, \sigma_0, \sigma, \Omega_0, \beta_0, \chi_e, \chi_m\} \\ = \{0.5 \text{ fm/c}, 0.1, 40 \text{ MeVc}, -0.1, 0.1, 0, 0\}, \quad (5.5)$$

and

$$\{\tau_0, \sigma_0, \sigma, \Omega_0, \beta_0, \chi_e, \chi_m\} \\ = \{0.5 \text{ fm/c}, 10, 40 \text{ MeVc}, -0.1, 0.1, 0, 0\}, \quad (5.6)$$

are used in Figs. 7(a) and 7(b), respectively. As it turns out from the results of Fig. 7, for B/B_0 , the SR approximate solution (red dashed curves) is more reliable than the PL solution (red solid curves). On the contrary, for E/E_0 , the errors for PL solutions (black solid curves) in the whole range of $\tau \in [0, 10] \text{ fm/c}$ are smaller than those for the SR solution (black dashed curves) in the same proper time interval. Except for the deviation of PL from numerical solutions for E/E_0 in Fig. 7(a) for $\sigma_0 = 0.1$ (black solid curve), the errors increase with increasing τ . Moreover, in contrast to the deviations of B/B_0 from the numerical solutions, which are in general lower than 20%, the deviations of E/E_0 are larger, and, depending on the choice of free parameters raise up to 80%. Increasing σ_0

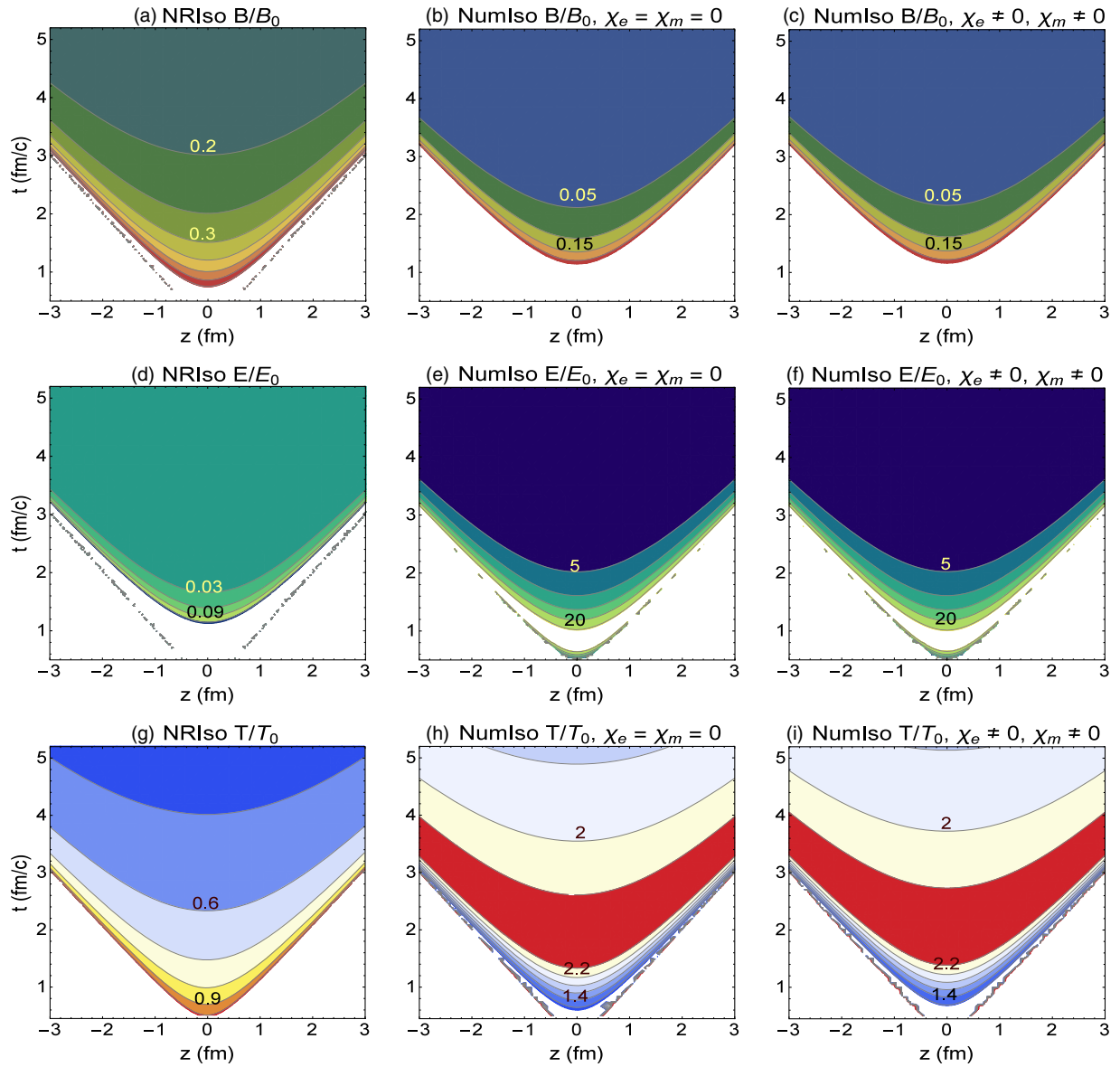


FIG. 6. Contour plots for B/B_0 , E/E_0 , and T/T_0 arising from NR [(a), (d), and (g)] and numerical solutions of rotating electromagnetic fields [(b) and (c), (e) and (f), and (h) and (i)]. The set of free parameters (5.1), (5.2), and (5.3) is chosen to determine the NR [(a), (d), and (g)] and rotating solutions corresponding to vanishing [(b), (e), and (h)] and nonvanishing [(c), (f), and (i)] susceptibilities. Qualitatively speaking, nonvanishing ω_0 affects the space-time evolutions of B , E , and T . Moreover, nonvanishing electric and magnetic susceptibilities, χ_e and χ_m , slightly affect the numerical rotating solutions for B , E , and T fluxes.

from $\sigma_0 = 0.1$ to $\sigma_0 = 10$ does not change this picture too much.

In Fig. 8, the τ dependence of the deviation of PL (solid curves) and SR (dashed curves) solutions of T/T_0 from its numerical solution is plotted for two set of free parameters

$$\begin{aligned} \text{A set: } & \{\tau_0, \sigma_0, \sigma, \Omega_0, \beta_0, \chi_e, \chi_m\} \\ & = \{0.5 \text{ fm/c}, 0.1, 4 \text{ MeVc}, -0.1, 1, 0, 0\}, \\ \text{B set: } & \{\tau_0, \sigma_0, \sigma, \Omega_0, \beta_0, \chi_e, \chi_m\} \\ & = \{0.5 \text{ fm/c}, 0.1, 40 \text{ MeVc}, -0.1, 0.1, 0, 0\}, \end{aligned} \quad (5.7)$$

in Fig. 8(a), and

$$\begin{aligned} \text{A set: } & \{\tau_0, \sigma_0, \sigma, \Omega_0, \beta_0, \chi_e, \chi_m\} \\ & = \{0.5 \text{ fm/c}, 10, 4 \text{ MeVc}, -0.1, 1, 0, 0\}, \\ \text{B set: } & \{\tau_0, \sigma_0, \sigma, \Omega_0, \beta_0, \chi_e, \chi_m\} \\ & = \{0.5 \text{ fm/c}, 10, 40 \text{ MeVc}, -0.1, 0.1, 0, 0\}, \end{aligned} \quad (5.8)$$

in Fig. 8(b). The green (blue) solid and dashed curves correspond to A (B) sets defined in (5.7) and (5.8). Comparing with the errors of B/B_0 and E/E_0 , presented

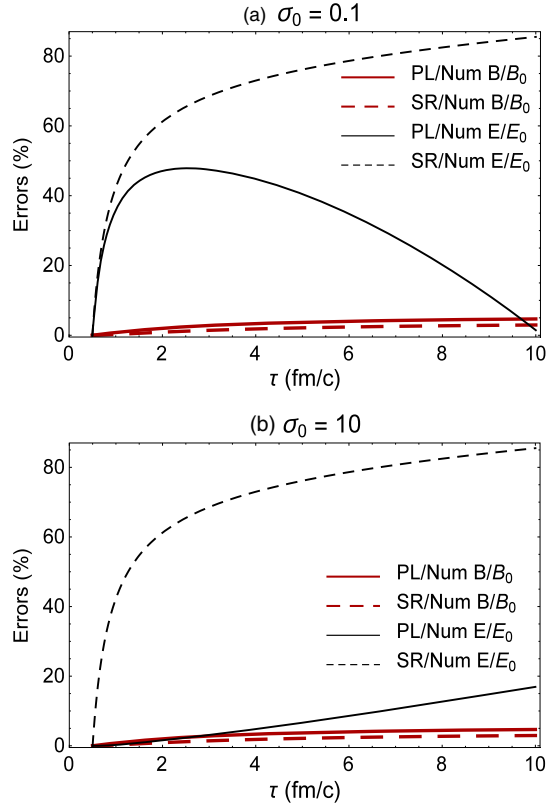


FIG. 7. The τ dependence of the deviation of PL and SR approximate analytical solutions of B/B_0 (red solid and dashed curves) and E/E_0 (thin black solid and dashed curves) from the corresponding numerical solutions is plotted for two sets of free parameters (5.5) (a) and (5.6) (b). The results for these deviations are strongly affected by the choice of free parameters, and increase, in general, with increasing τ . For B (E), the SR (PL) solution is more reliable than the PL (SR) solution.

in Fig. 7, the errors for T/T_0 are much smaller. They increase with increasing τ , and strongly depend on the choice of free parameters, especially σ_0 [compare Figs. 8(a) with 8(b)] and $\{\sigma, \beta_0\}$ pairs (compare the results for A and B sets). In general, similar to the case of E/E_0 , the PL solution for T/T_0 is more reliable than the SR solution.

In summary, the above analysis shows that the deviation of analytical PL and SR solutions to (3.39) from the numerical solution to the same equation depends strongly on the choice of the set of free parameters $\{\tau_0, \sigma_0, \sigma, \Omega_0, \beta_0, \chi_e, \chi_m\}$. In what follows, we focus solely on B , E , and T , arising from numerical solution of (3.39).

C. Effects of Ω_0 , σ , χ_m , and σ_0 on B , E , and T fields

In this section, we study the dependence of numerical results for B , E , and T on the angular velocity $\Omega_0 = \ell\omega_0$, the electric conductivity σ , the magnetic susceptibility χ_m , and $\sigma_0 = \frac{B_0^2}{\epsilon_0}$. The latter is originally introduced in [33], and is a measure for the strength of the magnetic field at τ_0 . We focus on the effects of these parameters on the τ

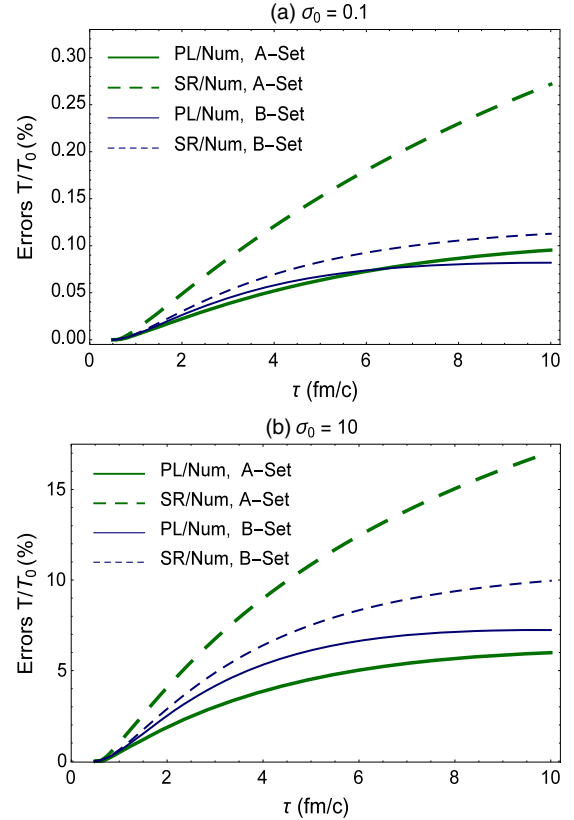


FIG. 8. The τ dependence of the deviation of PL and SR approximate analytical solutions of T/T_0 from the corresponding numerical solutions to T/T_0 is plotted for two sets of free parameters (5.7) (a) and (5.8) (b). The green (blue) solid and dashed curves correspond to A (B) sets defined in (5.7) and (5.8). As expected, the deviations of PL and SR solutions from numerical solution for T/T_0 are strongly affected by the choice of parameters.

dependence of electromagnetic fields B , E , and temperature T . We also study the effect of Ω_0, σ, χ_m , and σ_0 on the behavior of $B/B_0, E/E_0$, and T/T_0 for fixed proper time points. As aforementioned, for the choice of free parameters, we have strongly oriented ourselves to sets that may be relevant for QGP.

1. Ω_0 dependence of B , E , and T

Let us start by exploring the effect of angular velocity Ω_0 on B , E , and T . In Fig. 9, the τ dependence of B/B_0 [Fig. 9(a)], E/E_0 [Fig. 9(b)], and T/T_0 [Fig. 9(c)] is plotted for four different sets of free parameters with fixed $\{\tau_0, \sigma_0, \sigma, \beta_0, \chi_e, \chi_m\}$ and different Ω_0 s. The Ω_0 sets, denoted by O sets in Fig. 9, are characterized by

$$\begin{aligned} & \{\tau_0, \sigma_0, \sigma, \Omega_0, \beta_0, \chi_e, \chi_m\} \\ & = \{0.5 \text{ fm/c}, 10, 400 \text{ MeVc}, \Omega_0, 0.01, 0, 0\}, \quad (5.9) \end{aligned}$$

with

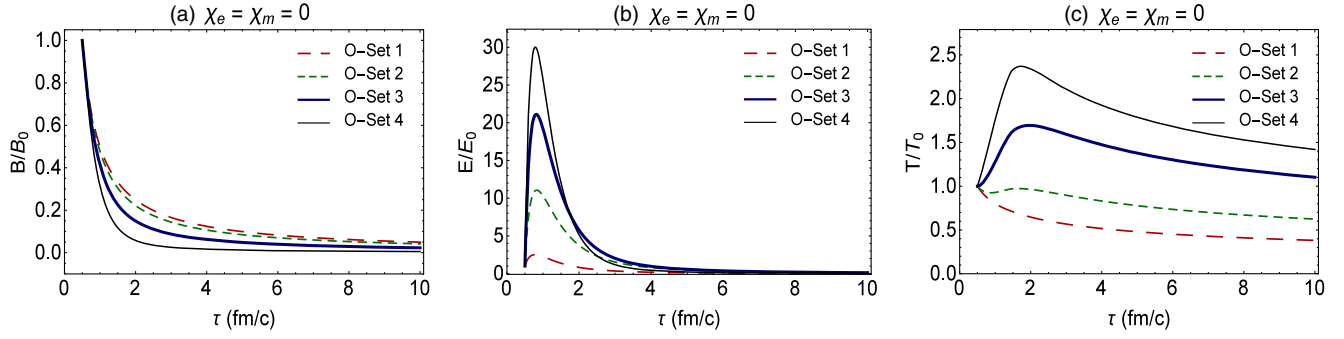


FIG. 9. The τ dependence of B/B_0 (a), E/E_0 (b), and T/T_0 (c), arising from the numerical solution of (3.39), is plotted. The O set i 's, $i = 1, 2, 3, 4$ correspond to Ω_0 sets from (5.9) and (5.10). Nonvanishing Ω_0 strongly affects the τ dependence and the lifetime of B , E , and T .

$$\begin{cases} \text{O set 1: } & \Omega_0 = -0.1, \\ \text{O set 2: } & \Omega_0 = -0.5, \\ \text{O set 3: } & \Omega_0 = -1.0, \\ \text{O set 4: } & \Omega_0 = -1.5. \end{cases} \quad (5.10)$$

We exclusively work with negative $\Omega_0 = \ell\omega_0$, because, as it turns out, positive Ω_0 leads to unphysical negative amplitudes for E/E_0 [see, in particular, Fig. 11(b) and our explanations in Appendix B]. Assuming ω_0 to be positive, $\Omega_0 < 0$ corresponds to antiparallel \mathbf{B} and \mathbf{E} fields. As it is shown in Fig. 9(a), for our specific choice of free parameters, B/B_0 monotonically decreases with increasing τ , while E/E_0 exhibits a certain peak in the proper time interval $0.5 < \tau < 2$ fm/c, and rapidly decreases for $\tau \geq 2$ fm/c [see Fig. 9(b)]. As concerns the effect of Ω_0 on the lifetime of B/B_0 and E/E_0 , it turns out that the lifetime of B/B_0 increases with increasing Ω_0 , or equivalently decreasing ω_0 , while faster rotating electric fields, with larger ω_0 , have larger lifetimes. The position and amplitude of E -peaks depend also on ω_0 ; as it is shown in Fig. 9(b), for larger ω_0 , the E -peaks arise with larger amplitudes at later proper times.

As concerns the τ dependence of T/T_0 , demonstrated in Fig. 9(c), T -peaks arise only for $\omega_0 \geq 0.5$. In contrast to E -peaks, T -peaks occur at $\tau \geq 2$ fm/c. Similar to E -peaks, the positions and amplitudes of T -peaks are affected by ω_0 ; for larger ω_0 , the T -peaks arise with larger amplitude at later proper times. After these peaks, T decreases slowly at $\tau \geq 3$ fm/c to $T \approx T_0$. The slope of this temperature decrease is slightly affected by ω_0 . However, since T -peaks are higher for larger ω_0 , the system remains hot longer for faster rotating B and E fields, e.g., for $\omega_0 = 1.5$, $T \sim 1.5T_0$ at $\tau \sim 10$ fm/c, while for $\omega_0 = 0.5$, $T \sim 0.5T_0$ at the same $\tau \sim 10$ fm/c. The fact that in the realistic QGP the temperature decreases to values $T < T_0$ within $\tau \sim 10$ fm/c indicates that ω_0 either vanishes or is small ($\omega_0 \approx 0.1$). Let us notice that this conclusion is only true for transverse MHD within our above-mentioned approximations. In Appendix B, we analyze the general behavior of the

solutions of (3.39), and present a detailed discussion on E and T reapeaking.

To study the effect of susceptibilities, χ_e and χ_m , the τ dependence of T/T_0 is plotted in Fig. 10 for the set of free parameters

$$\{\sigma_0, \sigma, \beta_0, \chi_e\} = \{10, 400 \text{ MeVc}, 0.01, 0.01\}, \quad (5.11)$$

with three different sets of χ_m ,

$$\begin{aligned} \chi_m &= 0 && \text{(thick solid curves),} \\ \chi_m &= +0.01 && \text{(thin solid curves),} \\ \chi_m &= -0.01 && \text{(dashed curves),} \end{aligned} \quad (5.12)$$

and $\Omega_0 = -0.2$ [Fig. 10(a)] and $\Omega_0 = -1$ [Fig. 10(b)].²² As expected from the results of Fig. 9(c), T -peaks appear only for large $\omega_0 = 1$ [Fig. 10(b)]. Moreover, it turns out that for a fixed τ , T/T_0 increases (decreases) for positive (negative) χ_m . The shape of T/T_0 is, however, not affected by nonvanishing susceptibilities. The results presented in Fig. 10, arising within our aforementioned approximations, thus show that whereas T remains high longer in a paramagnetic fluid, with $\chi_m > 0$, a diamagnetic fluid, with $\chi_m < 0$, cools faster. This result is independent of the choice of Ω_0 .

In Figs. 11(a)–11(c), the Ω_0 dependence of B/B_0 , E/E_0 , and T/T_0 is plotted for fixed $\tau = 1$ fm/c (blue curves) $\tau = 2$ fm/c (green curves). Here, we have used the set of free parameters

$$\begin{aligned} \{\tau_0, \sigma_0, \sigma, \beta_0, \chi_e\} \\ = \{0.5 \text{ fm/c}, 10, 400 \text{ MeVc}, 0.01, 0.01\}, \end{aligned} \quad (5.13)$$

with three different sets of χ_m ,

²²We later show that the effect of χ_m on the τ dependence of B/B_0 and E/E_0 can be neglected. This is why we have focused, at this stage, only on the effect of susceptibilities on T/T_0 .

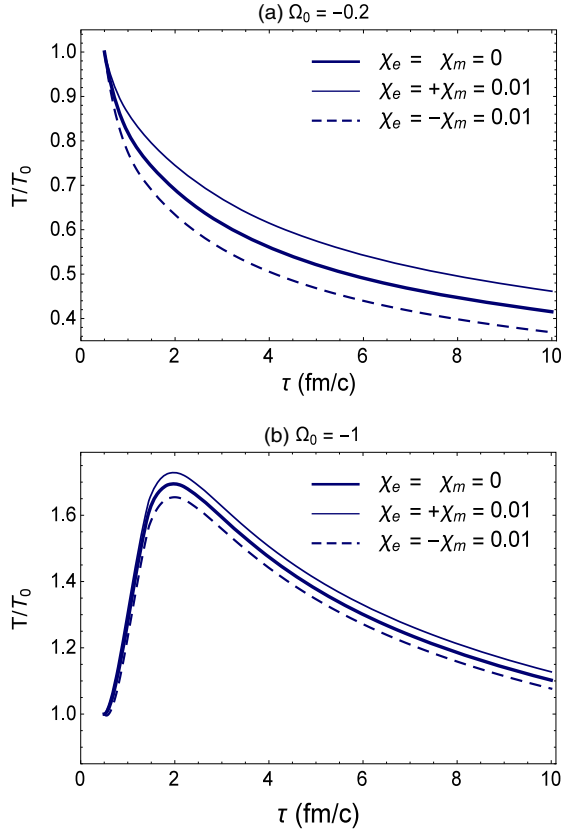


FIG. 10. The τ dependence of T/T_0 arising from the numerical solution of (3.39) is plotted for the set of free parameters (5.11) with $\chi_m = 0$ (thick solid curve), $\chi_m = +0.01$ (thin solid curve), and $\chi_m = -0.01$ (dashed curve), and $\Omega_0 = -0.2$ (a) as well as $\Omega_0 = -1$ (b). As it turns out, a diamagnetic fluid cools faster than a paramagnetic fluid.

$$\begin{aligned}
 \chi_m = 0 & \quad (\text{thick solid curves}), \\
 \chi_m = +0.01 & \quad (\text{thin solid curves}), \\
 \chi_m = -0.01 & \quad (\text{dashed curves}).
 \end{aligned} \tag{5.14}$$

These plots show that B/B_0 and T/T_0 are even in Ω_0 , while E/E_0 changes its sign by flipping the sign of Ω_0 from negative to positive. This behavior originates from the fact that E is essentially determined by $E = \frac{B}{\Omega_0} \frac{d\mathcal{M}}{du}$ [see (3.54)]. Bearing in mind that \mathcal{M} arises from the master equation (3.39), which is even in Ω_0 ,²³ E turns out to be odd in Ω_0 , as it is shown in Fig. 11(b). Let us notice that since $E = |\mathbf{E}|$ is always positive, the regime $\Omega_0 > 0$, where E/E_0 becomes negative, is to be excluded [see also Appendix B for a more detailed analysis of rotating solutions for B , E , and T]. A comparison between the curves for positive and negative Ω_0 shows that for negative Ω_0 , whereas B/B_0 increases with decreasing ω_0 , E/E_0 and T/T_0 increase with decreasing ω_0 . The dependence of

²³In (3.39), $\omega_0^2 = \ell^2 \Omega_0^2 = \Omega_0^2$.

B/B_0 and E/E_0 on $\Omega_0 < 0$, described above, is indeed expected, because the larger the ω_0 , the faster the \mathbf{B} and \mathbf{E} rotate in a medium with temperature T . In this case, whereas the magnitude of the magnetic field B decreases, E becomes larger, and the energy is thus pumped into the medium whose temperature increases consequently.

As it is shown in Fig. 10, the effects of χ_m on B/B_0 and T/T_0 are similar, and differ from the effect of χ_m on E/E_0 : For $\Omega_0 < 0$, at each fixed proper time, the amplitudes of B/B_0 and T/T_0 become larger for $\chi_m > 0$ (paramagnetic fluid) and smaller for $\chi_m < 0$ (diamagnetic fluid). On the contrary, the amplitude of E/E_0 becomes larger for $\chi_m > 0$ (paramagnetic fluid) and smaller for $\chi_m < 0$ (diamagnetic fluid).

Let us notice that in some specific regions of Ω_0 and for some specific choices of χ_m , T/T_0 becomes unphysically negative [see Fig. 11(c), where T/T_0 becomes negative for $\chi_m = -0.2$ in the regime $-0.5, \Omega_0 < +0.5$].²⁴ This regime of parameters is to be excluded from the parameter space. We also notice that $\Omega_0 = 0$ is to be excluded from the plots of Fig. 11, because, as it is argued in Sec. IV, this case corresponds to $\frac{d\mathcal{M}}{du} = 0$ from (3.38), and leads to non-rotating parallel or antiparallel \mathbf{B} and \mathbf{E} fields. The analytical solution of (3.38), as well as the τ and η evolutions of \mathbf{B} and \mathbf{E} , is already presented in that section. In Fig. 11, we have exclusively demonstrated the results arising from numerical solutions to (3.39), which lead to rotating parallel or antiparallel \mathbf{B} and \mathbf{E} fields with $\Omega_0 \neq 0$.

2. σ dependence of B , E , and T

In this part, we focus on the σ dependence of B , E , and T . In Fig. 12, the τ dependence of B/B_0 [Fig. 12(a)], E/E_0 [Fig. 12(b)], and T/T_0 [Fig. 12(c)] is plotted for four different sets of free parameters with fixed $\{\tau_0, \sigma_0, \Omega_0, \chi_e, \chi_m\}$ and different $\{\sigma, \beta_0\}$. The latter are chosen in a way that $\sigma\beta_0 \sim 4$ MeVc. The σ sets, denoted by S sets in Fig. 12, are characterized by

$$\{\tau_0, \sigma_0, \Omega_0, \chi_e, \chi_m\} = \{0.5 \text{ fm/c}, 10, -0.2, 0, 0\}, \tag{5.15}$$

with

$$\begin{cases}
 \text{S set 1: } \sigma = 4 \text{ MeVc}, & \beta_0 = 1, \\
 \text{S set 2: } \sigma = 40 \text{ MeVc}, & \beta_0 = 0.1, \\
 \text{S set 3: } \sigma = 400 \text{ MeVc}, & \beta_0 = 0.01, \\
 \text{S set 4: } \sigma = 4000 \text{ MeVc}, & \beta_0 = 0.001.
 \end{cases} \tag{5.16}$$

As it is demonstrated in Fig. 12(a), for our specific choice of free parameters, B/B_0 monotonically decreases to $B \ll B_0$. For fixed τ , B/B_0 essentially increases with increasing σ . However, no significant difference occurs

²⁴This does not happen for more relevant values of $\chi_m \sim -0.01$.

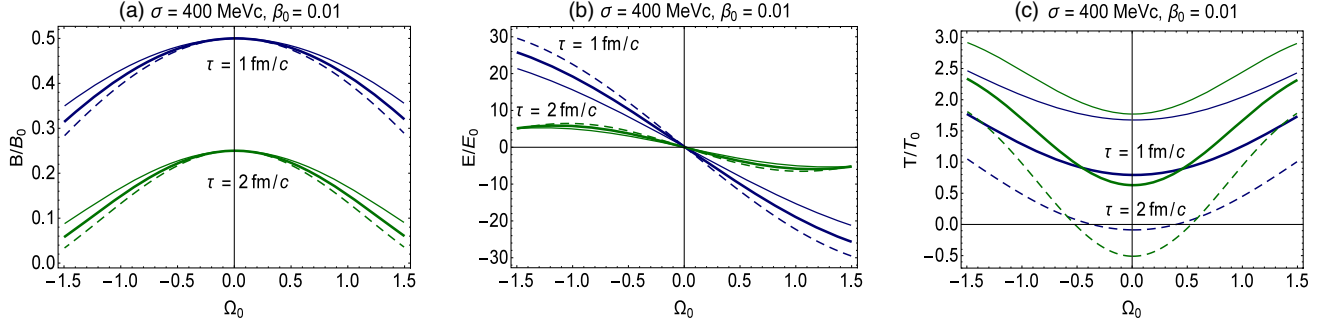


FIG. 11. The Ω_0 dependence of B/B_0 (a), E/E_0 (b), and T/T_0 (c) is plotted for $\tau = 1, 2$ fm/c (blue and green solid and dashed curves). The sets of free parameters (5.13) with $\chi_m = 0$ (thick solid curves), $\chi_m = +0.2$ (thin solid curves), and $\chi_m = -0.2$ (dashed curves) are used to determine B , E , and T from numerical solution of (3.39).

between the curves corresponding to S set 2 (green dashed curve), S set 3 (thick blue curve), and S set 4 (thin black curve). They almost coincide. For larger values of $\sigma \geq 40$ MeVc, the lifetime of B/B_0 becomes larger, as the slopes of the curves corresponding to S set i , $i = 2, 3, 4$ are smaller than those corresponding to S set 1. This is in contrast to the τ dependence of E/E_0 , demonstrated in Fig. 12(b). Whereas certain peaks occur in E/E_0 for large $\sigma = 400, 4000$ MeVc (thick blue and thin black curves) in the interval $0.5 < \tau < 2$ fm/c, for small $\sigma = 4, 40$ MeVc (green and red dashed curves), E/E_0 monotonically decreases. The positions of the peaks are slightly affected by σ . However, the peaks become sharper for large $\sigma = 4000$ MeVc and $\beta_0 = 0.001$. The lifetime of E/E_0 is smaller for smaller values of σ . The τ dependence of T/T_0 is demonstrated in Fig. 12(c). As it turns out, T/T_0 decreases monotonically for all σ sets (5.16). Moreover, for a fixed τ , T/T_0 decreases with increasing σ , and, as it turns out, a fluid with smaller electric conductivity remains hot longer, as the slope of the curves corresponding to small σ is significantly smaller than the slopes of curves corresponding to larger σ .

In Figs. 13(a), 13(b), and 14, the σ dependence of B/B_0 , E/E_0 , and T/T_0 for $\tau = 1$ fm/c (blue curves), $\tau = 2$ fm/c (green curves), and $\tau = 3$ fm/c is plotted. To determine the

amplitudes of B , E , and T in Figs. 13 and 14, we used the following sets of free parameters:

$$\{\tau_0, \sigma_0, \Omega_0\} = \{0.5 \text{ fm/c}, 10, -0.2\}, \quad (5.17)$$

with $\sigma \in [4, 40]$ MeVc, $\beta_0 = 4/\sigma$ and

$$\begin{aligned} \{\chi_e, \chi_m\} &= \{0, 0\}, \\ \{\chi_e, \chi_m\} &= \{0.01, +0.2\}, \\ \{\chi_e, \chi_m\} &= \{0.01, -0.2\}. \end{aligned} \quad (5.18)$$

The amplitude of B/B_0 for each fixed τ is almost not affected by σ [see Fig. 13(a)]. It increases with σ in the regime $\sigma \leq 10$ MeVc, and then remains almost constant. Different choices of $\{\chi_e, \chi_m\}$ have also no effects on the σ dependence of B/B_0 , as the curves corresponding to the sets (5.18) exactly coincide. This is in contrast to the behavior of E/E_0 for different sets of parameters (5.17) and (5.18), as it is demonstrated in Fig. 13(b). Here, thick solid curves correspond to $\{\chi_e, \chi_m\} = \{0, 0\}$, thin solid curves to $\{\chi_e, \chi_m\} = \{0.01, +0.2\}$, and dashed curves to $\{\chi_e, \chi_m\} = \{0.01, -0.2\}$. The amplitudes of E/E_0 essentially increase with increasing σ . For a fixed σ , E/E_0

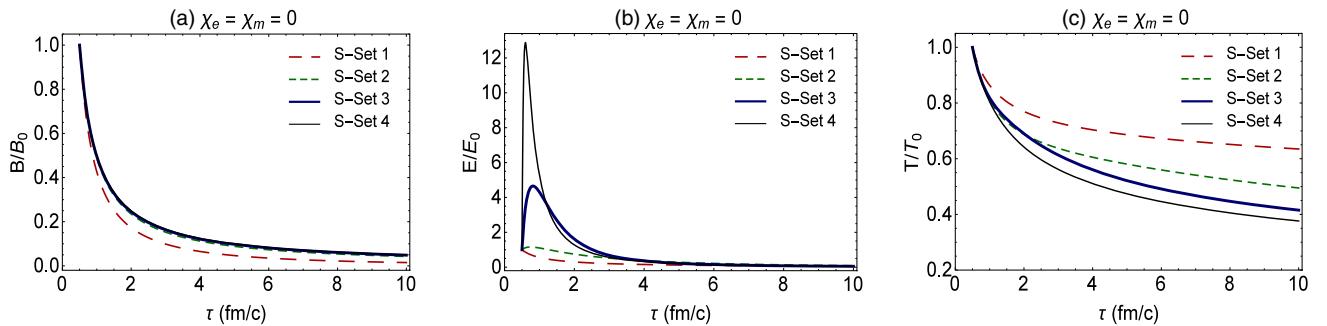


FIG. 12. The τ dependence of B/B_0 (a), E/E_0 (b), and T/T_0 (c) arising from the numerical solution of (3.39) is plotted. The S set i 's, with $i = 1, 2, 3, 4$ correspond to σ sets from (5.15) and (5.16). Nonvanishing σ affects the τ dependence and the lifetime of B , E , and T .

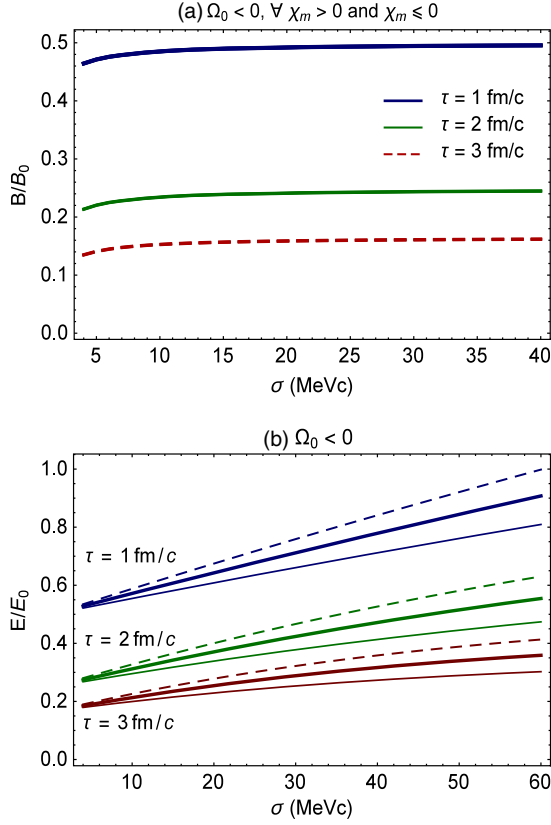


FIG. 13. The σ dependence of B/B_0 (a) and E/E_0 (b) is plotted at $\tau = 1, 2, 3$ fm/c (blue, green, and red solid and dashed curves). The sets of free parameters (5.17) and (5.18) are used to plot these curves. In b, thick solid curves correspond to $\{\chi_e, \chi_m\} = \{0, 0\}$, thin solid curves to $\{\chi_e, \chi_m\} = \{0.01, +0.2\}$, and dashed curves to $\{\chi_e, \chi_m\} = \{0.01, -0.2\}$. Whereas different choices of χ_m have no significant effect on the σ dependence of B/B_0 (see also Fig. 15), positive and negative χ_m affect the σ dependence of E/E_0 .

decreases (increases) in a para- (dia-) magnetic fluid. This effect enhances for larger values of σ .

The σ dependence of T/T_0 for different sets of parameters (5.17) and (5.18) and $\tau = 1, 2, 3$ fm/c is plotted in

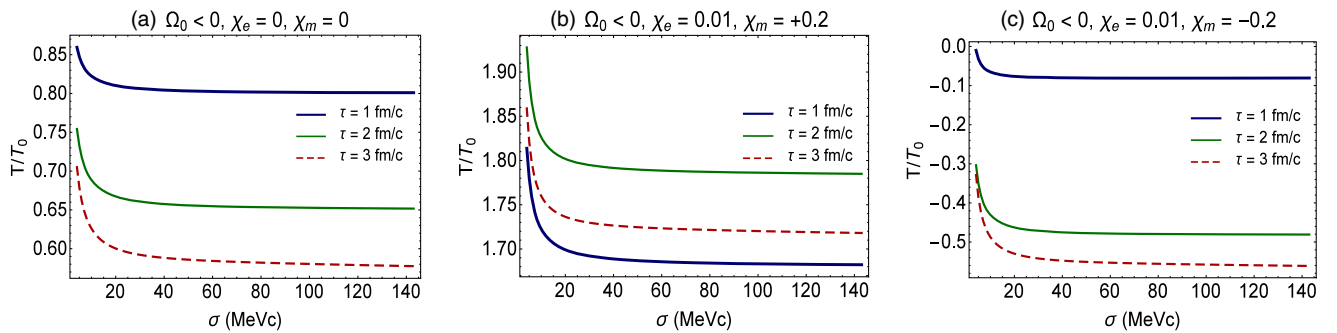


FIG. 14. The σ dependence of T/T_0 is plotted at $\tau = 1, 2, 3$ fm/c (blue, green, and red solid and dashed curves). The sets of free parameters (5.17) and (5.18) with $\chi_m = 0$ (a), $\chi_m = +0.2$ (b), and $\chi_m = -0.2$ (c) are used to determine T/T_0 from the numerical solution of (3.39).

Fig. 14. Apart from the fact that for $\{\chi_e, \chi_m\} = \{0.01, -0.2\}$, T/T_0 becomes unphysically negative, the amplitudes of T/T_0 decrease with increasing σ for $4 \leq \sigma \leq 20$ MeVc. For $\sigma > 20$ MeVc, however, T/T_0 does not change with increasing σ .

3. χ_m dependence of B , E , and T

To explore the χ_m dependence of B , E , and T , we have plotted in Fig. 15 B/B_0 , E/E_0 , and T/T_0 for two sets of free parameters

$$\{\tau_0, \sigma_0, \sigma, \Omega_0, \beta_0, \chi_e\} = \{0.5 \text{ fm/c}, 10, 400 \text{ MeVc}, -0.1, 0.01, 0.01\} \quad (5.19)$$

[see Figs. 15(a)–15(c)] and

$$\{\tau_0, \sigma_0, \sigma, \Omega_0, \beta_0, \chi_e\} = \{0.5 \text{ fm/c}, 10, 400 \text{ MeVc}, -1, 0.01, 0.01\} \quad (5.20)$$

[see Figs. 15(d)–15(f)] and for $\chi_m \in [-0.1, +0.1]$. This is the interval that may be relevant for QGP. As it is shown in Figs. 15(a) and 15(d), B/B_0 is almost not affected by χ_m . The same is also true for E/E_0 [see Figs. 15(b) and 15(e)]. For $\tau = 1$ fm/c, E/E_0 decreases with increasing χ_m , but remains almost constant for $\tau = 2, 3$ fm/c. Apart from the fact that at each fixed τ , E/E_0 becomes larger when ω_0 increases from $\omega_0 = 0.1$ to $\omega_0 = 1$, the χ_m dependence of E/E_0 remains almost unaffected by Ω_0 . Comparing with B/B_0 and E/E_0 , T/T_0 is strongly affected by χ_m . As it is shown in Figs. 15(c) and 15(f), T/T_0 increases, in general, with increasing χ_m . Moreover, as expected, the temporal sequence of T/T_0 changes for faster rotating electromagnetic fields [compare this sequence in Figs. 15(c) and 15(f)]. Let us notice that a change in the temporal sequence of T/T_0 in Fig. 15(c) comparing with Fig. 15(f) is mainly caused by the appearance of a T -peak in the regime $1 < \tau < 2$ fm/c for large ω_0 . The same effect occurs in the plots demonstrated in Fig. 10, where,

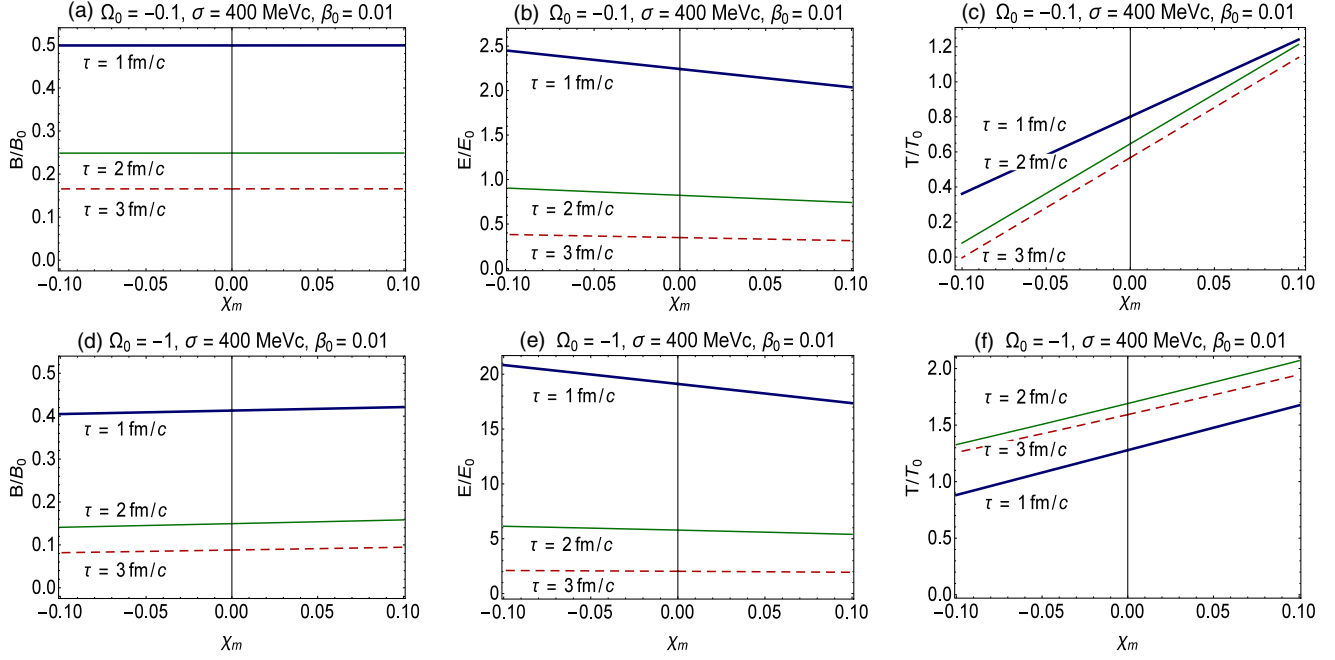


FIG. 15. The χ_m dependence of B/B_0 [(a) and (d)], E/E_0 [(b) and (e)], and T/T_0 [(c) and (f)] is plotted at $\tau = 1, 2, 3$ fm/c (blue, green solid curves, and red dashed curves). The sets of free parameters (5.19) [(a)–(c)] and (5.20) [(d)–(f)] are used to determine B/B_0 , E/E_0 , and T/T_0 from the numerical solution of (3.39).

comparing with the case of $\Omega_0 = -0.1$ in Fig. 10(a), for $\Omega_0 = -1$ in Fig. 10(b) a T -peak arises.

4. σ_0 dependence of B , E , and T

As it turns out, the numerical solutions of B and E are independent of $\sigma_0 = \frac{B_0^2}{e_0}$. We thus focus, in this part, on the dependence of T/T_0 on σ_0 .²⁵ This seems to be interesting also with regard to the evolution of the temperature in HIC experiments: As aforementioned, it is believed that in HIC experiments very strong magnetic fields are created at early stages of the collision (small τ). Depending on the impact parameter and collision energy, their strengths at the RHIC and LHC are estimated to be $eB_0 \sim 1.5m_\pi^2$ and $eB_0 \sim 15m_\pi^2$, respectively [18,19]. In what follows, after presenting the σ_0 dependence of T , we use the dependence of σ_0 on B_0 , and plot, in particular, T/T_0 as a function of eB_0/m_π^2 for nonvanishing angular velocity and electric as well as magnetic susceptibilities. To emphasize the effect of rotating electromagnetic fields, we also compare these results with the corresponding results for T/T_0 from nonrotating solutions, previously presented in Sec. IV A.

In Fig. 16, the σ_0 dependence of T/T_0 is plotted for $\tau = 1, 2, 3$ fm/c (blue and green solid and red dashed curves). To solve (3.39), we have used the set of free parameters

$$\{\tau_0, \sigma, \beta_0\} = \{0.5 \text{ fm/c}, 400 \text{ MeV/c}, 0.01\}, \quad (5.21)$$

with

$$\begin{aligned} \{\chi_e, \chi_m\} &= \{0, 0\}, \\ \{\chi_e, \chi_m\} &= \{0.01, +0.02\}, \\ \{\chi_e, \chi_m\} &= \{0.01, -0.02\}, \end{aligned} \quad (5.22)$$

and $\Omega_0 = -0.1$ [Figs. 16(a)–16(c)] as well as $\Omega_0 = -1$ [Figs. 16(d)–16(f)].

The results presented in Fig. 16 show that the σ_0 dependence of T/T_0 is strongly affected by Ω_0 , χ_e , and χ_m ; let us first consider the case of small $\omega_0 = 0.1$ in Figs. 16(a)–16(c). The slope of T/T_0 is affected by susceptibilities: Whereas T/T_0 increases with increasing σ_0 for $\{\chi_e, \chi_m\} = \{0, 0\}$ and $\{\chi_e, \chi_m\} = \{0.01, +0.02\}$ in a paramagnetic fluid [see Figs. 16(a) and 16(b)], it decreases with increasing σ_0 in a diamagnetic fluid with $\{\chi_e, \chi_m\} = \{0.01, -0.02\}$ [see Fig. 16(c)]. For large $\omega_0 = 1$, a completely different picture arises. Here, the effect of large angular velocity dominates the above-mentioned effect of nonvanishing susceptibilities. As it is shown in Figs. 16(d)–16(f), T/T_0 increases with increasing σ_0 for all sets of χ_e and χ_m from (5.22). Moreover, as expected, a change in the temporal sequence of T/T_0 amplitudes occurs for large $\omega_0 = 1$ in Figs. 16(d)–16(f) comparing with small $\omega_0 = 0.1$ from Figs. 16(a)–16(c). The same behavior was previously observed in Figs. 10 and 15(c) in comparison with Fig. 15(f).

²⁵See (3.36) from which T/T_0 is determined through (3.31). Here, it is enough to replace $\frac{E_0^2}{e_0}$ with $\frac{E_0^2}{e_0} = \sigma_0 \beta_0^2$.

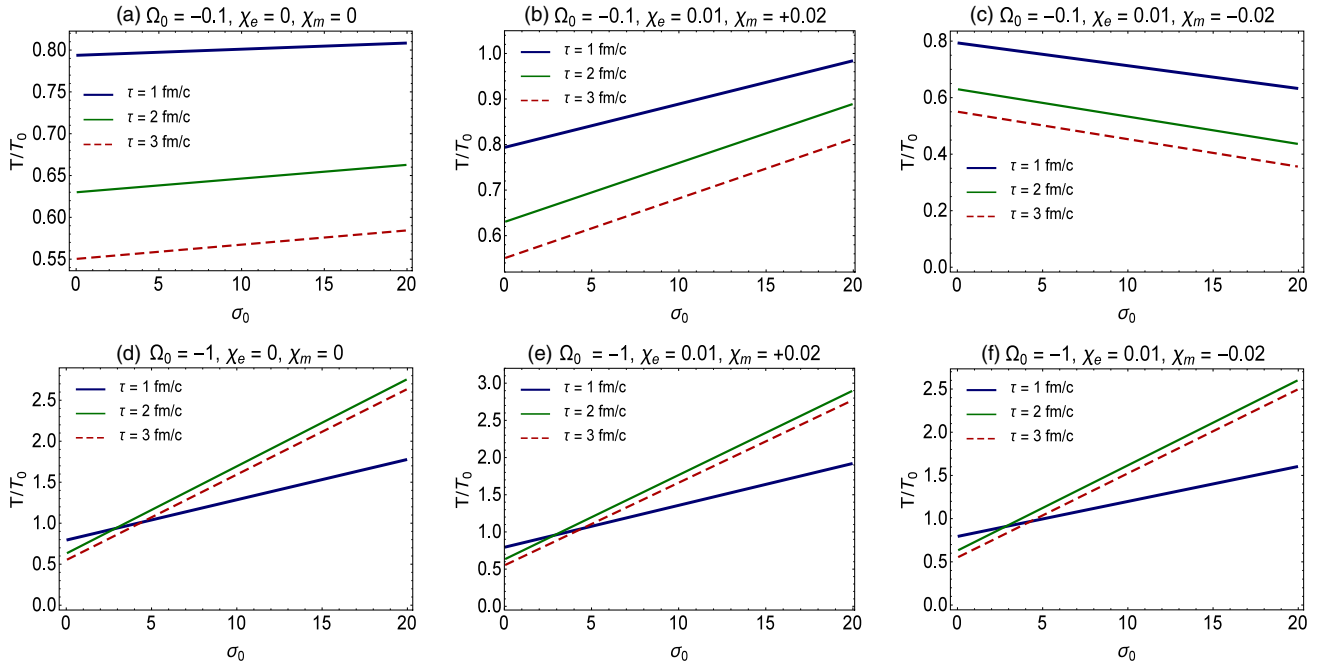


FIG. 16. The σ_0 dependence of T/T_0 is plotted at $\tau = 1, 2, 3$ fm/c (blue, green solid curves, and red dashed curves). The sets of free parameters (5.21) and (5.22) with $\Omega_0 = -0.1$ [(a)–(c)] $\Omega_0 = -1$ [(d)–(f)] are used to determine T/T_0 from the numerical solution of (3.39). The amplitude T/T_0 is strongly affected by angular velocity Ω , and electric and magnetic susceptibilities, χ_e and χ_m .

In Fig. 17, we have plotted the same numerical results from Fig. 16 in terms of eB_0/m_π^2 instead of σ_0 . The former seems to be a more appropriate measure in relation to HIC experiments. The aim is to look for a possibility to

emphasize the effects of Ω_0 , χ_e , and χ_m in a more phenomenological language.

To evaluate T/T_0 in terms of eB_0/m_π^2 , it is necessary to express eB_0 in terms of σ_0 . This is given by

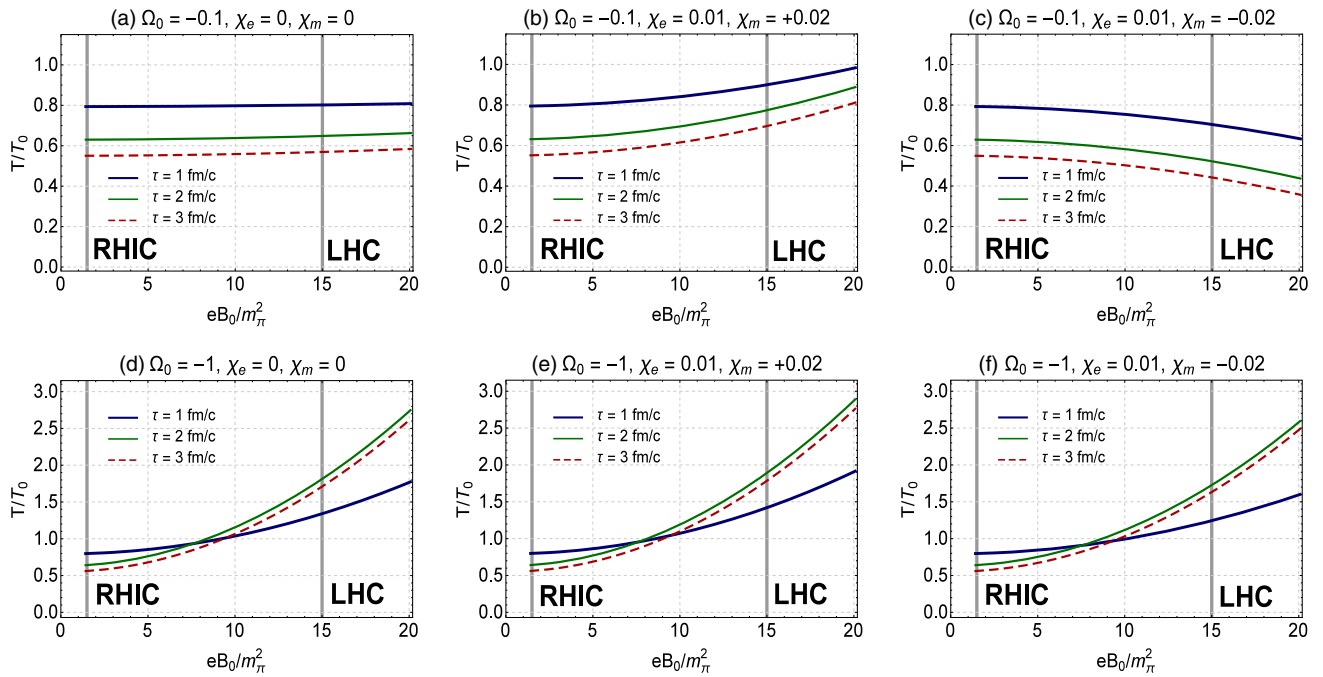


FIG. 17. The eB_0/m_π^2 dependence of T/T_0 is plotted at $\tau = 1, 2, 3$ fm/c (blue, green solid curves, and red dashed curves). The sets of free parameters (5.21) and (5.22) with $\Omega_0 = -0.1$ [(a)–(c)] $\Omega_0 = -1$ [(d)–(f)] are used to determine T/T_0 from the numerical solution to (3.39). The amplitude T/T_0 is strongly affected by angular velocity Ω_0 as well as electric and magnetic susceptibilities χ_e and χ_m .

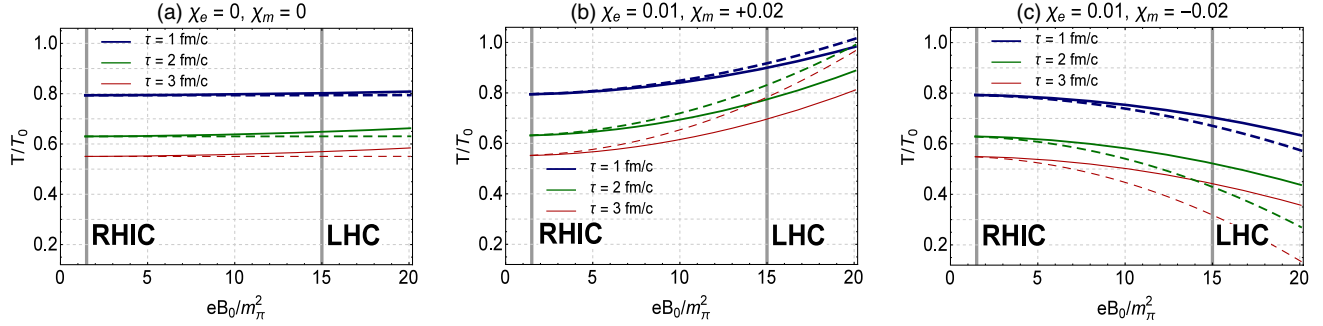


FIG. 18. The eB_0/m_π^2 dependence of T/T_0 corresponding to rotating (solid curves) and nonrotating (dashed curves) solutions is plotted at $\tau = 1, 2, 3$ fm/c (blue, green, and red solid curves). Here, we used three different sets of free parameters from (5.22) [(a)–(c)]. For the rotating solution, we have particularly used $\Omega_0 = -0.1$. Apart from different behavior of T/T_0 for vanishing and nonvanishing susceptibilities χ_e and χ_m , the deviation of nonrotating from the rotating solutions strongly depends on whether the fluid is para- or diamagnetic.

$$\frac{eB_0}{m_\pi^2} \sim 1.34(\epsilon_0\sigma_0)^{1/2}. \quad (5.23)$$

To arrive at (5.23), let us recall that $\sigma_0 = \frac{(eB_0)^2}{e^2\epsilon_0}$ is dimensionless, provided eB_0 is in GeV^2 and ϵ_0 in $\text{GeV fm}^{-3} \sim 8 \times 10^{-3} \text{ GeV}^4$. Using $m_\pi = 0.14 \text{ GeV}$, we have $1 \text{ GeV}^2 \sim 50m_\pi^2$. Replacing $e^2 = 4\pi\alpha_e \sim 0.09$ with the fine structure constant $\alpha_e = 1/137$, we arrive at (5.23). Here, ϵ_0 is in GeV fm^{-3} . For the energy density $\epsilon_0 \sim 10 \text{ GeV fm}^{-3}$ arising in a typical Au-Au collision with impact parameter $\sim 10 \text{ fm}$ and $\sqrt{s_{NN}} \sim 200 \text{ GeV}$ [34], we have

$$\frac{eB_0}{m_\pi^2} \sim 4.5\sigma_0^{1/2}. \quad (5.24)$$

The results presented in Fig. 17 have essentially the same feature as the results presented in Fig. 16. Vertical thick solid lines in the plots of Fig. 17 denote the values of eB_0 at the RHIC and LHC in m_π^2 units (see above). Remarkable is the difference between the dependence of T/T_0 on eB_0/m_π^2 for vanishing and nonvanishing susceptibilities for small angular velocity $\omega_0 = 0.1$. In this case, whereas for a fluid with $\chi_m = 0$, T remains almost constant with increasing eB_0/m_π^2 , for a para- (dia-) magnetic fluid with positive (negative) χ_m , T/T_0 increases (decreases) with increasing eB_0/m_π^2 . In contrast for large angular velocity $\omega_0 = 1$, T/T_0 increases for all values of χ_m .

To emphasize the effect of the rotation of electromagnetic fields on the dependence of T/T_0 on eB_0/m_π^2 , we have plotted in Fig. 18 the eB_0/m_π^2 dependence of T/T_0 for vanishing and nonvanishing Ω_0 . For nonrotating solutions of T/T_0 , we have used the analytical result (3.31) with $\mathbb{V} = 1$ and $\exp(\frac{\mathcal{L}}{\kappa})$ given in (4.10). For rotating solutions, the same numerical results for T/T_0 previously demonstrated in Figs. 16 and 17 are used. In both cases the set of parameters (5.21) and (5.22) is applied. For the rotating

solution, we set, in particular, $\Omega_0 = -0.1$. The blue, green, and red solid (dashed) curves correspond to rotating (nonrotating) solutions. For $\{\chi_e, \chi_m\} = \{0, 0\}$ in Fig. 18(a), the nonrotating solution is slightly deviated from the numerical solution with small $\omega_0 = 0.1$. In both cases amplitude T/T_0 remains almost constant once eB_0/m_π^2 is increased. In a paramagnetic fluid with $\{\chi_e, \chi_m\} = \{0.01, +0.02\}$, however, in both rotating and nonrotating cases, T/T_0 increases with increasing eB_0/m_π^2 , while the deviation of nonrotating solutions [dashed curves in Fig. 18(b)] from rotating solutions [solid curves in Fig. 18(b)] is positive. The opposite is true for a diamagnetic fluid with $\{\chi_e, \chi_m\} = \{0.01, -0.02\}$. As it is demonstrated in Fig. 18(c), the fluid becomes cooler once eB_0/m_π^2 increases. However, for nonvanishing ω_0 , the slope of T/T_0 as a function of eB_0/m_π^2 is smaller than that for vanishing ω_0 [compare the slope of solid and dashed curves in Fig. 18(c)]. These results, together with the data of T/T_0 from the RHIC and LHC, may provide an experimental tool to check whether in HIC experiments, like those at the RHIC and LHC, the angular velocity of ω_0 vanishes or not.

VI. SUMMARY AND CONCLUSIONS

The search for self-similar analytical solutions of RIHD exhibiting various geometrical symmetry properties has attracted much attention in recent years [16]. Being, in particular, nonboost invariant, they represent extensions to the well-known one-dimensional, longitudinally boost-invariant Bjorken flow of RIHD [11,12]. The goal is, among others, to develop new analytical solutions, which overcome the shortcomings of Bjorken flow in reproducing experimental data of the RHIC and LHC. Here, very large magnetic fields are shown to be created during early stages of HICs. Numerous attempts have already been undertaken to study the impact of these magnetic fields on electromagnetic and thermal properties of QGP created in HICs. Bearing in mind that the electromagnetic properties of

QGP, such as its electric conductivity or its response to external electromagnetic fields, may elongate the lifetime of the magnetic fields produced in these collisions, they may affect the evolution of thermodynamic quantities, such as the temperature, pressure, and energy density of QGP.

Motivated by the above facts, the boost-invariant motion of an ideal magnetized fluid is recently studied in the framework of ideal transverse MHD [33,34]. It is shown that the (proper) time evolution of the energy density of the fluid depends on whether the magnetic field decays as $B(\tau) \sim \tau^{-a}$ with the free parameter a being either $a = 1$ or $a \neq 1$. In the present work, we have extended the studies performed in [33,34] to the case of nonideal transverse MHD, where electric conductivity as well as electric and magnetic susceptibilities of the fluid are assumed to be finite. The aim was to study the evolution of electromagnetic fields satisfying Maxwell and MHD equations. Assuming the electric and magnetic fields to be transverse to the fluid velocity, and parametrizing the corresponding partial differential equations in terms of $B = |\mathbf{B}|$ and $E = |\mathbf{E}|$ as well as ϕ and ζ , their angles to a certain fixed axis in the transverse plane, we arrived at two distinct differential equations for a certain function \mathcal{M} , which appears in the inhomogeneous continuity equation $\partial^\mu (Bu_\mu) = B\mathfrak{D}\mathcal{M}$. For any $\mathcal{M} \neq 0$, the latter represents a deviation from the frozen-flux theorem. Whereas boost-invariant solutions for the evolution of B , E , and T arise from $\frac{d\mathcal{M}}{du} = 0$, another, second-order quadratic differential equation for \mathcal{M} eventually leads to nonboost-invariant solutions to B , E , and T . The latter are essentially characterized by rotating, parallel, or antiparallel electric and magnetic fields in the LRF of the fluid.²⁶ The rotation occurs with increasing rapidity η and with a constant angular velocity $\omega_0 = \frac{d\phi}{d\eta} = \frac{d\zeta}{d\eta}$. The exact analytical solution for nonrotating electromagnetic fields arises once \mathcal{M} satisfies $\frac{d\mathcal{M}}{du} = 0$. Other approximate analytical solutions arise for rotating electric and magnetic fields with E/B being constant (power-law solution) or \mathcal{M} being linear in ω_0 (slowly rotating solution). We have, in particular, shown that the power-law decay $B(\tau) \sim \tau^{-a}$ with $a \neq 1$, previously introduced in [33,34] as an example for the violation of frozen-flux theorem in ideal transverse MHD, naturally arises as one of the approximate solutions of rotating electromagnetic fields in the framework of nonideal transverse MHD with constant E/B . We have also shown that \mathcal{M} plays a major role in determining the thermodynamic fields T , p , and ϵ , which exhibit self-similar solutions arising from our method of self-similar solutions of non-conserved charges.

²⁶As concerns the relative angle δ' between the electric and magnetic vector fields in the laboratory (lab) frame, it is given by an appropriate boost transformation of \mathbf{E} and \mathbf{B} from the LRF of the fluid to the lab frame. As it turns out, $\delta' \neq \delta$. Here, δ is the relative angle between \mathbf{E} and \mathbf{B} in the LRF of the fluid.

Choosing appropriate sets of free parameters for electric conductivity σ and susceptibilities χ_e, χ_m of the electromagnetized fluid, we numerically studied the solutions to the second-order, nonlinear differential equations for \mathcal{M} with a given $\Omega_0 = \ell\omega_0$. Here, $\ell = \pm 1$ indicates parallel ($\ell = +1$) or antiparallel ($\ell = -1$) electric and magnetic vectors. We compared these numerical solutions with the approximate power-law and slowly rotating solutions for B , E , and T , arising from nontrivial solutions of \mathcal{M} , and checked, in this way, the reliability of these approximations. We further focused on the interplay between the angular velocity ω_0 and σ, χ_m in connection with their potential effects on the lifetime of B and E fields as well as the evolution of the temperature T . We have shown that for large enough ω_0 , E and T exhibit certain peaks at early times after the collision, whereas B monotonically decays. In a general analysis of the solutions to the master equation for \mathcal{M} , we also discussed the conditions under which these kinds of peaks occur (see Appendix B). The effects of Ω_0, σ , and χ_m on the amplitudes $B/B_0, E/E_0$, and T/T_0 for fixed proper times τ have also been separately studied. We have, in particular, shown that for free parameters chosen according to their relevance for QGP produced in HICs, $\Omega_0 > 0$ leads to unphysical negative values for E/E_0 . This indicates that within our transverse MHD approximations \mathbf{B} and \mathbf{E} in these kinds of experiments have to be antiparallel to each other.

We have further considered the dependence of B , E , and T on the phenomenologically relevant parameter $\sigma_0 = \frac{B_0^2}{\epsilon_0}$, which appears also in [33,34]. Through its dependence on the magnetic field B_0 and energy density ϵ_0 at the initial (proper) time τ_0 , we plotted the temperature gradient of the electromagnetized fluid as a function of eB_0/m_π^2 . We have shown that for small values of ω_0 , the eB_0/m_π^2 dependence of T/T_0 at fixed $\tau \gtrsim \tau_0$ is significantly affected by χ_m , whereas for large values of ω_0 , T/T_0 increases with increasing eB_0/m_π^2 for all values of $\chi_m = 0, \chi_m > 0$, and $\chi_m < 0$. Bearing in mind that the magnetic fields created in HICs are estimated to be $B \sim 1.5m_\pi^2$ at the RHIC and $15m_\pi^2$ at the LHC, a possible difference between the temperature of QGP at the RHIC and LHC may provide information about the onset of rotation of electromagnetic fields in these kinds of experiments.

Let us finally note that the method of self-similar solutions for nonconserved charges, developed and used in the present work, is derived under the assumption of a simple EoS, $\epsilon = \kappa p$ with constant $\kappa = c_s^{-2} = 3$, which is only valid in the ultrarelativistic limit [33,34]. The above results can thus be improved by choosing more realistic EoS, arising, e.g., from lattice QCD, where c_s turns out to be T dependent. Apart from the sound velocity c_s , the electric conductivity and magnetic susceptibility, σ and χ_m , can also be chosen to be T dependent. In a magnetized medium, a dependence of c_s, σ , and χ_m on B and E is also

possible. All these may lead to more complicated differential equations for \mathcal{M} , which eventually results in more realistic results for the τ dependence of B , E , and T . We postpone these studies to our future works. As it is emphasized in the discussion below (3.11), another extension of the results presented in this work arises when p , E , and B are not assumed to be boost invariant. In this case, the uniform expansion of the fluid (i.e., $\mathfrak{D}u_\mu = 0$) is guaranteed once the numerator of (3.11) vanishes. More complicated solutions for the space and time evolution of the electromagnetic and thermodynamic fields may arise, which are presented elsewhere [41].

ACKNOWLEDGMENTS

The authors thank F. Taghinavaz and S. M. A. Tabatabaee for useful discussions.

APPENDIX A: USEFUL PROOFS

1. Proof of $\rho_e = 0$ in two-dimensional transverse MHD

As we have noticed in Sec. III, the electric charge density ρ_e vanishes in transverse MHD. To show this, let us contract the inhomogeneous Maxwell equation (3.9) with u_ν . Using the definition of $F^{\mu\nu}$ from (3.5), we arrive first at

$$u_\nu \partial_\mu F^{\mu\nu} = u_\nu \partial_\mu (E^\mu u^\nu - E^\nu u^\mu - \epsilon^{\mu\nu\alpha\beta} B_\alpha u_\beta) = u_\nu J^\nu. \quad (\text{A1})$$

Evaluating the derivatives on the lhs and using $\partial \cdot E = 0$, $(u \cdot E) = 0$ and $u_\nu (u \cdot \partial) E^\nu = 0$, which are valid in transverse MHD, together with $u \cdot E = 0$, we arrive first at

$$u_\nu \partial_\mu F^{\mu\nu} = 2B \cdot \omega, \quad (\text{A2})$$

where $\omega^\mu \equiv \frac{1}{2} \epsilon^{\mu\nu\alpha\beta} u_\nu \partial_\alpha u_\beta$ is the vorticity of the fluid. Bearing in mind that in transverse MHD the nonzero components of u_μ and ∂_μ are in $\mu = 0, 3$ directions, it turns out that the vorticity of the fluid vanishes in the transverse MHD. We therefore arrive at

$$u_\nu \partial_\mu F^{\mu\nu} = 0. \quad (\text{A3})$$

This leads to $u_\nu J^\nu = 0$. Plugging at this stage J^ν from (3.10) into this relation, and using similar arguments as above, it can be shown that $u_\nu \partial_\rho M^{\rho\nu} = 0$ and thus $u_\nu J^\nu = \rho_e = 0$.

2. Notes on the symmetry properties in transverse MHD

In Sec. III, we have introduced the setups of nonideal transverse MHD. Here, B^μ and E^μ are defined by $B^\mu = \frac{1}{2} \epsilon^{\mu\nu\alpha\beta} F_{\nu\alpha} u_\beta$ and $E^\mu = F^{\mu\nu} u_\nu$, where $F^{\mu\nu}$ is the electromagnetic field strength tensor and $u^\mu = \gamma(1, \mathbf{v})$ the fluid

velocity. Using these definitions together with symmetry properties of $F^{\mu\nu}$, it is easy to show $u \cdot B = 0$ and $u \cdot E = 0$. Combining these relations with $\mathbf{v} \cdot E = 0$ and $\mathbf{v} \cdot B = 0$, which characterize transverse MHD, we have, in particular,²⁷

$$B_0 = B_z = 0 \quad \text{and} \quad E_0 = E_z = 0. \quad (\text{A4})$$

We thus have

$$B^\mu = (0, B_x, B_y, 0), \quad E^\mu = (0, E_x, E_y, 0), \quad (\text{A5})$$

as already pointed out in Sec. III. Using the definitions of B^μ and E^μ in terms of $F^{\mu\nu}$,²⁸

$$\begin{aligned} B_0 &= +F_{12}u_3 = -\sinh \eta F_{12}, \\ B_z &= -F_{12}u_0 = -\cosh \eta F_{12}, \end{aligned} \quad (\text{A6})$$

as well as

$$\begin{aligned} E_0 &= -F^{30}u_3 = \sinh \eta F^{30}, \\ E_z &= +F^{30}u_0 = \cosh \eta F^{30}, \end{aligned} \quad (\text{A7})$$

(A4) leads, in general, to

$$F_{12} = 0, \quad \text{and} \quad F^{30} = 0. \quad (\text{A8})$$

In what follows, we use the above properties of transverse MHD, and, in particular, the translational invariance in the x - y plane, to show that B_i , $i = 0, z$, and E_i , $i = 0, z$ do not evolve with τ and η , i.e.,

$$\frac{\partial B_i}{\partial \tau} = \frac{\partial B_i}{\partial \eta} = 0 \quad i = 0, z, \quad (\text{A9})$$

$$\frac{\partial E_i}{\partial \tau} = \frac{\partial E_i}{\partial \eta} = 0 \quad i = 0, z. \quad (\text{A10})$$

To prove (A9), let us start with the homogeneous Maxwell equation

$$\partial_\gamma F_{\alpha\beta} + \partial_\beta F_{\gamma\alpha} + \partial_\alpha F_{\beta\gamma} = 0. \quad (\text{A11})$$

For $(\alpha, \beta, \gamma) = (0, 1, 2)$, we have

$$\partial_2 F_{01} + \partial_1 F_{20} + \partial_0 F_{12} = 0. \quad (\text{A12})$$

Using the translational invariance in the transverse x - y plane, we have $\partial_2 F_{01} = \partial_1 F_{20} = 0$. We thus arrive at

²⁷Here, for a generic four-vector a^μ , the notation $a^\mu = (a^0, a^1, a^2, a^3) = (a_0, a_x, a_y, a_z)$ is used.

²⁸Here, $u^\mu = (\cosh \eta, 0, 0, \sinh \eta)$ is used.

$$\frac{\partial F_{12}}{\partial t} = 0. \quad (\text{A13})$$

Plugging $(\alpha, \beta, \gamma) = (3, 1, 2)$ into (A11) leads to

$$\partial_2 F_{31} + \partial_1 F_{23} + \partial_3 F_{12} = 0. \quad (\text{A14})$$

Again the translational invariance in the transverse x - y plane yields $\partial_2 F_{31} = \partial_1 F_{23} = 0$. We thus obtain

$$\frac{\partial F_{12}}{\partial z} = 0. \quad (\text{A15})$$

Using at this stage the definition of $\frac{\partial}{\partial t}$ and $\frac{\partial}{\partial z}$ from (3.14), (A13) and (A15) read

$$\begin{aligned} \left(\cosh \eta \frac{\partial}{\partial \tau} - \frac{1}{\tau} \sinh \eta \frac{\partial}{\partial \eta} \right) F_{12} &= 0, \\ \left(-\sinh \eta \frac{\partial}{\partial \tau} + \frac{1}{\tau} \cosh \eta \frac{\partial}{\partial \eta} \right) F_{12} &= 0. \end{aligned} \quad (\text{A16})$$

Combining these relations, we arrive at

$$\frac{\partial F_{12}}{\partial \tau} = 0, \quad \text{and} \quad \frac{\partial F_{12}}{\partial \eta} = 0. \quad (\text{A17})$$

Using at this stage the definitions (A6) of B_0 and B_z in terms of F_{12} as well as $F_{12} = 0$ from (A8), we arrive finally at $\frac{\partial B_i}{\partial \tau} = \frac{\partial B_i}{\partial \eta} = 0, i = 0, z$ from (A9).

As concerns the τ and η dependence of $E_i, i = 0, 3$ from (A10), we have to start from the equation of motion (3.9), with the electromagnetic current J^μ given in (3.10). For $\nu = 0, 3$, we have

$$\frac{\partial F^{30}}{\partial t} = -J^3, \quad \text{and} \quad \frac{\partial F^{30}}{\partial z} = J^0. \quad (\text{A18})$$

Plugging at this stage $\rho_e = 0$ from Appendix A 1 and $E_0 = E_z = 0$ from (A4), $J^i, i = 0, 3$ are first given by

$$J^i = \partial_\rho M^{\rho i}, \quad i = 0, 3. \quad (\text{A19})$$

Using the definition of $M^{\rho\mu}$ from (3.5) and the properties $\partial \cdot E = 0, E \cdot \partial = 0$ of transverse MHD, we obtain

$$J^i = \partial_\rho M^{\rho i} = \chi_e \frac{\partial E^i}{\partial \tau} - \chi_m \partial_\rho B^{\rho i}, \quad i = 0, 3, \quad (\text{A20})$$

where $B^{\mu\nu} \equiv \epsilon^{\mu\nu\alpha\beta} B_\alpha u_\beta$. For $\partial_\mu = (\partial_0, 0, 0, \partial_3)$ and $u^\mu = (u_0, 0, 0, u^3)$, we have $\partial_\rho B^{\rho i}, i = 0, 3$. We are therefore left with

$$J^0 = \chi_e \frac{\partial E^0}{\partial \tau}, \quad J^3 = \chi_e \frac{\partial E^3}{\partial \tau}. \quad (\text{A21})$$

Plugging $E_i, i = 0, 3$ from (A7) into (A21), and the resulting expression into (A18), we arrive at

$$\begin{aligned} \frac{\partial F^{30}}{\partial t} &= -\chi_e \cosh \eta \frac{\partial F^{30}}{\partial \tau}, \\ \frac{\partial F^{30}}{\partial z} &= \chi_e \sinh \eta \frac{\partial F^{30}}{\partial \tau}. \end{aligned} \quad (\text{A22})$$

Using (3.14) to write ∂_t and ∂_z in terms of ∂_τ and ∂_η , (A22) reads

$$\begin{aligned} \left((1 + \chi_e) \cosh \eta \frac{\partial}{\partial \tau} - \frac{1}{\tau} \sinh \eta \frac{\partial}{\partial \eta} \right) F^{30} &= 0, \\ \left(-(1 + \chi_e) \sinh \eta \frac{\partial}{\partial \tau} + \frac{1}{\tau} \cosh \eta \frac{\partial}{\partial \eta} \right) F^{30} &= 0. \end{aligned} \quad (\text{A23})$$

Combining these relations, we arrive for $\chi_e \neq -1$ at

$$\frac{\partial F^{30}}{\partial \tau} = 0, \quad \text{and} \quad \frac{\partial F^{30}}{\partial \eta} = 0. \quad (\text{A24})$$

Using at this stage the definitions (A7) of E_0 and E_z in terms of F^{30} as well as $F^{30} = 0$ from (A8), we arrive finally at $\frac{\partial E_i}{\partial \tau} = \frac{\partial E_i}{\partial \eta} = 0, i = 0, z$ from (A10).

The above results (A9) and (A10) show that in a transverse MHD setup, which is in particular characterized by translational invariance in the transverse x - y plane, the longitudinal components of \mathbf{E} and \mathbf{B} fields, E_i and $B_i, i = 0, z$, vanish during the uniform expansion of the fluid. The proof performed in this section can be viewed as a self-consistency check for the method used in Sec. III to determine the space and time evolution of electromagnetic and thermodynamic fields within a transverse nonideal MHD setup.

APPENDIX B: GENERAL ANALYSIS OF THE SOLUTIONS TO THE MASTER EQUATION FOR \mathcal{M}

The analysis of the master equation without actually solving it gives us important insights about the qualitative behavior of B, E , and T fields. One of the accessible results is the prediction of reapeaking in B, E , and T , i.e., the appearance of maxima after the initial time. These kinds of maxima do not occur in ideal MHD. Interestingly, for $\chi_m > 1$, it is also possible for the above fields to have a minimum before rising to a peak. However, as far as the HIC physics is concerned, $\chi_m > 1$ is not physically relevant. In what follows, we find the necessary conditions for a reapeaking of E and T fields, and prove that in the physically relevant case of $\chi_m < 1$ and $\chi_e > -1$, we must have $\Omega_0 \equiv \ell \omega_0 < 0$. This guarantees B, E , and T to be positive. We, in particular, show that for $\chi_m < 1$, B is monotonically decreasing, and find certain conditions for

which E and T have only one single maximum shortly after the initial time. To this purpose, we first prove a number of lemmas.

Lemma 1: For \tilde{u} being the extrema of

$$f(\tau) = f_0 \left(\frac{\tau_0}{\tau} \right) e^{\lambda(\tau)}, \quad (\text{B1})$$

we have

$$\frac{d\lambda}{du} \Big|_{\tilde{u}} = 1. \quad (\text{B2})$$

In addition, \tilde{u} is a maximum (minimum) if $\frac{d^2\lambda}{du^2} \Big|_{\tilde{u}}$ is negative (positive). Here, $u = \ln\left(\frac{\tau}{\tau_0}\right)$. For $f = \{B, E, T\}$, we have $\lambda = \{\mathcal{M}, \mathcal{N}, \mathcal{L}\}$, respectively.

Proof:—The proof is straightforward. One first finds the derivative with respect to τ in terms of the derivative with respect to u . By setting the first derivative equal to 0, (B2) is derived. The second derivative test then translates into the second claim.

Lemma 2: A differentiable function $f(u)$ either does not have two subsequent extrema of the same kind (maximum or minimum) or is constant in between.

Proof:—Consider two extrema of the same kind at points u_1 and u_2 . Then, for some ϵ we have $f'(u_1 + \epsilon) f'(u_2 - \epsilon) < 0$, and thus another extremum exists in the interval between u_1 and u_2 . This is either of the same or opposite kind. If it is of the same kind, this procedure can be repeated until an extremum of opposite kind is found or $f'(u) = 0$ for all points $u \in [u_1, u_2]$.

Lemma 3: If the sign of the second derivative of a differentiable function $f(u)$ in its possible extremum is forced to be negative and nonzero, then

- (1) If $\left(\frac{df}{du}\Big|_0\right)\left(\frac{df}{du}\Big|_{u \gg 1}\right) < 0$, f has exactly one maximum somewhere in $[0, \infty)$.
- (2) If $\left(\frac{df}{du}\Big|_0\right)\left(\frac{df}{du}\Big|_{u \gg 1}\right) > 0$, f is monotonically decreasing or increasing.

Proof:—If the second derivative is negative at any possible extremum, then the function is neither constant nor does it have a minimum by lemma 2. By Bolzano's theorem, the function has a maximum in $[0, \infty)$ if the first derivative has opposite signs in 0 and $u \gg 1$. Now consider the case that the derivative is negative both initially ($u = 0$) and asymptotically ($u \rightarrow \infty$), and assume that $f'(u) = 0$ at some point u^* . Then, u^* needs to be a maximum of $f'(u)$. If it is not, then there exists a point such that $f'(u) > 0$, and therefore $f'(u)$ vanishes in another point other than u^* . This is not possible by lemma 2. Being a maximum of $f'(u)$, we have $f''(u) = 0$ at u^* . This is again not possible, and therefore $f(u)$ is monotonically decreasing. A similar argument shows that $f(u)$ is monotonically increasing if the first derivative is positive both initially and asymptotically.

Lemma 4: At the initial time, i.e., $u = 0$, the derivatives of functions of interest are given by

$$\frac{d\mathcal{M}}{du} \Big|_{u=0} = \beta_0 \Omega_0, \quad (\text{B3})$$

$$\frac{d^2\mathcal{M}}{du^2} \Big|_{u=0} = - \left\{ \frac{\Omega_0 \beta_0 \sigma \tau_0 + \Omega_0^2 [1 - \chi_m + \beta_0^2 (1 + \chi_e)]}{1 + \chi_e} \right\}, \quad (\text{B4})$$

$$\frac{d\mathcal{N}}{du} \Big|_{u=0} = - \left[\frac{\Omega_0 (1 - \chi_m) + \beta_0 \sigma \tau_0}{\beta_0 (1 + \chi_e)} \right], \quad (\text{B5})$$

$$\begin{aligned} \frac{d\mathcal{L}}{du} \Big|_{u=0} = \frac{\sigma_0}{c_s^2} \left\{ \right. & \left. \left[\sigma \tau_0 \right. \right. \\ & + \chi_e \left(\frac{\Omega_0 (1 - \chi_m) + \beta_0 (1 + \sigma \tau_0 + \chi_e)}{\beta_0 (1 + \chi_e)} \right) \left. \right] \beta_0^2 \\ & \left. + \chi_m (1 - \beta_0 \Omega_0) \right\}. \end{aligned} \quad (\text{B6})$$

Proof:—The first relation (B3) was already used in Sec. III [see (3.54) and evaluate it at $u = 0$]. Plugging $\frac{d\mathcal{M}}{du}$ from (B3) into (3.39), (B4) is found. As concerns (B5), one uses

$$\frac{d\mathcal{M}}{du} \frac{d\mathcal{N}}{du} = \frac{d^2\mathcal{M}}{du^2} + \left(\frac{d\mathcal{M}}{du} \right)^2, \quad (\text{B7})$$

along with earlier results, and arrives at (B5). Finally, from (3.29), one finds

$$\frac{d\mathcal{L}}{du} = \frac{\kappa B^2}{\epsilon} \left\{ \left[\sigma \tau - \chi_e \left(\frac{d\mathcal{N}}{du} - 1 \right) \right] \frac{E^2}{B^2} + \chi_m \left(1 - \frac{E}{B} \Omega_0 \right) \right\}, \quad (\text{B8})$$

which at $u = 0$ yields the desired relation (B6).

Lemma 5: The asymptotic behavior of quantities of interest at $u \gg 1$ is given by

$$\frac{d\mathcal{M}}{du} \Big|_{u \gg 1} \sim - \frac{\Omega_0^2 (1 - \chi_m)}{\sigma \tau_0} e^{-u}, \quad (\text{B9})$$

$$\frac{d^2\mathcal{M}}{du^2} \Big|_{u \gg 1} \sim - \frac{d\mathcal{M}}{du}, \quad (\text{B10})$$

$$\mathcal{M}(u) \Big|_{u \gg 1} \sim - \frac{\Omega_0^2 (1 - \chi_m)}{\sigma \tau_0} (1 - e^{-u}), \quad (\text{B11})$$

$$\frac{d\mathcal{N}}{du} \Big|_{u \gg 1} \sim -1 - \frac{\Omega_0^2 (1 - \chi_m)}{\sigma \tau_0} e^{-u}, \quad (\text{B12})$$

$$\mathcal{N}(u) \Big|_{u \gg 1} \sim -u - \frac{\Omega_0^2 (1 - \chi_m)}{\sigma \tau_0} (1 - e^{-u}), \quad (\text{B13})$$

and

$$\begin{aligned}
e^{\mathcal{L}/\kappa}|_{u \gg 1} &\sim 1 + \sigma_0 \exp\left(-\frac{2(1-\chi_m)\Omega_0^2}{\sigma\tau_0}\right) \\
&\times \left\{ \frac{\chi_m}{1-c_s^2} (1 - e^{-(1-c_s^2)u}) \right. \\
&+ \frac{1}{2-c_s^2} \left(\beta_0^2 \sigma\tau_0 + \frac{\chi_m \Omega_0^2 (1-\chi_m)}{\sigma\tau_0} \right) \\
&\times (1 - e^{-(2-c_s^2)u}) + \frac{2\beta_0^2 \chi_e}{3-c_s^2} (1 - e^{-(3-c_s^2)u}) \\
&\left. + \frac{\beta_0^2 \chi_e \Omega_0^2 (1-\chi_m)}{\sigma\tau_0 (4-c_s^2)} (1 - e^{-(4-c_s^2)u}) \right\}, \quad (\text{B14})
\end{aligned}$$

as well as

$$\frac{d}{du} (e^{\mathcal{L}/\kappa})|_{u \gg 1} \sim \chi_m \sigma_0 \exp\left(-\frac{2(1-\chi_m)\Omega_0^2}{\sigma\tau_0}\right) e^{-(1-c_s^2)u}. \quad (\text{B15})$$

Proof:—We start by inspecting the master equation (3.39) at $u \gg 1$. To do so, we reevaluate it in terms of $w \equiv \frac{1}{u}$. Using

$$\frac{d\mathcal{M}}{du} = -w^2 \frac{d\mathcal{M}}{dw}, \quad \frac{d^2\mathcal{M}}{du^2} = w^3 \left(2 \frac{d\mathcal{M}}{dw} + w \frac{d^2\mathcal{M}}{dw^2} \right), \quad (\text{B16})$$

keeping nonvanishing terms in $w \rightarrow 0$, and rewriting the result in terms of u , we find the asymptotic equation as

$$\frac{d\mathcal{M}}{du} e^u \sigma\tau_0 + \omega_0^2 (1-\chi_m) = 0. \quad (\text{B17})$$

This immediately leads to (B9). Equations (B10) and (B11) are found by differentiating and integrating (B9) with respect to u . Here, $\mathcal{M}(0) = 0$ is assumed. Using (B7), and earlier results, we arrive at (B12). The result is then integrated to give (B13). We use $\mathcal{N}(0) = 0$. In order to find (B14), we first rewrite (3.36) as

$$\begin{aligned}
e^{\mathcal{L}/\kappa} &= 1 + \sigma_0 \left[\sigma\tau_0 \beta_0^2 \int_0^u du' e^{2\mathcal{N}(u') + c_s^2 u'} \right. \\
&+ \chi_e \beta_0^2 \int_0^u du' \left(1 - \frac{d\mathcal{N}}{du'} \right) e^{2\mathcal{N}(u') - (1-c_s^2)u'} \\
&\left. + \chi_m \int_0^u du' \left(1 - \frac{d\mathcal{M}}{du'} \right) e^{2\mathcal{M}(u') - (1-c_s^2)u'} \right]. \quad (\text{B18})
\end{aligned}$$

Then, plugging earlier results into (B18), and performing the corresponding integrals, we arrive at (B14). Here,

$$e^{2\mathcal{N}(u')} \sim e^{-2u' - \frac{2\Omega_0^2(1-\chi_m)}{\sigma\tau_0}}$$

is used. Taking finally the derivative of (B14), all terms except the first one are suppressed at $u \gg 1$. We thus arrive at (B15).

We are now in the position to analyze the rotating solutions for B , E , and T in the following theorems:

Theorem 1: In order for the system to be physical (i.e., $E > 0$)

$$\Omega_0(1-\chi_m) < 0. \quad (\text{B19})$$

In other words, the sign of $\frac{d\mathcal{M}}{du}$ does not change during the time evolution.

Proof:—From (3.54), it is evident that, in order for E to be non-negative, we must have

$$\frac{1}{\Omega_0} \frac{d\mathcal{M}}{du} > 0, \quad (\text{B20})$$

provided $B > 0$. In other words, $\frac{d\mathcal{M}}{du}$ does not change sign in the whole interval of u . Moreover, according to (B9), for $\chi_m < 1$ ($\chi_m > 1$), $\frac{d\mathcal{M}}{du}$ becomes asymptotically negative (positive). Multiplying (B9) with $1/\Omega_0$, we obtain

$$\frac{1}{\Omega_0} \frac{d\mathcal{M}}{du} \sim -\Omega_0(1-\chi_m)\xi, \quad \text{with} \quad \xi \equiv \frac{e^{-u}}{\sigma\tau_0} > 0,$$

which leads to (B19), upon using (B20).

Theorem 2: For $\chi_m < 1$, the magnetic field monotonically decreases.

Proof:—According to theorem 1, $\chi_m < 1$ leads to $\Omega_0 < 0$. Negative Ω_0 thus leads to $\frac{d\mathcal{M}}{du} < 0 < 1$, $\forall u \in [0, \infty)$ [see (B20)]. This shows that B has always a negative derivative, and is thus monotonically decreasing.

Theorem 3: For $\chi_m < 1$ and $\chi_e > -1$, the electric field repeats exactly once if

$$\Omega_0 < -\frac{\beta_0(1+\chi_e + \sigma\tau_0)}{1-\chi_m}. \quad (\text{B21})$$

Otherwise, it is monotonically decreasing.

Proof:—Let us determine the sign of

$$\frac{dE}{du} = E \left(\frac{d\mathcal{N}}{du} - 1 \right),$$

at $u = 0$ and $u \gg 1$ by separately inspecting the sign of $\frac{d\mathcal{N}}{du} - 1$ at $u = 0$ and $u \gg 1$. Using (B5) and (B12), we have

$$\begin{aligned}
\left. \frac{d\mathcal{N}}{du} \right|_{u=0} - 1 &\sim -\frac{[\Omega_0(1-\chi_m) + \beta_0\sigma\tau_0 + \beta_0(1+\chi_e)]}{\beta_0(1+\chi_e)}, \\
\left. \frac{d\mathcal{N}}{du} \right|_{u \gg 1} - 1 &\sim -2 - \frac{\Omega_0^2(1-\chi_m)}{\sigma\tau_0} e^{-u}. \quad (\text{B22})
\end{aligned}$$

For $\chi_m < 1$ and $\chi_e > -1$, $\frac{dN}{du}|_{u \gg 1} - 1$ and thus $\frac{dE}{du}|_{u \gg 1}$ are always negative. Hence, in order for E to reapek only once, $\frac{dN}{du}|_{u=0} - 1$ and thus $\frac{dE}{du}|_{u=0}$ are to be positive (see lemma 3). This fixes Ω_0 to be

$$\Omega_0 < -\frac{\beta_0(1 + \chi_e + \sigma\tau_0)}{1 - \chi_m},$$

as claimed in (B21). Moreover, according to lemma 3, E is monotonically decreasing for

$$\Omega_0 \geq -\frac{\beta_0(1 + \chi_e + \sigma\tau_0)}{1 - \chi_m}.$$

This completes the proof.

Theorem 4: Causality ensures $T \rightarrow 0$ when $\tau \gg \tau_0$. However, the parameters have to be constrained in order for T to be positive. The constraint is roughly given by $\chi_m \gtrsim -\sigma_0^{-1}$.

Proof:—According to (3.31), for $\mathbb{V} = 1$, the self-similar solution of T/T_0 is given by

$$\frac{T}{T_0} = \left(\frac{\tau_0}{\tau}\right)^{\frac{1}{\kappa}} e^{\frac{\mathcal{L}}{\kappa}}. \quad (\text{B23})$$

As we have seen in (B14), the asymptotic form of T/T_0 contains terms of $1 - e^{-(k-c_s^2)u}$, with $k = 1, \dots, 4$. Since $c_s \leq 1$ by causality, for all $k = 1, \dots, 4$ we have $1 - e^{-(k-c_s^2)u} \rightarrow 1$ as $u \rightarrow \infty$. The factor $e^{\mathcal{L}/\kappa}$ in (B23) becomes therefore constant at $u \gg 1$. Hence, the behavior of T/T_0 is exclusively dictated by the Bjorken factor $\tau^{-c_s^2}$ that vanishes at $\tau \gg \tau_0$. We therefore have $T \rightarrow 0$ at large $\tau \gg \tau_0$, as claimed.

Inspecting now the limit of $e^{\mathcal{L}/\kappa}$ at $u \gg 1$, it may becomes negative, especially for $\chi_m, \chi_e < 0$. An exact constraint, which ensures T to be positive, reads

$$\sigma_0 \left(\frac{\chi_m}{1 - c_s^2} + \mathcal{R} \right) \geq -1, \quad (\text{B24})$$

with \mathcal{R} defined by

$$\begin{aligned} \mathcal{R} \equiv & \exp\left(-\frac{2(1 - \chi_m)\Omega_0^2}{\sigma\tau_0}\right) \\ & \times \left[\frac{1}{2 - c_s^2} \left(\beta_0^2 \sigma\tau_0 + \frac{\chi_m \Omega_0^2 (1 - \chi_m)}{\sigma\tau_0} \right) \right. \\ & \left. + \frac{\beta_0^2 \chi_e}{3 - c_s^2} + \frac{\beta_0^2 \chi_e \Omega_0^2 (1 - \chi_m)}{\sigma\tau_0 (4 - c_s^2)} \right]. \end{aligned} \quad (\text{B25})$$

Assuming

$$\frac{\Omega_0^2}{\sigma\tau_0} \ll 1, \quad (\text{B26})$$

the second and the last term in the bracket appearing in \mathcal{R} are suppressed, and it becomes always positive for $\chi_e, \sigma > 0$. In this case, neglecting \mathcal{R} , the positivity condition (B24) is roughly given by $\chi_m \gtrsim -\sigma_0^{-1}$, as claimed.

Theorem 5: For $\chi_m < 1$, the temperature reapeks exactly once if

$$\begin{aligned} \frac{d\mathcal{L}}{du}\Big|_{u=0} = & \frac{\sigma_0}{c_s^2} \left\{ \left[\sigma\tau_0 \right. \right. \\ & \left. \left. + \chi_e \left(\frac{\Omega_0(1 - \chi_m) + \beta_0(1 + \sigma\tau_0 + \chi_e)}{\beta_0(1 + \chi_e)} \right) \right] \beta_0^2 \right. \\ & \left. + \chi_m(1 - \beta_0\Omega_0) \right\} > 1. \end{aligned} \quad (\text{B27})$$

Proof:—To determine the sign of

$$\frac{dT}{du} = T \left(\frac{d\mathcal{L}}{du} - 1 \right),$$

at $u = 0$ and $u \gg 1$, we separately inspect the sign of $\frac{d\mathcal{L}}{du} - 1$ at $u = 0$ and $u \gg 1$. According to (B15), $\frac{d}{du}(e^{\mathcal{L}}) \rightarrow 0$ for $u \gg 1$. This translates into $\frac{d\mathcal{L}}{du} = 0$. Hence, in the limit of large $u \gg 1$, $\frac{dT}{du}|_{u \gg 1}$ is always negative. According to lemma 3, T peaks only once if $\frac{dT}{du}|_{u=0} > 0$. Using (B6), we thus arrive at (B27), as claimed.

-
- [1] D. Teaney, J. Lauret, and E. V. Shuryak, Flow at the SPS and RHIC as a Quark Gluon Plasma Signature, *Phys. Rev. Lett.* **86**, 4783 (2001); A hydrodynamic description of heavy ion collisions at the SPS and RHIC, [arXiv:nucl-th/0110037](https://arxiv.org/abs/nucl-th/0110037).
- [2] P. F. Kolb, P. Huovinen, U. W. Heinz, and H. Heiselberg, Elliptic flow at SPS and RHIC: From kinetic transport to hydrodynamics, *Phys. Lett. B* **500**, 232 (2001).

- [3] E. Shuryak, Why does the quark gluon plasma at RHIC behave as a nearly ideal fluid?, *Prog. Part. Nucl. Phys.* **53**, 273 (2004).
- [4] M. Gyulassy and L. McLerran, New forms of QCD matter discovered at RHIC, *Nucl. Phys.* **A750**, 30 (2005).
- [5] T. Hirano and M. Gyulassy, Perfect fluidity of the quark gluon plasma core as seen through its dissipative hadronic corona, *Nucl. Phys.* **A769**, 71 (2006).

- [6] P. Romatschke and U. Romatschke, Viscosity Information from Relativistic Nuclear Collisions: How Perfect is the Fluid Observed at RHIC?, *Phys. Rev. Lett.* **99**, 172301 (2007).
- [7] T. Schäfer and D. Teaney, Nearly perfect fluidity: From cold atomic gases to hot quark gluon plasmas, *Rep. Prog. Phys.* **72**, 126001 (2009).
- [8] L. D. Landau, On the multiparticle production in high-energy collisions, *Izv. Akad. Nauk Ser. Fiz.* **17**, 51 (1953).
- [9] S. Z. Belenkij and L. D. Landau, Hydrodynamic theory of multiple production of particles, *Usp. Fiz. Nauk* **56**, 309 (1955) [*Nuovo Cimento Suppl.* **3**, 15 (1956)].
- [10] I. M. Khalatnikov, Nekotorye voprosy nerelativistskoi gidrodinamiki (Some questions of relativistic hydrodynamics), *Zh. Eksp. Teor. Fiz.* **27**, 529 (1954).
- [11] R. C. Hwa, Statistical description of hadron constituents as a basis for the fluid model of high-energy collisions, *Phys. Rev. D* **10**, 2260 (1974).
- [12] J. D. Bjorken, Highly relativistic nucleus-nucleus collisions: The central rapidity region, *Phys. Rev. D* **27**, 140 (1983).
- [13] J. P. Bondorf, S. I. A. Garpman, and J. Zimanyi, A simple analytic hydrodynamic model for expanding fireballs, *Nucl. Phys. A* **296**, 320 (1978).
- [14] P. Csizmadia, T. Csörgö, and B. Lukács, New analytic solutions of the nonrelativistic hydrodynamical equations, *Phys. Lett. B* **443**, 21 (1998).
- [15] T. S. Biró, Analytic solution for relativistic transverse flow at the softest point, *Phys. Lett. B* **474**, 21 (2000).
- [16] R. D. de Souza, T. Koide, and T. Kodama, Hydrodynamic approaches in relativistic heavy ion reactions, *Prog. Part. Nucl. Phys.* **86**, 35 (2016).
- [17] T. Csörgö and G. Kasza, New exact solutions of hydrodynamics for rehadronizing fireballs with lattice QCD equation of state, [arXiv:1610.02197](https://arxiv.org/abs/1610.02197).
- [18] D. E. Kharzeev, L. D. McLerran, and H. J. Warringa, The effects of topological charge change in heavy-ion collisions: “Event by event P and CP violation”, *Nucl. Phys. A* **803**, 227 (2008).
- [19] V. Skokov, A. Y. Illarionov, and V. Toneev, Estimate of the magnetic field strength in heavy-ion collisions, *Int. J. Mod. Phys. A* **24**, 5925 (2009).
- [20] K. Tuchin, Particle production in strong electromagnetic fields in relativistic heavy-ion collisions, *Adv. High Energy Phys.* **2013**, 1 (2013); Time and space dependence of the electromagnetic field in relativistic heavy-ion collisions, *Phys. Rev. C* **88**, 024911 (2013).
- [21] U. Gürsoy, D. Kharzeev, and K. Rajagopal, Magnetohydrodynamics, charged currents and directed flow in heavy-ion collisions, *Phys. Rev. C* **89**, 054905 (2014).
- [22] B. G. Zakharov, Electromagnetic response of quark-gluon plasma in heavy-ion collisions, *Phys. Lett. B* **737**, 262 (2014).
- [23] S. Fayazbakhsh and N. Sadooghi, Color neutral 2SC phase of cold and dense quark matter in the presence of constant magnetic fields, *Phys. Rev. D* **82**, 045010 (2010).
- [24] S. Fayazbakhsh and N. Sadooghi, Phase diagram of hot magnetized two-flavor color superconducting quark matter, *Phys. Rev. D* **83**, 025026 (2011).
- [25] K. G. Klimenko, Three-dimensional Gross-Neveu model at nonzero temperature and in an external magnetic field, *Z. Phys. C* **54**, 323 (1992).
- [26] V. P. Gusynin, V. A. Miransky, and I. A. Shovkovy, Dimensional reduction and catalysis of dynamical symmetry breaking by a magnetic field, *Nucl. Phys. B* **462**, 249 (1996).
- [27] G. S. Bali, F. Bruckmann, G. Endrodi, Z. Fodor, S. D. Katz, S. Krieg, A. Schäfer, and K. K. Szabo, The QCD phase diagram for external magnetic fields, *J. High Energy Phys.* **02** (2012) 044.
- [28] N. Sadooghi and F. Taghinavaz, Dilepton production rate in a hot and magnetized quark-gluon plasma, *Ann. Phys. (Amsterdam)* **376**, 218 (2017).
- [29] A. Bandyopadhyay, C. A. Islam, and M. G. Mustafa, Electromagnetic spectral properties and Debye screening of a strongly magnetized hot medium, *Phys. Rev. D* **94**, 114034 (2016).
- [30] A. Ayala, J. D. Castano-Yepes, C. A. Dominguez, and L. A. Hernandez, Thermal photon production from gluon fusion induced by magnetic fields in relativistic heavy-ion collisions, *EPJ Web Conf.* **141**, 02007 (2017).
- [31] J. O. Andersen, W. R. Naylor, and A. Tranberg, Phase diagram of QCD in a magnetic field: A review, *Rev. Mod. Phys.* **88**, 025001 (2016).
- [32] V. A. Miransky and I. A. Shovkovy, Quantum field theory in a magnetic field: From quantum chromodynamics to graphene and Dirac semimetals, *Phys. Rep.* **576**, 1 (2015).
- [33] V. Roy, S. Pu, L. Rezzolla, and D. Rischke, Analytic Bjorken flow in one-dimensional relativistic magnetohydrodynamics, *Phys. Lett. B* **750**, 45 (2015).
- [34] S. Pu, V. Roy, L. Rezzolla, and D. H. Rischke, Bjorken flow in one-dimensional relativistic magnetohydrodynamics with magnetization, *Phys. Rev. D* **93**, 074022 (2016).
- [35] L. Rezzolla and O. Zanotti, *Relativistic Hydrodynamics* (Oxford University Press, Oxford, 2013); L. D. Landau and E. M. Lifshitz, *Fluid Mechanics*, 2nd ed. (Pergamon Press, New York, 1987).
- [36] S. Pu and D. L. Yang, Transverse flow induced by inhomogeneous magnetic fields in the Bjorken expansion, *Phys. Rev. D* **93**, 054042 (2016).
- [37] T. Csörgö, F. Grassi, Y. Hama, and T. Kodama, Simple solutions of relativistic hydrodynamics for longitudinally expanding systems, *Heavy Ion Phys. A* **21**, 53 (2004); Simple solutions of relativistic hydrodynamics for longitudinally and cylindrically expanding systems, *Phys. Lett. B* **565**, 107 (2003).
- [38] T. Csörgö, L. P. Csernai, Y. Hama, and T. Kodama, Simple solutions of relativistic hydrodynamics for systems with ellipsoidal symmetry, *Heavy Ion Phys. A* **21**, 73 (2004).
- [39] S. S. Gubser, Symmetry constraints on generalizations of Bjorken flow, *Phys. Rev. D* **82**, 085027 (2010).
- [40] J. Y. Ollitrault, Relativistic hydrodynamics for heavy-ion collisions, *Eur. J. Phys.* **29**, 275 (2008).
- [41] M. Shokri and N. Sadooghi (to be published).